Heinrich-Heine-University Düsseldorf
Department of Mathematics and Natural Science
Institute of Physical Biology

New avenues in the characterization of Membrane Systems

Inaugural dissertation

for the attainment of the title of doctor
in the Faculty of Mathematics and Natural Sciences
at the Heinrich Heine University Düsseldorf

presented by

Fátima Carolina Escobedo González
from México

Düsseldorf, March 2023

-

From the Institute for Physical Biology
at the Heinrich Heine University Düsseldorf

Published by permission of the Faculty of Mathematics and Natural Sciences at Heinrich Heine University Düsseldorf

Supervisor: Dr. Manuel Etzkorn

Co-supervisor: Dr. Matias Zurbriggen

Date of the oral examination: 29/03/2023

-

Declaration

I hereby declare that the present dissertation is written independently, without outside help and without using sources other than those specified. All of the outside works taken over directly or indirectly are marked as such. This dissertation was not submitted in any other doctoral procedure. I declare under oath that I have produced my thesis independently and without any undue assistance by third parties under consideration of the “Principles for the Safeguarding of Good Scientific Practice at Heinrich-Heine Universität Düsseldorf”.

Düsseldorf den 29.03.2023

-

Acknowledgements

This work was done at the Institut für Physicalische Biologie der Heinrich Heine Universität Düsseldorf and at the Institute of Complex Systems des Forschungszentrum Jülich

I am deeply grateful to Dr. Manuel Etzkorn for granting me the opportunity to work in his research group, supervising my project, and providing exceptional guidance and support throughout all these years. My thanks are extended to Prof. Dr. Henrike Heise for her support during the final stages of this project.

I also would like to express my sincere gratitude to all my collaborators who have contributed to this work through their valuable input: Dr. Nils Lakomek, Dr. Boran Uluca, Dr. Shanta Elter, Celina Schulz, Achraf Ayadi, Lora Denson, Dr. Soumav Nath, Laetitia Heid, everyone who has been a part of the AG-Etzkorn, either currently or previously and Prof. Dr. Dieter Willbod for provide all the facilities and suitable environment.

-

Zusammenfassung

Membranproteine spielen eine wichtige Rolle in der Regulierung biologischer Prozesse und deren Untersuchung und Charakterisierung ist für das Verständnis von Zellfunktionen unerlässlich. Diese Proteine interagieren komplex mit anderen Proteinen und der Lipiddoppelschicht der Zellmembran, was für die Aufrechterhaltung der Zellfunktion wichtig ist. Ein tieferes Verständnis dieser Interaktionen ist auch für die Entwicklung neuer Medikamente und therapeutischer Maßnahmen, die die Aktivität dieser Proteine beeinflussen können, von großer Bedeutung. Pharmakologische Ansätze, die auf Membranproteine abzielen, haben das Potenzial, die Behandlung von vielen Krankheiten zu beeinflussen, weshalb dieser Bereich in der Biologie und Medizin hohe Priorität hat. Die Molekularbiologie hat in den letzten Jahren große Fortschritte gemacht, insbesondere bei der Herstellung und Reinigung rekombinanter Proteine. Die gleichzeitige Entwicklung biophysikalischer Techniken hat es ermöglicht, die Strukturen und Wechselwirkungen von Proteinen genauer zu untersuchen und wertvolle Informationen über ihr Verhalten und ihre Funktion zu erhalten. Eine der größten Herausforderungen bei der Untersuchung von Membranproteinen in vitro besteht jedoch darin, ein geeignetes mimetisches System zu finden, um sie zu untersuchen. Dies ist wichtig, da Lipiddoppelschichten und die Wechselwirkungen von Membranproteinen mit anderen Proteinen eine entscheidende Rolle bei der Aufrechterhaltung einer ordnungsgemäßen Zellfunktion spielen. Ein mimisches System muss die Eigenschaften der natürlichen Umgebung dieser Proteine so gut wie möglich nachahmen und sie stabil halten. Daher ist die Entwicklung von Membranimitaten nach wie vor ein wichtiges Forschungsgebiet. Diese Arbeit befasst sich mit der Entwicklung neuer Membranmimiken und der Untersuchung und Charakterisierung ausgewählter Proteine.

Das erste Kapitel dieser Arbeit gibt einen Überblick über die Zellmembran, einschließlich ihrer Eigenschaften und der Arten von Proteinen, mit denen sie verbunden ist. Außerdem werden die Techniken und Methoden zur Gewinnung rekombinanter Proteine erörtert.
Kapitel 2 gibt einen Überblick über die Vor- und Nachteile der wichtigsten Membranmimetika, die bei der Untersuchung von Membranproteinen verwendet werden, sowie über die biophysikalischen Techniken, die zur Charakterisierung von Proteinen, Protein-Protein- und Protein-Lipid-Wechselwirkungen eingesetzt werden.
Kapitel 3 konzentriert sich auf die Erforschung des potenziellen Einsatzes von Escin-Saponin bei der Bildung von Lipiddoppelschichten als neues Membranmimetikum, das verschiedene Größen von Doppelschichtsystemen erzeugt und somit eine geeignete Umgebung für die Untersuchung von Membranproteinen darstellt. Das Transmembranprotein Bacteriorhodopsin wurde erfolgreich

rekonstituiert, was die Gültigkeit dieses vorgeschlagenen neuen Membranmimetikums zur Nachahmung der nativen Umgebung von Membranproteinen und zur Förderung ihrer Stabilität beweist. Die erfolgreiche Rekonstitution von Bacteriorhodopsin zeigt, dass Aescin-Saponin das Potenzial hat, als wertvolles Werkzeug für die Untersuchung von Membranproteinen eingesetzt zu werden.

Kapitel 4 befasst sich mit den Schwierigkeiten bei der Charakterisierung von Protein-Membran-Wechselwirkungen und stellt einen neuartigen Ansatz vor, der dies ermöglicht. Die Studie verwendet das Protein α-Synuclein und POPG-Nanodiscs als Modellsysteme zur Untersuchung von Protein-Membran-Wechselwirkungen. Die Methode umfasst die Bewertung des Systems, das sowohl aus löslichen als auch aus membrangebundenen Proteinen im Gleichgewicht besteht. Der Schwerpunkt liegt dabei auf der selektiven Untersuchung von membranassoziierten Zuständen, d.h. von wenig besiedelten, aber wichtigen Zuständen, die sonst nur schwer zu charakterisieren wären. Dank dieser innovativen Methode ist es möglich, die Komplexität der Wechselwirkungen zwischen Proteinen und Membranen zu erforschen, die für das Verständnis verschiedener biologischer Prozesse und die Entwicklung wirksamer therapeutischer Strategien, z. B. bei neurodegenerativen Erkrankungen, von entscheidender Bedeutung sind.

Kapitel 5 präsentiert eine in-vitro-Untersuchung der Expression und Reinigung der Melanocortin Receptor Accessory Proteine 1 und 2 (MRAP1 und MRAP2). Beide sind essentielle transmembranäre Proteine, die an der Modulation der Aktivität mehrerer GPCRs beteiligt sind. Unsere Studie ist pionierhaft, da es das erste Mal ist, dass MRAP1 und MRAP2 erfolgreich in vitro exprimiert und gereinigt wurden, was eine weitere Charakterisierung und Analyse ihrer strukturellen und funktionellen Eigenschaften ermöglich.

In Kapitel 6 schließlich wird die Charakterisierung von MRAP1 und MRAP2 vorgestellt, die erstmals als eisenbindende Proteine identifiziert wurde

Summary

Membrane proteins play a crucial role in regulating various biological processes, which makes their study and characterization essential for advancing our understanding of cellular function. These proteins can interact with other proteins and the lipid bilayer of the cell membrane in complex ways, and these interactions are critical for maintaining proper cellular function.

A deeper understanding of these interactions is also crucial for developing new drugs and therapeutic interventions that can modulate the activity of these proteins. The development of pharmacological methods that target membrane proteins has the potential to significantly impact the treatment of a wide range of diseases, making this area of research a high priority in the biological and medical fields.

The field of molecular biology has seen significant advancements in recent years, particularly in the production and purification of recombinant proteins; The simultaneous development of biophysical techniques has allowed for a more detailed study of protein structures and interactions, providing valuable information about the behavior and function of these proteins. However, one of the biggest challenges in studying membrane proteins in vitro is find an appropriate mimetic system to study them. This is essential because the lipid bilayer and the interactions of membrane proteins with other proteins play a critical role in maintaining proper cellular function. A mimetic system should closely resemble the characteristics of the native environment of these proteins, keeping them stable. Therefore, the development of membrane mimetics continues to be a critical area of research. This work addresses the development of new membrane mimetics as well as the study and characterization of selected proteins.

The first chapter provides an overview of the cell membrane, including its characteristics and the types of proteins with which it is associated. In addition, the techniques and methodologies used to obtain recombinant proteins are discussed.

Chapter 2 provides a review of the advantages and disadvantages of the main membrane mimetics used in the studying membrane proteins, as well as of the biophysical techniques used to characterize proteins, protein-protein, and protein-lipid interactions.

Chapter 3 focuses on exploring the potential use of aescin saponin in the formation of lipid bilayers as a new membrane mimetic, generating different sizes of bilayer system making it a suitable environment for the study of membrane proteins. The transmembrane protein Bacteriorhodopsin was successfully reconstituted, thus proving the validity of this proposed new membrane mimetic to

mimic the native environment of membrane proteins and favor its stability. The successful reconstitution of Bacteriorhodopsin indicates that aescin saponin has the potential to be used as a valuable tool for the study of membrane proteins.

Chapter 4 aims to address the difficulties in characterizing protein-membrane interactions and presents a novel approach to do so. The study uses protein α-synuclein and POPG nanodiscs as model systems to investigate protein-membrane interactions. The method involves the evaluation of the system comprised of both soluble and membrane-bound proteins at equilibrium. Focusing on the selective study of membrane-associated states; sparsely populated but important states that would otherwise have been difficult to characterize. Thanks to this innovative method, it is possible to delve into the complexities of protein-membrane interactions, which are crucial for understanding various biological processes and developing effective therapeutic strategies, as in the case of neurodegenerative diseases.

Chapter 5 presents in vitro investigation of the expression and purification of Melanocortin Receptor Accessory Proteins 1 and 2 (MRAP1 and MRAP2). Both are essential transmembrane proteins involved in the modulation of the activity of several GPCRs. Our study is pioneering as it is the first time that MRAP1 and MRAP2 have been successfully expressed and purified in vitro allowing for further characterization and analysis of their structural and functional properties.

Finally, chapter 6 presents the characterization of MRAP1 and MRAP2, identifying them for the first time as iron-binding proteins

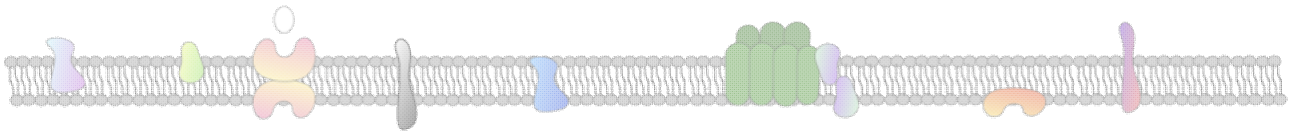

Contents

-

-

List of figures

Protein figures were created using protein imaging server [1]

-

List of abbreviations and acronyms

7-TM - Seven-transmembrane

αS- α-Synuclein

Bb- Biobeads

B-MeETOH- β-mercaptoethanol

BO - Bacteriohopsin

BR - Bacteriorhodopsin

CECF - Continuous-exchange cell-free expression

CMC - Critical micelle concentration

δ – Chemical shift

D-CF - Detergent-based cell-free expression

DLS – Dynamic light scattering

DMPC -1,2-dimyristoyl-sn-glycero-3-phosphocholine

DNP – Dynamic nuclear polarization

ECL - Extracellular loop

FM - Feeding mixture

FP - Fusion protein

GPCR - G protein-coupled receptors

GUV - giant unilamellar vesicle

HSQC -Heteronuclear Single Quantum Coherence

IMPs- Integral membrane proteins

IBs- Inclusion bodies

IMAC - Immobilized metal affinity

L-CF - Lipid-based cell-free expression

ICL- Intracellular loop

LUV - Large unilamellar vesicle

MCR- Melanocortin receptor

IMP- Integral membrane protein

M1- Melanocortin accessory protein1a

M2- Melanocortin accessory protein 2a

M22- construct M2-TEV-M2

MRAP- Melanocortin accessory protein

MSP- Membrane scaffold protein

ND- Nanodisc

NMR- Nuclear Magnetic Resonance

PAGE- Polyacrylamide gel electrophoresis

P-CF- Precipitate-based cell-free expression

PM- Purple membrane

PM- Purple membrane

POPG- 1-palmitoyl-2-oleoyl-sn-glycero-3-phospho-(1'-rac-glycerol)

PRE – Paramagnetic Relaxation Enhancement

RM - Reaction mixture

SEC - Size exclusion chromatography

SUV - Small unilamellar vesicle

TEV- Tobacco Etch Virus

TROSY - Transverse Relaxation Optimized Spectroscopy

Aims of the project

Membrane proteins (MP) represent 30% of the human genome; they play key roles in many essential life processes, including structural functions, signal transduction, cell-to-cell communication, energy production, immune responses, and even the regulation of transport between intracellular and extracellular compartments of a wide variety of drugs and compounds. Due to the significant role MPs play in physiology, it is important that their study and characterization are carried out in conditions as close as possible to the native lipid environments; this represents a great challenge due to the low expression rate in heterologous systems, low solubility, low stability, and their tendency to form aggregates.

To keep membrane proteins stable and functional during their study and characterization, it is essential to use membrane mimetics that resemble as reliably as possible the native environment of membrane proteins.

This work focuses on the development of new membrane mimetics as well as their feasibility in the study of proteins, for which the following objectives were set:

1) To evaluate the properties of Aescin-DMPC particles and confirm their ability to incorporate MPs. In addition, the study aims to investigate the effect of Aescin saponin concentration on the stability and size adjustment capacity of the bicelles.
2) To develop a methodology capable of selectively studying membrane-interacting proteins using nanodiscs as membrane mimetics.
3) Express for the first time in vitro melanocortin 1a and -2a receptor accessory proteins. To establish and optimize the expression conditions for their study, characterization, and reconstitution in different membrane mimetics.

The successful completion of these objectives will provide new and improved tools for studying and understanding the structure and function of membrane-interacting proteins.

Chapter 1: General introduction

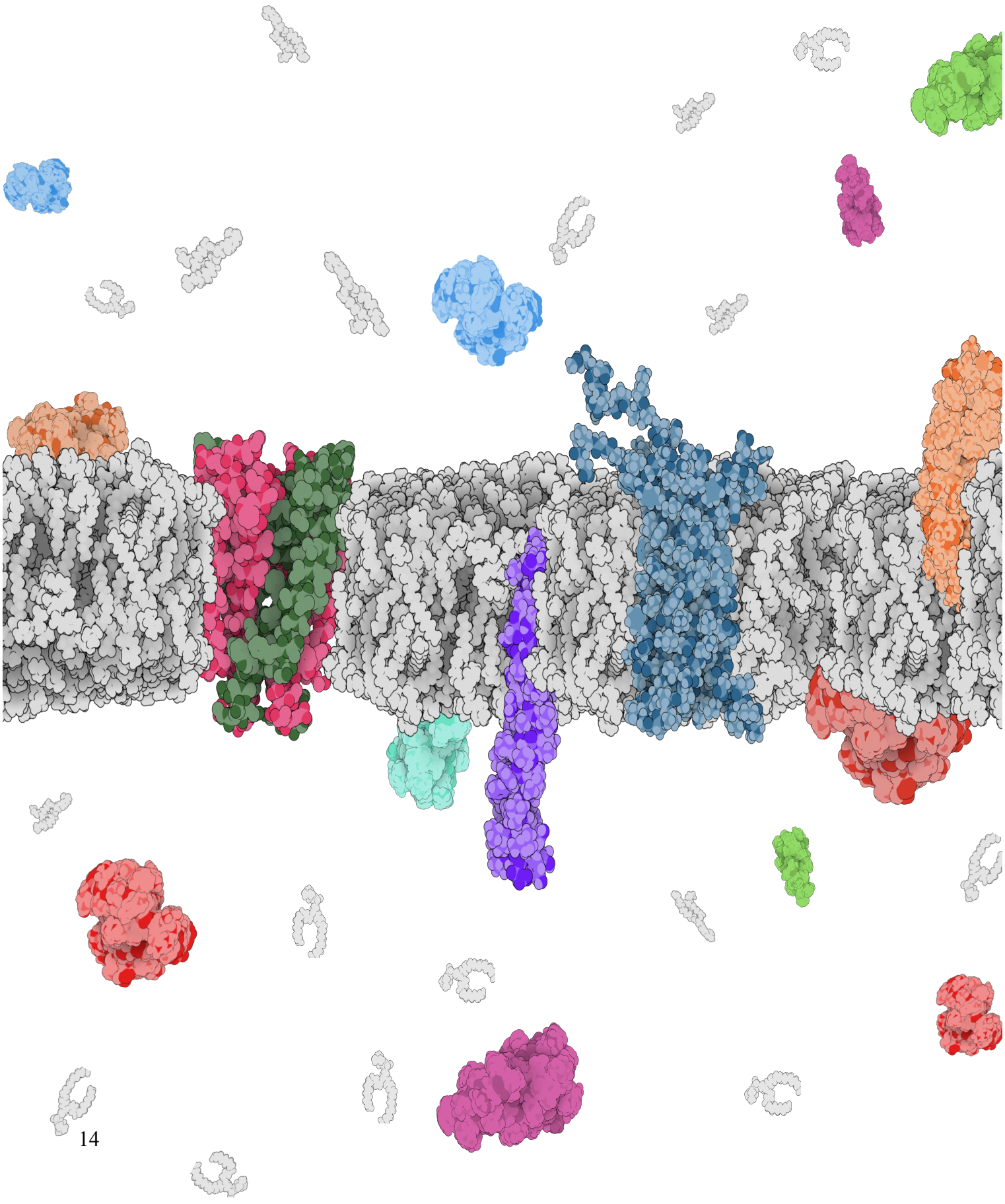

-

Chapter 1: General introduction

The cell membrane

Biological membranes are semi-permeable hydrophobic barriers essential for life. They keep cells protected by defining their boundaries and allowing differentiation between the cytosol and the extracellular medium [2]. These hydrophobic barriers restrict the diffusion of solutes from the external environment to the interior of the cell and vice versa. Additionally, in eukaryotic cells, membranes delimit sections with specific chemical conditions ideal for each organelle, as in the case of the mitochondria, the Golgi apparatus, and the cell nucleus [3], [4].
Cell membranes also regulate the transfer and storage of energy in the form of transmembrane ions and information since the assembly of various metabolic pathways takes place on their surface [5], [6].

Each membrane has its particular composition; however, all are fluid structures that have general structural characteristics in common. Membranes are mainly composed of lipids, carbohydrates, and membrane proteins [7].

Lipids

Lipids are the major component of biological membranes and the only structural elements of cells that adapt to external environmental conditions [8]. The membrane´s lipids are grouped by non-covalent interactions, forming double-layer structures of approximately 5 nm thickness in which lipid head groups are projected toward the aqueous environment while the acyl chains are facing the interior of the bilayer (figure 1.1). In addition to acting as physical barriers, cell membranes play a role as solvents, anchors, and activators of proteins and other membrane constituents, allowing their conformational stabilization and correct functionality [2], [9].

-

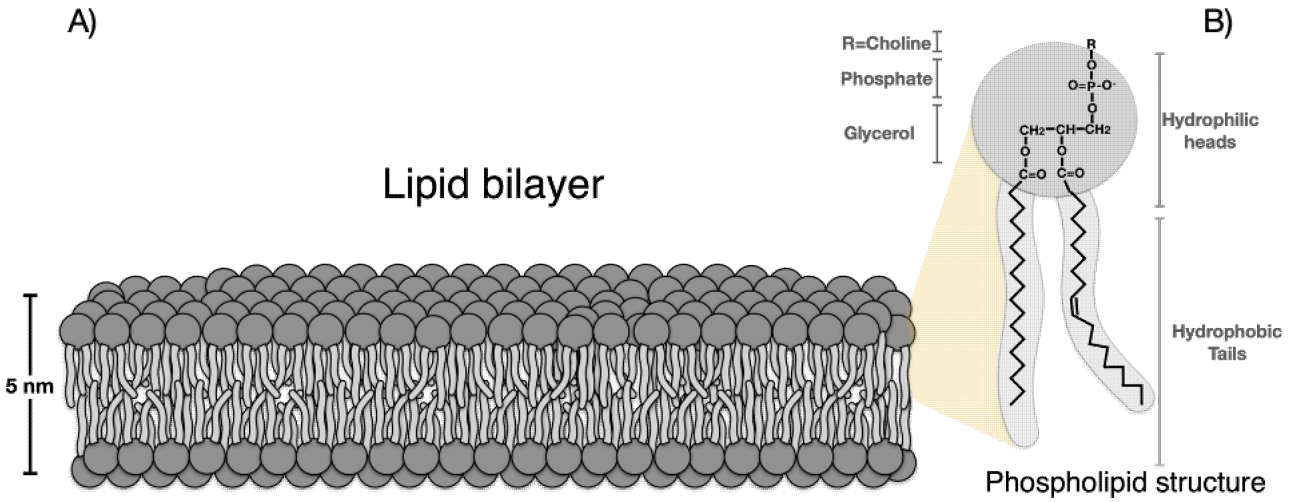

Figure 1.1 Three-dimensional schematic lipid bilayer. A) Lipid molecules generate a 5 nm thick bilayer structure in which, hydrophilic head groups are directed to the aqueous environment and hydrophobic tails are directed inside the membrane. B) Basic structure of an amphipathic phospholipid, which is a component of most cell membranes.

The lipids that constitute the membrane are classified into phospholipids, sterols, sphingolipids, and fatty acids. Although the lipid composition in the membrane varies depending on the type of organism, cell, organelle, and even differs depending on the monolayer region, in animal eukaryotic cells they are mainly composed of a mixture of phospholipids and cholesterol, while in plants, cholesterol is replaced by ergosterol, sitosterol, and lanosterol [8], [10].

Phospholipids are polymorphic molecules whose physicochemical properties, phase properties, and even membrane order are sensitive and dependent on conditions such as pH, temperature, pressure [5], [11].

Since lipids are the major component of the membrane, the characteristics of the latter depend, to a larger extent, on the properties of the phospholipids that compose it; for example, membranes composed mainly of lipids with long-chain saturated fatty acids are thicker and less fluid than those that contain a higher proportion of unsaturated lipids because lipid-lipid interactions are stronger in the former. In the same way, the size and charge of the lipid head group affect the natural curvature of the membrane (figure 1.2). These structural differences directly influence the functionality of the membrane, given that some specific lipids also participate in a wide variety of processes, which include the essential role of stabilization and activity of the second major component of biological membranes: proteins [9], [12].

-

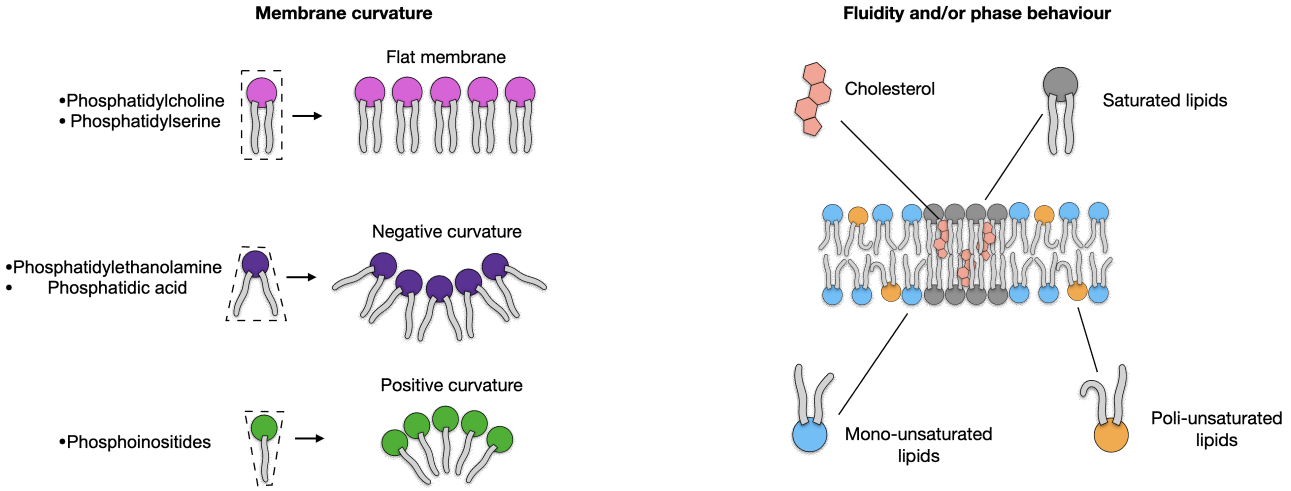

Figure 1.2 Membrane curvature. The curvature of the cell membrane could be regulated by the composition and nature of the lipids that compose it. The fluidity and phase behavior of the membrane will also be regulated by the composition of the phospholipids as well as other lipids such as cholesterol [9].

Proteins and membrane proteins

Proteins play key roles in many essential life processes, including structural functions, signal transduction, cell-to-cell communication, energy production, immune responses, and the regulation of transport between intracellular and extracellular compartments of a wide variety of drugs and compounds. Due to their influence on all these essential processes, it is not surprising that more than 60% of all FDA-approved drugs target membrane proteins (MPs). Enzymes, transporters, ion channels, and receptors are the main drug targets [13]–[15].

Membrane proteins are amphiphilic proteins located in the cell membrane, as their name suggests. They represent 30% of the human genome and constitute the second main component of cell membranes after lipids. They can be classified into two large groups, depending on the interaction they have with the biological membrane: peripheral and integral membrane proteins [13], [14].

-

Peripheral membrane proteins

Peripheral membrane proteins interact superficially with the cell membrane; that is, they never cross the hydrophobic side of the membrane. Hence, they interact exclusively with the hydrophilic sides of the lipid bilayer, either inside or outside the cell. Peripheral proteins interact with other membrane proteins through non-covalent interactions [16]. This interaction could be transient due to a conformational change of a soluble protein by exposing a hydrophobic patch region or permanent due to the presence of a lipid anchor covalently bound to it. These protein-protein interactions can be easily altered by extreme changes in both pH and ionic strength [3]. Membrane-protein interactions can be governed, in this case, through a lipid anchor formed by fatty acid chains or prenyl groups [17].

Integral membrane proteins

Integral membrane proteins (IMPs) are amphipathic proteins that have one or more hydrophobic regions in their structure. These regions span the bilayer of the cell membrane, interacting with the hydrophobic tails of phospholipids, while its hydrophilic regions are exposed on both sides of the cell membrane [3], [18].

IMPs can be classified according to the number of times they cross the lipid bilayer. Proteins that cross the membrane only once are called simple transmembrane proteins, and multipass transmembrane proteins are those in which several fragments of their structure cross the hydrophobic core of the membrane. The membrane-spanning fragments made up mostly of non-polar amino acids are called transmembrane domains (TMDs). Transmembrane proteins generally have well-defined characteristics and functions in their cytosolic and non-cytosolic domains so that when inserted into the lipid bilayer, they do so with a specific and asymmetric orientation [3]. However, as mentioned below, in this work, we study a family of proteins with an unusual topology in which their intracellular and extracellular domains can switch [19].

Approximately 30% of the encoded proteins of organisms in all living kingdoms are IMPs [20]. Numerous inherited diseases are associated with deletions, point mutations, overexpression, or misassembly of membrane proteins [21], [22]. Due to the significant

role, IMPs play in physiology, it is essential that their study and characterization must be carried out in certain conditions that resemble, as close as possible, the native lipid environments [20].

Despite their undeniable importance, the study of IMPs is limited compared to soluble proteins. Even today, IMPs are a big challenge for researchers for reasons such as their low expression rate in heterologous systems, low solubility, low stability, and their tendency to form aggregates [20], [23].

Due to the highly hydrophobic environment in the core of the lipid membrane, the amino acids that form the transmembrane region(s) of IMPs acquire specific structures to stabilize their backbones. One way to do this is to maximize their interaction by forming hydrogen bonds with each other; this same structural arrangement occurs when there is a longitudinal difference between the TMD and the thickness of the lipid bilayer, resulting in the formation of the most popular secondary structure element seen in transmembrane segments: the alpha helix [24]. However, this conformational arrangement is not the only one that can stabilize TMD within the hydrophobic environment of the lipid bilayer. Another alternative to stabilize the backbone in the transmembrane region is the formation of several beta-sheets arranged in a compact structure called the β-barrel (figure1.3) [3], [13], [25].

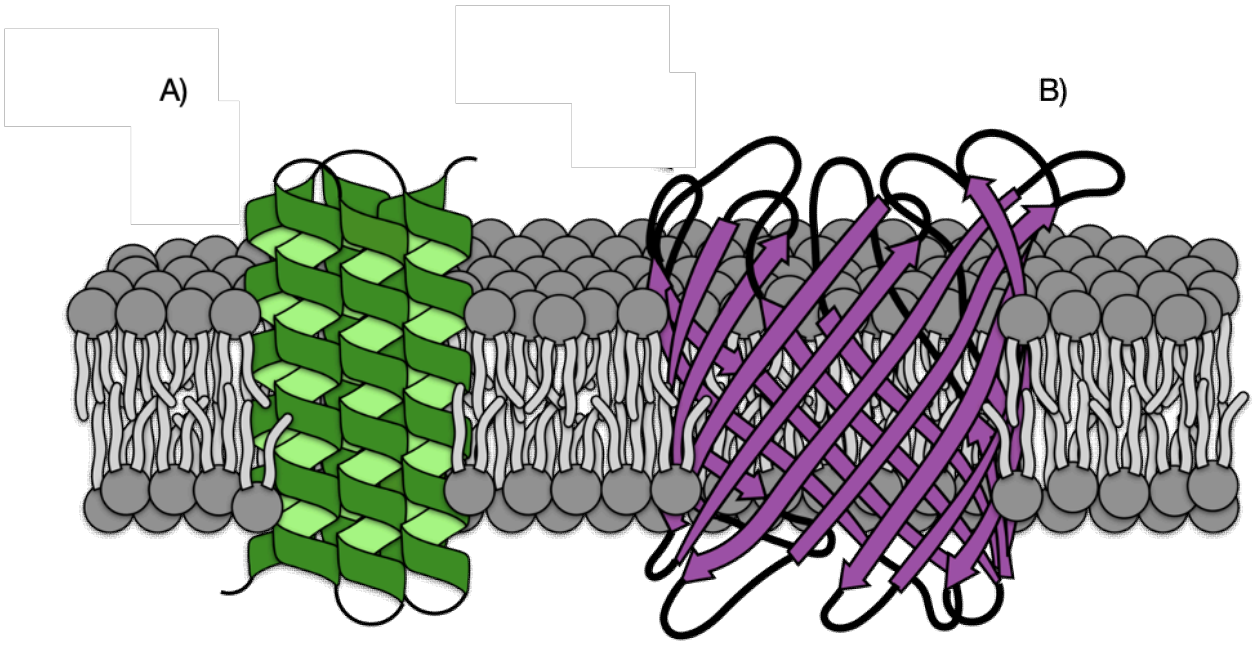

Figure 1.3 Most common structural motifs in transmembrane proteins. A) The alpha helix and B) beta barrel structures stabilize amino acids in the TM domain.

-

Membrane protein topology

TMDs do not only play a fundamental role in stabilizing proteins in the membrane but also direct the insertion and orientation that proteins adopt when inserted into the membrane, among other roles.

The topology of a membrane protein is usually determined when inserted into the membrane for the first time. Until now, the distribution of residues that compose the different domains of each protein is the most useful parameter for topological prediction [26]. According to statistical studies, it was found that hydrophobic residues (Ala, Ile, Val, and Leu) are present in greater quantity in the middle of the membrane, while in the lipid-water interface regions, there are abundant Tyr and Trp aromatic residues (but not Phe). The transmembrane regions, of course, are poor in charged and polar residues [27]. In contrast, it has been noted that the cytoplasmic regions are 25% richer in positively charged residues (Arg and Lys) than the rest of the protein domains. This guide is known as The Positive Inside Rule [28]–[30].

In addition to this, electrostatic and van der Waals interactions between TMD residues and the lipids that constitute the bilayers can also influence the topology that characterizes each transmembrane protein. According to their orientation and the mechanism of insertion in the membrane, transmembrane proteins can be classified into four groups (figure 1.4):

Membrane proteins Type I are oriented with the exoplasmic N-term and the cytoplasmic C-term (N_{out}/C_{in}) inserted via an N-terminal cleavable signal sequence of 7-15 a polar residue and another fragment of 20 hydrophobic residues, that acts as an anchor. The LDL receptor is an example of a protein with this topology.

Type II membrane proteins, unlike type I, cross the bilayer in the opposite direction (N_{in}/C_{out}) and lack a cleavage site. The transferrin receptor has this type of topology [31].

Type III proteins acquire the orientation (N_{out}/C_{in}) like those of type I. However, the proteins that compose type III also lack the cleavable sequence. Cytochrome P-450 has this topology.

-

Types I, II, and III are inserted by the same mechanism, which involves the SRP receptor. The last group consists of proteins that are found almost entirely on the cytoplasmic side, linked to the lipid bilayer only by an anchor located at its C-terminus. An example of this latter group is synaptobrevin [12], [31].

In the case of multipass transmembrane proteins, each TMD can vary individually, and their topologies are highly diverse. It has been shown that the topology of membrane proteins can be dynamic, reorienting themselves in response to drastic changes in membrane lipid composition [30].

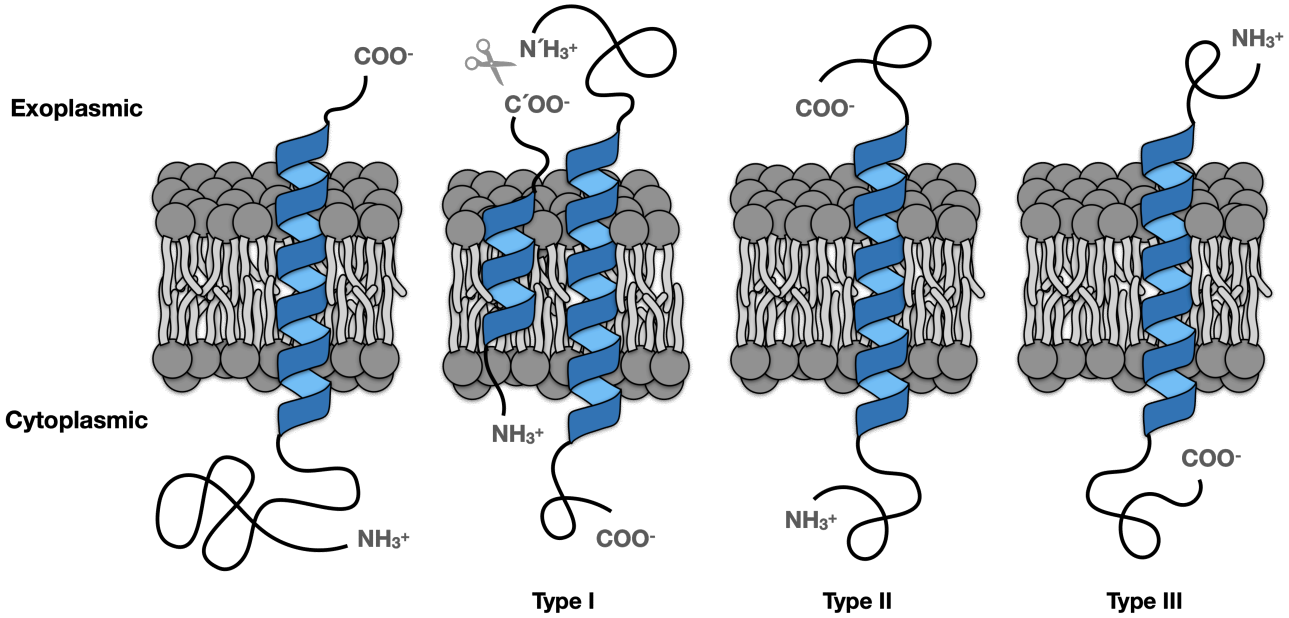

Figure 1.4 Membrane protein topology. Transmembrane proteins can be classified into four types based on their orientation and mechanism of insertion into the membrane [31].

Of all the topological variations, the most significant is that of certain proteins with dual topology. This topology type is associated with the conservation of a domain of basic residues (LKAHKYS) in a position close to TMD. Dual topology proteins do not have a defined orientation and can insert in either N_{in}/C_{out} or N_{out}/C_{in} orientations or even acquire structures with parallel or antiparallel domains.

TMDs not only have a fundamental role in the stabilization, insertion, orientation, and oligomerization of proteins in the membrane through promoting protein-protein interactions

(PPI) within the biological membrane, but they are also responsible for promoting lipids-protein interactions [13], [25].

Molecular interactions between lipids and proteins

As mentioned, biological membranes are fluid structures whose conformational molecules are distributed asymmetrically on each side of the bilayer. The lipid molecules that conform to biological membranes may or may not interact with membrane-associated proteins. These interactions, whether intracellular, transmembrane, or extracellular, may be specific, nonspecific, or simply nonexistent [12].

Lipid molecules that do not interact with proteins are called bulk lipids; an example of this type of lipid is phosphatidylcholine. Nonspecific interactions between lipid and protein molecules generally occur with the lipids surrounding integral proteins. These lipids are called "Annular lipids" since they form a ring that surrounds the protein, acting as a "solvent" for the transmembrane protein.
Due to the lack of specific interactions, these molecules are easily interchangeable with bulk lipids. On the other hand, the specific interactions between proteins and the so-called non-annular lipids can be of the electrostatic type, van der Waals interactions, hydrogen bonds, etc. Lipids such as cholesterol and sphingolipids are typical examples of non-annular lipids; lipids that specifically interact and modify protein activity through the generation of conformational changes (figure1.5) [12].

-

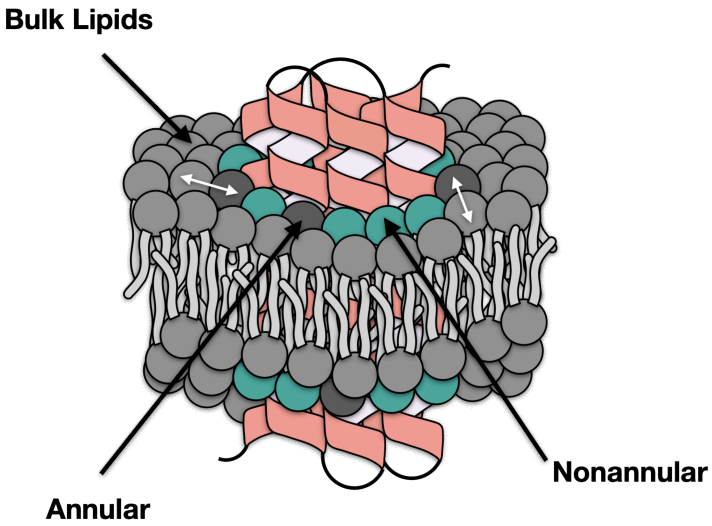

Figure 1.5 Lipid classification according to their interaction with membrane proteins. The bulk lipids do not interact with proteins; Annular lipids interact nonspecifically with surrounding proteins; these lipids are interchangeable with bulk lipids. Non-annular lipids have specific lipid-protein interactions and are not interchangeable [12].

The most straightforward mechanism governing protein-lipid interactions is found in electrostatic interactions, which happen through complementary electrical charges between phospholipids and the protein domain with which they interact. Some phospholipids, such as phosphatidylserine (PS), have a net negative charge at physiological pH and hence are predominantly distributed in the inner lamina of the membrane. On the other hand, and following the positive interior rule, the cytoplasmic domains of transmembrane proteins are rich in lysine and/or arginine cationic motifs, capable of interacting with the negative charges mainly of the PS head groups; however, it has also been shown that the acyl chains that anchor the phospholipid in the membrane are essential for interactions [12]. Such is the case for the protein associated with Parkinson's disease, α-synuclein, which forms electrostatic interactions between its lysine-rich helical cationic motif and those phospholipids whose net charge is negative, although this interaction is highly dependent on acyl chains [12], [21], [32], [33].

Cholesterol interaction is an example of specific transmembrane interactions. The mechanism of this interaction is governed by hydrophobic interactions, van der Waals interactions, CH–π stacking, and hydrogen bonds between the domains called “CRAC and CARC” of the protein. These motives are formed by either one valine or leucine in the N-terminal domain, an aromatic residue in the transmembrane region, and one arginine or lysine located in the C-terminal domain that these residues interact with the isooctyl chain

of the sterol, with some sterane ring and with the OH group of the sterol group respectively [12]. In this way, membrane proteins type I, III, and GPCR TM-1, 3, 5, and 7 domains interact with cholesterol molecules found on the inner side of the membrane and type II and GPCR TM-1 domains. 2, 4, and 6 interact with cholesterol bound in the outer layer of the biological membrane [12].

Another example of specific protein-lipid interaction is the one that occurs between sphingolipids and proteins that contain in their structure a symmetrical motif whose aromatic center is surrounded by acidic or basic amino acids (SBD motif). Hydrophobic interactions between the SBD motif and the polar regions of lipids occur, for example, in amyloid proteins, membrane receptors, and viral proteins, among others.

The chaperone effect of lipids (lipo chaperones or lipid cofactors) is another example of highly relevant lipid-protein interaction. This effect is generated by lipid molecules whose electrostatic interactions with charged residues (generally lysine) in the N-terminal domain of proteins promote correct folding into functional units. This process occurs just after a protein is inserted into the lipid bilayer and is known as lipid-dependent renaturation. It generally occurs with highly specific lipids such as sphingolipids PE and phosphatidylserine (PS), also found in non-annular positions. Classic examples of this type of interaction that promotes a conformational adjustment are observed between amyloid proteins such as a-synuclein or Synaptobrevin, which interact with the charged lipids that form the membrane of brain cells. They transform their disordered structure acquiring a helical structure. Therefore, if the lipid composition of the membranes of these cells changes, as has been observed during aging, so will the membrane-protein interactions, which could trigger a wide variety of neurological pathologies [12], [34].

G protein-coupled receptors

The guanine nucleotide-binding protein (G protein)-coupled receptor (GPCR) is one of the largest families of integral membrane proteins in the human genome [35], [36] and is also present in a wide range of species. GPCRs have control over many critical physiological processes, such as intracellular responses to extracellular stimuli, among many others.

The activity of GPCRs is regulated by their interaction with different types of ligands as neurotransmitters, ions, hormones, peptides, and proteins. The binding of these ligands to receptors triggers a heterotrimeric G-protein response on the cytosolic side, which in turn generates a second messenger system modulated by the activity of various enzymes.

-

The main structural characteristic of GPCRs is that they have conserved the extracellular N-terminal domain, the heptahelical (TM) transmembrane domain, three extracellular and three intracellular loops, and the cytoplasmic C-terminal domain, which contains serine residues that are the sites where the ligand-induced phosphorylation occurs (figure 1.6) [36]–[38].

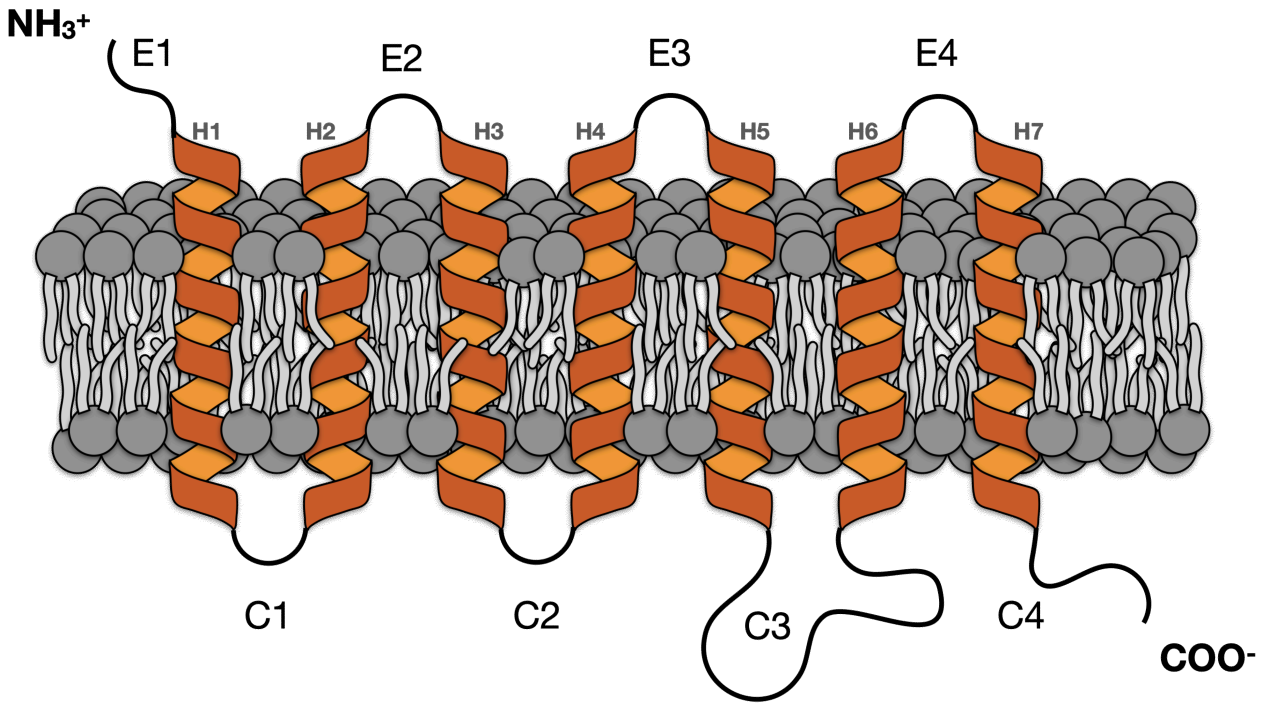

Figure 1.6 General scheme of GPCR structure. All GPCR superfamily members are characterized by having an extracellular N-terminal domain, a heptahelical transmembrane domain, three extracellular- (E) and three intracellular loops (C) and the cytoplasmic C-terminal domain.

GPCRs can be classified into different systems. The most widely used system is based on amino acid sequence homology and functional similarity to classify the GPCR superfamily into three main families (A, B, C) [37] and three other mini types, for a total of six families [39], [40]:

Class A (rhodopsin-like superfamily, RLF) is the largest subfamily of GPCR receptors. These receptors are involved in response to hormones, neuropeptides, pheromones, glycoproteins, and sensory stimuli such as light, odor, and taste. Protein members of this class have two conserved structural motifs. The NPXXY motif and the DRY (Asp-Arg-Tyr)

motif are located in the third transmembrane domain in which the Arg is highly conserved in all the receptors of this subfamily [41], [42].

Class B (secretin receptor family, SRF). Members of this family play a key role in hormonal homeostasis. They are characterized by having an N-terminal domain of about 120 residues, rich in cysteines, and highly conserved [43]. The dactyloscopic motifs of the family are the REY and VAVLY motifs. Members of this class are activated by peptides such as glucagon and glucagon-like peptide 1 (GLP-1), family B and A receptors, which are important drug targets due to their influence on many human disorders and diseases such as neurodegeneration, obesity, diabetes, osteoporosis, etc. [44],[43], [45], [46].

Class C (metabotropic glutamate/pheromone receptors), the receptors that form this family have small molecules such as amino acids, ions, and sugar molecules as endogenous agonists. Examples of receptors belonging to this family are aminobutyric acid receptor B (GABAB) [47], pheromone receptors, calcium-sensitive receptors (CaR), and the metabotropic glutamate receptor (mGlu). The main structural feature of this family of receptors is the presence of an unusually large N-terminal domain (500-600 residues) and its orthosteric site [36], [40], [47].

Class D (fungal mating pheromone receptors). These receptors are found exclusively in fungi, where they regulate nutrient sensing, fungal metabolism, sexual development, virulence, and mycotoxin production. Depending on their structural similarity, they can be classified into up to ten categories. All of them have weak similarities to mammalian receptors; however, they are of great interest for research aimed at the development of new antifungal drugs [48], [49].

Class E (cyclic AMP receptors). Cyclic adenosine monophosphate receptors. These receptors are unique to Dictyostelium. Its main functions are associated with the regulation of cytodifferentiation and aggregation of individual amoebas in a multicellular organism, as well as the expression of a large number of developmental regulatory genes [50], [51].

The F class (Frizzled/Smoothened receptors) consists of SMO and FZD receptors, which play a critical role in embryonic development, body conformation, and the maintenance and regeneration of adult stem cells. FZDs and SMOs are recognized as oncoproteins and play relevant roles in a wide variety of cancer types and other disorders, such as fibrosis

neurodegeneration. Its inhibitory ligands are currently under clinical investigation to develop new tumor suppressor agents [38], [52], [53].
The activity of G protein-coupled receptors (GPCRs) is so crucial that more than 33% of drugs target proteins belonging to this superfamily to promote or inhibit their activities [13].

Bacteriorhodopsin

Bacteriorhodopsin (BR) is a 27 kDa integral membrane protein. BR is part of the plasma membrane of Halobacterium salinarum [54], where it is grouped into trimers to form a network of hexagonal structures called the purple membrane (PM). BR was the first membrane protein to be structurally characterized and thus generated the classification of membrane proteins; the first and largest group (class A) takes it as a model. As mentioned above, essential proteins such as G protein-coupled receptors (GPCR) also belong to this class. Its structure is composed of seven transmembrane helixes (A-G) with a core containing a retinal molecule covalently bound to the G helix through the 216 Lys. The BR apoprotein is called bacteriodopsin (bO) [55]. It acts as a proton pump that is fueled by light: the small green-light-induced movements of its transmembrane helixes attract protons that unidirectionally translocate towards the exterior of the membrane against an electrochemical gradient (500-650 nm) [30], [56]. Afterward, this gradient is employed by DNA synthase to produce ATP.
BR has been the subject of multiple investigations since its stability and biophysical properties (such as molecular size, topology, and its characteristic purple color when in its functional conformation) make it the ideal model for structural, interaction, and functional studies of both membrane proteins and in the development of membrane mimetics that do not alter the native properties of the proteins under study [57], [58].

Membrane protein expression (*E. coli*)

Undoubtedly, the first aspect on which attention should be focused when researching a membrane protein is to find the most efficient way to obtain enough of the protein of interest for its subsequent functional, structural, or interactional characterization. In vitro, structural and functional studies of membrane proteins are a challenge due to the aforementioned intrinsic complexity, particularly in terms of expression and purification. The abundance of membrane proteins in their natural source is often very low in yield, so

heterologous expression is generally used as a more helpful tool to obtain them [23], [59]–[61].

The first step to follow is to choose the most appropriate system for MP expression, depending on the needs and resources of the research. Some of the most used systems are bacterial, eukaryotic, and cell-free. The main aspects to consider are the origin of the target protein, the existence of special codons, and post-translational modifications.

The *Escherichia coli* bacteria is the most widely used heterologous system for the overexpression of soluble and membrane proteins. It is a widely known system and, at least in theory, very simple to work with. Among these expression systems, the main advantages are their rapid growth, known culture conditions, low economic cost, and simple and robust protocols. Added to these, the possibility of producing genetically modified variants to enrich and facilitate the protein´s study by adding labels to improve its solubility, facilitate purification or promote the co-expression of post-translational machinery has positioned its popularity above other more expensive and slower systems such as yeast, fungi and eukaryotic cells of insects or mammals [60], [62].

The main disadvantage of using this system is the accumulation of proteins expressed in inclusion bodies, which may lead to low protein yield.

Within the *E. coli* bacterial system, there is a great variety of strains whose characteristics could greatly help to obtain MP. The E. coli BL21 (DE3) strain, for example, is the most widely used in the expression of recombinant proteins due to its economic cost, rapid replication, biological safety, and ease of genetic manipulation.

E. coli strains C43 (DE3) and C41 (DE3) are specially designed for the overexpression of eukaryotic membrane proteins [59], [63].

The *Rosetta* strain is used when the genetic sequence of the protein to be expressed has a high frequency of codons that are rarely used in *E. coli* but are commonly used in eukaryotic cells, especially the codons AGG, AGA, AUA, CUA, CCC, and GGA. Using this strain, a better expression yield can be obtained, avoiding changes in the translation framework or poor incorporation of amino acids [64].

To avoid these problems associated with differences in codon usage between organisms, it is recommended, in addition to using the *Rosetta* strain, to perform codon optimization of the target gene sequence for its use in the host organism without altering the amino acid sequence [64].

Despite the great advantages of using the bacterial system, experimentally, the overexpression of membrane proteins in this heterologous system can be toxic and, on occasions, lethal for the cells in which they are expressed; this translates into low or null productive yields, the generation of inclusion bodies from protein aggregates, possible contamination or degradation due to proteases from the host cell and misfolding of the target protein, which could lead to losing native activity [62] [65].

Cell-free expression

Cell-free expression (CF) systems do not involve the use of living cells and are another alternative to produce membrane proteins that are difficult to express, especially when MP expression produces toxicity to host cells [66], [67]. These systems commonly use cell extracts from bacteria, eukaryotic cells and wheat germ [68]; however, they can be obtained from any cells [69]. They all contain the active components of the cellular transcription/translation machinery, such as ribosomes, aminoacyl-tRNA synthetases and other essential translation factors [66], [70]. The use of this expression system has the great advantages of eliminating problems related to cell toxicity presented during recombinant expression, the formation of inclusion bodies, aggregation and degradation, its generally short reaction times and the possibility of adding substances, such as chaperones that favor the correct folding of the MP [70], [71]. Using cell-free system, proteins can be expressed as a precipitate (P-CF) or soluble using hydrophobic enviroments, such as detergents (D-CF), lipids (L-CF), or nanodiscs [44], [70], [71]. Cell-free reactions are generally performed in two types of formats: one-compartment or two-compartment, the latter also called continuous exchange (CECF). The one-compartment system consists of a reaction mixture (RM) which contains enzymes, plasmid DNA, transfer RNA and the ribosomes. In this type of system the reaction time is typically in the rang from 0.5 to 2 h, after which the reaction is stopped by the accumulation of inhibiting reaction products, such as inorganics phosphates [72]–[74]. The CECF format is usually more efficient than one-compartment system. since it consists of a feeding mixture (FM) containing low molecular weight precursors, energy sources and amino acids, separated by a semi-permeable membrane from a tank containing the reaction mixture (RM). This system of constant exchange between the RM and FM compartments favors the continuous supply of substrates and the elimination of residues that can inhibit the protein synthesis reaction, its ideal volume ratio RM:FM is from 1:10 to 1:30. This system allows

the extention of reaction time up to 12-24 hours. Using CFCE it is possible to achieve yields of up to milligrams of protein expressed in 1 mL of reaction [59], [71].

Successful protein production by cell-free systems crucially depends on the correct preparation and quality of the cell extract [75]. As mentioned above, cell extracts can be obtained from any living organism. The extracts obtained from *E. coli* cells are the most frequently used and are obtained from varius strains. However, it has been reported that the use of strains such as *E. coli K-12* strains *A19* or *D10* can promote substantial improvements in expression yields [76], [77] because these strains are deficient in ribonuclease Io, which helps stabilize mRNA during transcription/translation [71].

Once the membrane protein of interest has been synthesized, the next step is its purification and characterization. To know and understand its mechanisms of action, it is essential to previously carry out its structural characterization as well as to know how it interacts with other molecules associated with the cell membrane, such as proteins, nucleic acids, and, of course, lipids.
To keep membrane proteins stable and functional during purification and characterization processes, a wide variety of biomimetic systems have been developed that attempt to resemble as reliably as possible the native conditions of membrane proteins. Each of these systems has its strengths and weaknesses as membrane mimetics, and the choice of the most appropriate system will depend on the protein to be studied and the question to be answered with each investigation [57]. In general, a good membrane mimetic should be stable and resemble as closely as possible the specific native environment of each protein. The most widely used systems include detergent micelles, lipid-detergent bicelles, amphipathic polymers (amphipols), and nanodiscs [78].

Therefore, in the following chapter, a general review of the most used membrane mimetics and the biophysical and biochemical methods to characterize protein-membrane interactions both in vivo and in vitro will be carried out.

Technics

Dynamic Light Scattering (DLS)

Dynamic Light Scattering (also called Photon Correlation Spectroscopy (PCS) or Quasi-Elastic Light Scattering) is a noninvasive technique used to measure the mean particle

size and diameter distribution of nanometer-sized particles suspended in a fluid in which the intensity of scattered light is measured through particles that are moving freely due to random collisions with the surrounding solvent molecules (Brownian motion). The DLS correlates the fluctuation of the intensity of the scattered light as a function of time with the Brownian motion, and this, in turn, with the size of the particles [79].

When a monochromatic light beam passes through the sample, the particles scatter the light independently. The intensity of this scattered light will be the sum of the light scattered by each particle. Since the light-scattering particles are in random motion, the intensity of the scattered light will fluctuate in the same way as a function of time. Using the Stokes-Einstein model, it is possible to correlate the intensity fluctuation of scattered light as a function of time with the Brownian motion of the particles. This movement depends on the temperature of the solution and the friction experienced by the particles as they move. The friction is proportional to both the solution's viscosity and the particle's radius. A sample's radius can therefore be related to its dynamic scattering of light [80].

DLS is a widely used technique to study protein homogeneity, the dynamics of protein aggregation, protein-protein, protein-nucleic acid, and protein-membrane interaction studies, as well as to test the stability of these systems over time. The main advantages of DLS are that it is a non-invasive method, does not require a large amount of sample, and the measurement times are short. On the other hand, some of its main disadvantages to taking into account are: 1) its low resolution, as it is often not possible to distinguish between molecules such as monomers and dimers 2) its high sensitivity to temperature variations, 3) the fact that the presence of large aggregates even if in a tiny proportion, will affect the measurement very significantly, since the intensity of scattering depends on the sixth power of the size of the macromolecules [79].

Nuclear Magnetic Resonance (NMR)

Understanding how proteins work is not easy, and it is even more complicated when studying such challenging systems as membrane proteins (IMPs). Due to their complexity, it is not surprising that the structures of IMP constitute only a small fraction of all the structures reported in the PDB (less than 4%), despite they constituted more than 50% of therapeutic drug targets [81].

Nowadays, X-ray crystallography and CryoEM are the common techniques for structural studies of membrane proteins; despite the difficulty involved in obtaining protein crystals,

crystallography is, so far, the most popular technique to have structures in atomic resolution. On the other hand, CryoEM has the advantage of the simplicity involved in sample preparation and is progressively reaching higher resolutions. However, although these techniques provide a clear image of the structures, dynamic information is still missing. The dynamic governs the functionality of proteins. While solution NMR is a technique limited by protein size, it is potentially the best tool for studying dynamics along with structure as well as interactions with other molecules, especially for systems that are difficult to crystallize or too small to measure in electron microscopy [81], [82].

Solution NMR

Nuclear magnetic resonance is a biophysical tool that takes advantage of the quantum mechanical properties of nuclei, obtaining details of the protein at atomic resolution. Under terrestrial conditions, the possible orientations associated with the magnetic moment of the nuclei are energetically equivalent, generating a set of degenerate states. If we apply an external magnetic field, the magnetic moments align and acquire a particular energy value, generating different population states. The energy difference between these states is determined by $\Delta E = \hbar\gamma B0$, where $\hbar$ is Planck's constant divided by 2π, is the gyromagnetic constant of the nucleus in question, and B0 is the magnetic field. This difference between the energy states is directly proportional to the external magnetic field, and its magnitude is in the radio frequency range [83].

One of the most important spectroscopic parameters is the chemical shift; for decades, spectroscopists have used chemical shift to map the covalent structure of organic molecules. The chemical shift is a robust parameter with great sensitivity to the geometry and electronegativity of atoms in molecules. This has allowed the development of simple rules and tables widely used for the structural analysis of small molecules. In the case of proteins, the panorama becomes extremely complex when moving to hundreds or thousands of atoms with practically uniform covalent structures distributed in the same 20 amino acids, differentiated by subtle but identifiable variations caused by their secondary or tertiary structure in the protein [84], [85].

The chemical shifts most frequently measured in proteins are isotropic chemical shifts (obtained in samples in the solution and represent a value averaged over time) corresponding to the ^{1}H, ^{13}C, and ^{15}N isotopes. Thanks to the accumulation of assigned

proteins, databases have been developed that not only helped to understand the relationship between chemical shifts and secondary structure but also helped the development of better protocols for the identification of secondary structures based on chemical shifts [86], [87]. It was generally observed that, for example, the α protons show a clear up field trend in the formation of helices and a clear downfield trend in the β sheets. In the same way, similar behaviors were observed in other nuclei, and the method called chemical shift Index (CSI) was developed. To quickly determine the secondary structure of proteins from chemical shifts [88]. This method uses a set of upper and lower thresholds to convert residue-specific secondary chemical shifts from backbone nuclei into three indices corresponding to the three states of secondary structure. Secondary chemical changes that exceed the upper threshold receive an index of 1, while those that fall below the lower threshold receive an index of -1. Finally, secondary changes with values between the upper and lower thresholds receive an index of 0. This type of analysis shows a bar graph indicating the start and end of α-helices, β-sheets, and random coil regions.

In addition to giving us a very approximate reference on the secondary structure, the chemical shift is also a key parameter in the study of protein interactions, whether they are interactions with other proteins or other types of molecules such as carbohydrates, nucleic acids, lipids, and organic or inorganic molecules. As mentioned above, the chemical environment of the atoms defines this parameter. Therefore, the atoms that interact, or in the case of proteins, the amino acids involved in said interaction, will experience a chemical environment different from that of the free state; therefore, the chemical shift values for the residues involved will be perturbed thus changing their chemical shift value [89].

TROSY

Although the size of proteins is one of the main limitations of NMR, the advent of multidimensional NMR, combined with isotopic labeling of proteins using active isotopes in NMR (^{15}N, ^{13}C, and ^{2}H), has allowed detailed structural and dynamic analyzes of soluble proteins with molecular weights up to 25 kDa [82], [90], [91]. However, NMR studies of proteins larger than 30 kDa, such as IMPs, are complicated by rapid signal decay due to the slow molecular tumbling of proteins within a membrane-like environment, producing spectra with low resolution and low signal-to-noise ratio.

The introduction of NMR methods based on optimized transverse relaxation spectroscopy (TROSY) opened new possibilities for the structural determination of larger biological macromolecules around 900 kDa [92]. The drawback of large NMR molecules is that they have longer rotational correlation times and, consequently, shorter transverse relaxation times (T2). Hence its signal decays faster and generates a wide line width and low resolution. The TROSY experiment is based on the fact that cross-relaxation resulting from the interference of dipole-dipole interaction (DD) and chemical shift anisotropy (CSA) results in much lower transverse relaxation rates at high fields. In a system of two coupled spins, as is the case with ^{15}N–^{1}H, this allows for much larger NMR studies of proteins and nucleic acids. This experiment requires high magnetic fields to achieve the necessary balance between the CSA and DD relaxation mechanisms [93].

Dynamic Nuclear Polarization (DNP)

One of the main problems that NMR has is its low detection sensitivity, which is related to the relative population difference of the Zeeman levels, which is extremely small but modifiable with hyperpolarization processes. In the last two decades, dynamic nuclear polarization (DNP) has become a key method to increase the sensitivity of NMR spectroscopy. This technique is based on the transfer of polarization between spins of unpaired electrons to surrounding nuclei. Samples are usually labeled with stable radicals called polarizing agents whose unpaired electrons are saturated by continuous microwave (MW) irradiation. This is achieved by using a gyrotron that operates in the required frequency range (140–600 GHz) and produces high-power microwaves increasing the sensitivity between 10 and 300 times in solid-state NMR [94], [95].

Chapter 2: Membrane mimetics

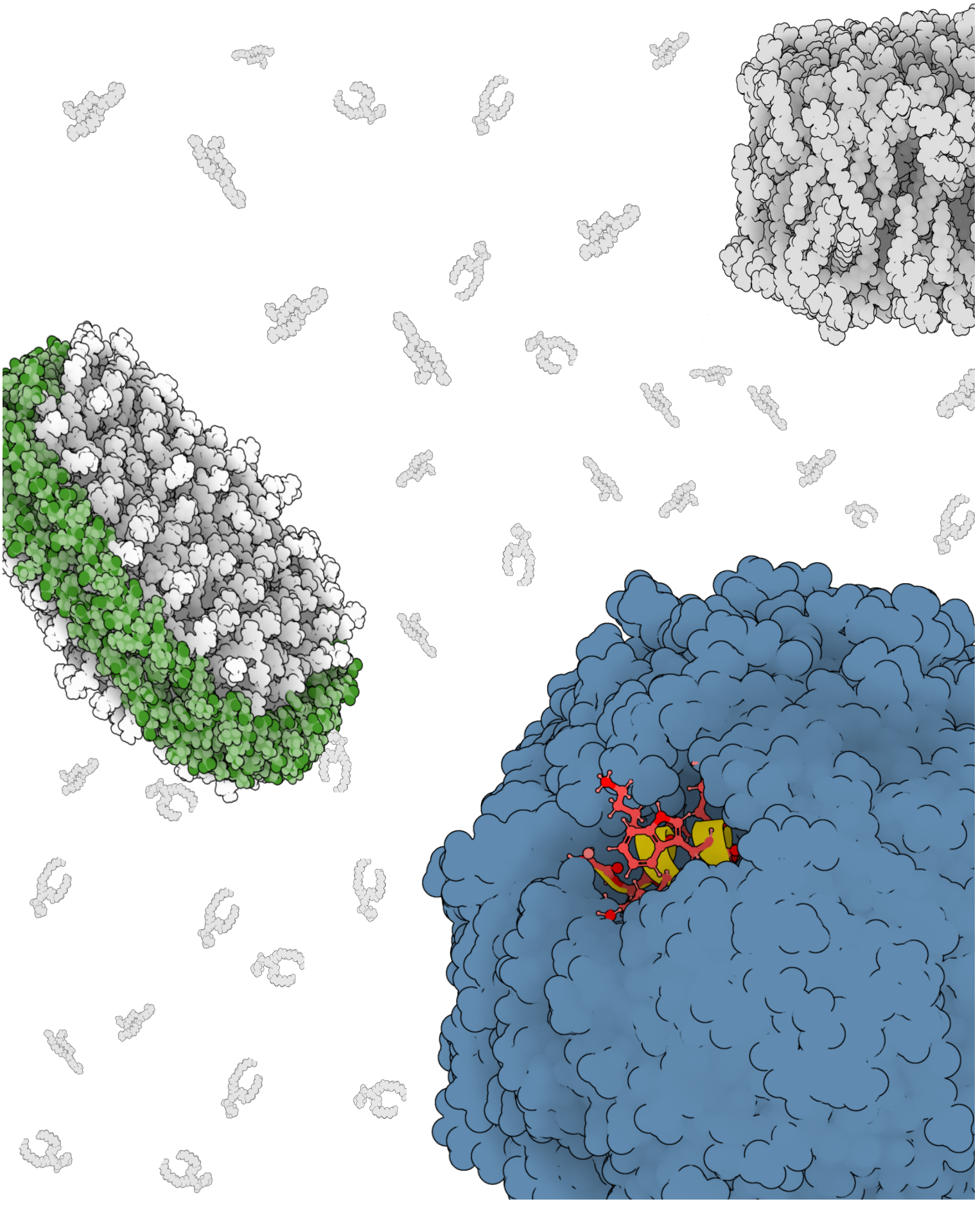

Chapter 2: Membrane mimetics

This chapter represents parts of an invited review manuscript (reference 1 in the List of publications). It summarizes currently available biochemical approaches to generate membrane-mimicking environments as well as biochemical and biophysical methods to characterize interactions between membranes and peptides/proteins. These aspects will be important for the subsequent research questions of this thesis, i.e., the use of the Aescin system as a new membrane mimetic environment (chapter 3) as well as the characterization of membrane binding modes of a-synuclein (chapter 4) and the first in vitro characterization of the MRAP system (chapters 5 and 6). In this respect, this chapter should bridge the introduction and result sections.

Biophysical and biochemical methods to characterize membrane systems and their (inter-) actions

Introduction

Cellular membranes predominantly consist of phospholipid bilayers, carbohydrates, and proteins. Their exact composition can considerably differ due to environmental factors, the state during the cell cycle, and the cell type. The cell membrane is at the center of numerous biochemical and physiological processes, such as molecular transport, enzymatic activity, and control of cell-to-cell interactions. In addition to the membrane proteins, which are established interfaces in membrane function and one of the key targets of modern drugs, the lipids themselves can carry out a wide variety of functions, e.g., by regulating membrane dynamics or membrane protein structure as well as recruiting molecules to the membrane surface.

The choice of an adequate membrane mimetic

Due to the importance and complexity of cell membranes, a broad assortment of biomimetic model systems has been developed, each of which possesses specific strengths and weaknesses in its capability to emulate a native biomembrane. Most prominent membrane mimetics include detergent micelles, bicelles, nanodiscs, and liposomes. Each system exhibits different characteristics, and the selection of the most suitable membrane mimetic is of fundamental importance and should always be made with

respect to the research question under consideration. As such, studies of integral membrane protein structure may, e.g., rely on substantially different features of the membrane mimetic as the investigation of interactions of peptides with lipid surfaces. While a good membrane mimetic should, in general, meet the criterion that the studied environment closely resembles the native one, the one feature that is at the center of the investigation should be particularly considered (e.g., MP structure determination requires an environment that stabilizes a relevant state, and lipid-peptide interactions requires the presence of chemical and physical properties of the lipid bilayer) [96]–[101]. Furthermore, care should be taken that the system is stable for the measurement periods to rely on the benefits of having a well-defined in vitro system.

Detergent micelles

Common mimetic systems are detergent micelles. They are amphipathic and spherical formations, constituted by aggregation of amphiphilic surfactant molecules (at concentrations above their specific critical micellar concentration, CMC) where their hydrophobic tails constitute an inside core and hydrophilic head groups exposed to the aqueous solution.There is a wide variety of detergents to choose from, and the ideal one should be able to keep the membrane target proteins soluble without producing changes in their native structure and functional activity as well as in their thermodynamic properties [102]. This system is easy to prepare and often exhibits good solubility of the target MP. Nevertheless, micelles' intrinsic instability and chemical and physical properties represent a poor mimetic of a native membrane. In this respect, the presence of high detergent concentration often alters the properties of the target proteins, including their structure, inducing conformational changes and aggregation, and consequently also, may alter their activity.

In general, due to their intrinsic properties, micelles are generally a rather poor mimetic of lipid surfaces. As such, care needs to be taken when interpreting results of peptide-detergent interactions concerning physiological relevant interactions, e.g., on the cell surface.

Liposomes

Liposomes are another system commonly used to study molecular interaction with membranes due to their considerably greater resemblance with a cell membrane.

Liposomes are spherical bilayer vesicles comprising normally phospholipids with an aqueous interior, where the polar head groups are oriented towards the aqueous phase. Their properties depend directly on the nature of the lipid molecules used for liposome assembly (charge, acyl chain length, etc.), as well as the number of bilayers that comprise the liposome and the preparation conditions. Therefore, the system enables the possibility to modify properties like surface charge, fluidity, elasticity, curvature, and size. The liposomes' size ranges from 30 nm to microns. It is reported, for example that the vesicles formed with unsaturated phosphatidylcholine have greater permeability than those formed with saturated phospholipids with long acyl chains [96], [103], [104].

Liposomes can be classified on the number of bilayers and size as small unilamellar vesicles (SUVs) have a diameter smaller than 0.1μm; large unilamellar vesicles (LUVs) have a diameter of up to 1 μm or giant unilamellar vesicles (GUVshave diameters greater than 1 μm. Likewise, multilamellar vesicles (MLV) can be generated due to the union of unilamellar vesicles [97], [104].

There are a wide variety of procedures to prepare liposomes that normally rely on a self-assembly reaction of the lipids that is promoted by increasing the aqueous proportion present in the medium, thus forcing the interaction among their hydrophobic tails [97], [105].

Overall, liposome systems provide a relatively fast and easy-to-prepare way to produce a native-like membrane environment in which the phospholipid composition can be well controlled. Nonetheless, the principal disadvantages of this biomimetic model are related to difficulties in obtaining homogenous and controlled sizes of the vesicles, as well as the lack of control in the lamellarity, encapsulation efficiency, and poor stability. Still, liposomes are promising systems also used as carriers of drugs, antimicrobials, antioxidants, and many other bioactive elements in food, cosmetics, and pharmaceutical industries [97], [98], [105].

Nanodiscs

Nanodiscs are discoidal phospholipid bilayers surrounded and stabilized by two copies of an amphipathic helical protein, i.e., the membrane scaffold protein MSP. Nanodiscs often provide increased stability and a more homogenous environment than other membrane mimetics [106]–[108].

Nanodiscs are also formed through a self-assembly reaction between lipids and two MSP proteins. The general protocol begins by solubilizing lipids in a detergent solution. Once the lipids are completely dissolved, the MSP is added. The self-assembly reaction is promoted by removing the detergent via dialysis or adsorption to hydrophobic beads. When the detergent is removed, the two MSPs encircle the lipid bilayer, generating the discoidal structure. The diameter of nanodiscs depends on the length of the used MSP variant and is approximately 6-17 nm [103], [107], [109].

Nanodiscs are a suitable membrane mimetic to obtain homogeneous size assemblies, which can be composed of different mixtures of phospholipid types. Nanodiscs have high stability, and their small size facilitates using different characterization techniques like NMR spectroscopy. Nanodiscs also provide suitable properties to maintain and promote the native structure and functionality of many membrane proteins by simultaneously eliminating common problems like aggregation [103]. However, optimizing the assembly conditions can be laborious [107], [109].

In addition to MSP-stabilized nanodiscs, other proteins can also assemble nanodiscs. Prominent examples include saponins such as Saponin A [110], alpha-synuclein [111], and an amphipathic 18 amino-acid-long peptide derived from apolipoprotein A-1 [110]. In these systems, the size of the nanodiscs is often easier to modify. However, this usually comes with the prize of increased polydispersity and decreased stability compared to MSP-derived nanodiscs.

In addition to proteins, other distinct polymers could be used to encircle lipid bilayer patches in the form of nanodiscs. These polymers include copolymers of styrene and maleic acid (SMA) or diisobutylene [112] / maleic acid copolymer (DIBMA) [113]. In the SMA system, amphipathic molecules surround the lipid bilayer, promoting styrene phenyl rings to interact with the hydrophobic edge of the bilayer, and the maleic acid is oriented towards the solvent, increasing the solubility of the nanodisc. The principal difference with DIMBA is that it has aliphatic rather than aromatic hydrophobic properties generating good homogeneity for the co-polymer, regardless of its length. A great advantage of polymer nanodiscs is that size modifications can be made directly by modifying the ratio of maleic acid to styrene. However, a disadvantage of polymer-based nanodiscs systems often include low solubility at low pH or high divalent metal ion concentrations as well as the

very high negative charge density of the polymers known to induce strong unspecific interactions with various biomolecules [110].

Characterization of lipid-peptide interactions

The investigation of interactions of biomolecules with membrane surfaces is an important yet often difficult-to-realize research area that strongly depends on the choice of an adequate membrane-mimicking system. Antimicrobial peptides (AMPs) provide just one example where these interactions are critical to understanding on a molecular level. In recent years, the alarming increase of antibiotic-resistant microorganisms represents a severe health risk worldwide. Wide families of molecules with potential therapeutic applications are antimicrobial peptides. These molecules take part in the immune system of many organisms. Several membrane-related factors modulate antimicrobial activity, such as membrane curvature, electric potential, architecture, and lipid composition. Liposomes can be used as a membrane model for interaction studies of drugs and biological membranes, for instance, on the passive diffusion of antibiotics across the cell membrane. The knowledge of the membrane-antibiotics interaction plays a central role in designing and developing processes of new antibiotics, understanding the pharmacological effect the potential toxicity; to predict their pharmacokinetic and pharmacodynamic properties as absorption, transport, and metabolization may be effective in obtaining antibiotics with strong therapeutic efficacy and less adverse effects [114], [115]. For example, using the aspiration method for giant unilamellar vesicles (GUVs), it has been possible to probe a multi-step membrane-peptide interaction that affects membrane permeability and results in cell damage through pore formation [115]. Due to their great importance, AMPs are currently studied using increasingly realistic membrane mimetics to better understand their interactions and mechanisms of action [106], [115], [116]. Still, the membrane mimetic and suitable read-outread-out assays that can ideally already report on the initial (often transient) interaction of the target molecule with the membrane surface are sparse. In the following, the established biophysical and biochemical methods to probe peptide-membrane interactions are outlined.

Commercial test stripes (lipid screening)

In order to study protein-membrane interaction, it is essential to identify the type of phospholipids with which the target protein can interact. Lipid-specific protein-membrane interactions are essential for many cell signaling processes. Knowledge of the occurrence,

mode of action, and means to modulate these interactions are therefore central, yet often unexplored, in our endeavor to understand life at the molecular level. Nowadays, the arguably easiest way to perform screening of lipid specificity is through commercial test strips.

Membrane Lipid Strips, often focusing on PIP (phosphatidylinositol phosphate) lipids, are pieces of hydrophobic membranes impregnated with small amounts (100 pmol) of different lipids. These lipids, which are mainly contained in biological cell membranes, are immobilized in the nitro-cellulose strip [117].

The lipid-protein interactions can be determined through a simple protein-lipid overlay experiment (PLO assay), whose protocol is quite similar to that of a western blot [118], [119]. Briefly, the assay consists in blocking the PIP membrane in a solution TBS-T for 1 h at room temperature; then, the strip is incubated with a protein of interest, and at the end, lipid-protein interaction is detected by enhanced chemiluminescence using antibodies [119]–[121].

The main advantages of the PIP strips assay are that the procedure is relatively simple and low time consuming, the required amount of protein (around 0.5mg/mL for every 15 lipids screening), and its reduced cost. On the other hand, possible disadvantages of this assay could be that the conditions and setting are far away from resembling a physiological membrane environment and that the protein-PIP strips binding may be poor or promiscuous, according to previous reports [120], [122].

As mentioned above, protein-PIP interactions play important roles in cell signaling and pathophysiology. Recognition of these specific interactions under membrane lipid strip test has been, for example, the starting point to recognize the antimicrobial action of defensins against different pathogens.

Defensins are one of the principal families of AMPs, constituted by small cationic peptides (less than 100 amino acids) stabilized by disulfide bounds [123], [124].

Like many other AMPs, defensins´ antimicrobial effect is involved in their interaction with the lipid bilayer of target cells; thereby, defensins exhibit antimicrobial activity depending on their ability to interact with lipids in the membrane of the pathogen agents. According to different researchers, defensin-lipid binding is mediated, among many other factors, by electrostatic interactions with the negatively charged cell envelope components and phospholipids. Hence lipid screening assays of defensins are very useful to clarify the factors involved in recognition of target molecules, being able to hypothesize the biological activity of new molecules based on their interaction with specific lipid targets [124], [125].

The commercial stripes are very useful as a first test to determine protein-lipid interaction, but it is highly recommendable to corroborate the obtained result using more reliable membrane mimetics in a secondary method since the behavior observed in a solid surface assay could be quite different from that in bilayer membranes [126].

Surface techniques (SPR, BLI)

Surface plasmon resonance (SPR) is a powerful technique used to study and characterize a wide diversity of binding interactions between biomolecules such as protein-protein, antibody-antigen, ligand-receptor, protein-nucleic acid, and protein-membrane interaction. It is one of the most useful techniques used in protein-membranes interaction studies since it can provide qualitative and quantitative information. Using SPR, it is possible to identify not only if molecule targets have the capability to interact with certain lipids but also to accurately characterize the binding kinetics. Therefore, SPR can detect rather subtle differences in the assay conditions, such as minor differences in membrane compositions or different variants (e.g., mutations) of the protein target [127].

In a standard SPR assay, a ligand (such as a membrane-mimetic) is immobilized on the surface of a sensor chip while a solution of analyte (a protein solution) flows over it. Surface plasmon resonance takes place when polarized laser light is aimed at a gold layer at a critical angle. The sensors are made of glass slides and have a thin layer of metal on their surface, which is where surface plasmon resonance occurs. The gold-free electrons oscillate coherently at the glass-metal interface, creating a charge density called surface plasmons. Surface plasmons are produced, and this process leads to light absorption. When a protein-membrane complex forms, it causes a change in the refractive index near the surface of the sensor, which results in an increase in the signal [97], [100], [127], [128].

One of the main advantages of SPR over other techniques is its high sensitivity, which allows for the detection of very small quantities of biomolecules. This means that only nanomolar (nM) concentrations of proteins, nucleic acids, or lipids are required for analysis. Additionally, SPR does not require the use of radioactive or fluorescent labels, which makes it a safer and more cost-effective option.

Another advantage of SPR is the ability to determine the affinity constants and the association or dissociation rates of binding. This information is critical for understanding

the kinetics and thermodynamics of biomolecular interactions. Additionally, SPR does not require a purified system, allowing for the study of heterogeneous membranes. This means that it is possible to study the interactions of proteins and other biomolecules with native membranes, as well as the monitoring of molecular binding can be done in real time, which enables the study of dynamic interactions. However, one of the main challenges of SPR is the selection of a suitable membrane mimetic. The stability of the lipids on the sensor is an important factor in the protein binding ability and can affect the sensitivity and specificity of the assay. Therefore, choosing a membrane mimetic that is stable and compatible with the biomolecules of interest is crucial. Another limitation of SPR is the sensor's sensitivity, which can be affected by the detection of low molecular weight molecules such as DNA, cancer biomarkers, and antigens [97], [127], [129].
As previously mentioned, SPR is a valuable tool for studying peptide-membrane interactions. These interactions play a crucial role in many biological processes, such as coagulation factor binding in cell signaling, attachment of pore-forming proteins (PFPs) in lipid membranes, and ligand binding between receptors like G-proteins in transmembrane signaling pathways. Using SPR, it is possible to obtain the binding affinity constants and stoichiometry of these complexes, providing insight into the kinetics and thermodynamics of these interactions [127].

Micro-fluidics differential sizing

Microfluidics (MDS) is another technique used to study biomolecular interactions. It uses microfluidic devices to separate particles or biomolecules based on their size. The technique is based on the principle that particles of different sizes will experience different flow dynamics and behavior in a microchannel because of hydrodynamic and Brownian motion, which means the larger particles will experience more resistance to flow than smaller particles. This technique can be used not only for studying interactions but also for functional and structural analysis of biomolecules, as well as for sample manipulation [130], [131].

One of the main advantages of microfluidics is the ability to create well-controlled microenvironments that closely mimic native conditions. This allows for the development of innovative techniques and equipment that can contribute to the advancement of quantitative protein science. Additionally, microfluidics can also be combined with other methods, such as SPR, to improve the accuracy and sensitivity of the analysis.

Furthermore, microfluidics is useful for high-throughput analysis and the miniaturization of samples, which makes it a cost-effective and efficient technique for large-scale studies [130], [131].
The determination of biomolecular interactions and binding can be achieved by monitoring the diffusion coefficients of the biomolecules. Diffusion is a molecular property that depends on both the size and structure of the biomolecule. It is directly correlated with the hydrodynamic radius (RH) of the molecule, which is a measure of the size and shape of the molecule in solution. By measuring the diffusion coefficients of biomolecules under different conditions, it is possible to gain valuable information about the nature of the binding interactions between molecules, such as the binding strength.

The Microfluidics device is used to measure the diffusion properties of molecules perpendicular to the flow direction; this is done by first determining the hydrodynamic radii of pure and free molecules in a denaturing solution (typically 20%v/v DMSO) to promote the presence of the molecule in a monomeric state. Measurements are then performed under close to native conditions, where larger species have diffused less than smaller ones. Finally, the molecules are labeled with fluorophores for detection. By characterizing these properties, interactions can be studied by comparing RH [130], [131].
The Microfluidics device can be used to study protein-protein interactions by measuring the size change of molecules before and after complex or aggregate formation using the space-time diffusion technique. The Microfluidics device can be used to study protein-protein interactions by measuring the size change of molecules before and after complex or aggregate formation using the space-time diffusion technique. Characterizing these aggregates is essential in medical science, as it provides evidence of primary and secondary nucleation in amyloid formation, a key factor in neurodegenerative diseases [132]. Additionally, the device can mimic in vivo environments and study the connection between the aggregation of biomolecules and a variety of functional and pathological cellular behaviors. It allows the acquisition of multiple diffusion profiles and an understanding of the influence of other components in heterogeneous assays [130], [131].
Microfluidics offers several advantages as a method for studying interactions between biomolecules. One of the main benefits is the ability to reproduce well-controlled microenvironments using small sample volumes and short time scales of analysis. Additionally, microfluidics allows for the detection of specific interactions between biomolecules without the need for any matrices or attachment to surfaces, enabling the

analysis of the behavior of specific molecules within polydisperse mixtures with high sensitivity. However, a disadvantage of this technique is that it requires the continuous generation of fluorophores in order to work under microfluidic conditions [130]–[132].

NMR

Nuclear Magnetic Resonance spectroscopy has been one of the most important techniques in the study of molecular biophysical properties in the last 30 years. Several studies have recently emerged, focusing on the functional dynamics of biomolecules, especially membrane proteins. Through NMR, it is possible to acquire unambiguous structural information regarding the aggregation, orientation, dynamics, and topology of membrane-inserted polypeptides; in addition, it allows the characterization of interactions at an atomic level. This level of resolution enables a detailed understanding of the chemical interactions between biomolecules, which can provide insights into their function and behavior in complex biological systems.
When studying interactions using NMR, it is also essential, as with other techniques reviewed before, to use a membrane mimetic that closely resembles the native environment and conditions of the membrane. This is important because the location, dynamics, and structural conformation of peptides or proteins are often influenced by their interactions with membrane mimetics such as detergents, liposomes, nanodiscs, etc. Using a membrane mimetic that closely mimics the native environment can provide a more accurate representation of the interactions being studied and help better to understand the behavior of biomolecules in their natural setting [133].

The basic principle of NMR spectroscopy involves the interaction of the magnetic properties of the nuclei (non-zero nuclear spin) with an externally applied magnetic field. This interaction causes the nuclei to absorb and emit electromagnetic radiation at a specific frequency.

This process generates energy states. The energy difference between these states depends on the nature of the nuclei (gyromagnetic constant γ) and the magnitude of the applied magnetic field (B0). This is low energy (in the range of radio frequencies). By measuring the emission of this radiation, it is possible to determine the sample's chemical composition, structure, and dynamics.

NMR spectroscopy is a powerful technique for studying the structure and dynamics of a wide range of samples, including small molecules and large biomolecules. The technique works by detecting subtle chemical shifts, coupling constants, and relaxation times can be measured to provide information about the local chemical environment, interactions, and dynamics of the nuclei. This makes NMR ideal for studying structural conformations or interaction processes. Different nuclei can be observed in NMR, such as ^{1}H, ^{2}H, ^{13}C, ^{15}N, and ^{19}F, each with advantages and limitations. For example, ^{1}H is commonly used for one- and two-dimensional experiments observing bond correlations or determining interatomic distances. ^{2}H, ^{13}C, and ^{15}N are essential for more complex systems, such as proteins, as they help in determine the backbone; ^{31}P is useful for studying membrane phospholipids. Apart from providing structural information, NMR can yield other essential parameters, such as the concentration of a compound (proportional to the integral of the signals) and specific correlations between atoms, which allows for the discrimination of other signals present in the compound [134]. NMR spectroscopy enables the analysis of interactions between biomolecules in a physiological environment and over a wide range of temperatures.

Additionally, it permits the determination of the atoms involved in the binding process. Nonetheless, there are also some limitations to using NMR for these studies. One of the main disadvantages is that NMR is less sensitive than other techniques, requiring a significant amount of samples to obtain accurate results. Additionally, isotope labeling is often necessary to achieve adequate sensitivity, and studying of large complexes may be challenging. These limitations must be considered when selecting NMR to study interactions between biomolecules.

NMR spectroscopy is a versatile tool that can be applied to a wide range of fields, including the study of ligand-receptor binding mechanisms and protein-lipid interactions. In the study of ligand-receptor binding, NMR can be used to identify potential ligands and determine which atoms are involved in the binding process. In the study of protein-lipid interactions, NMR can provide valuable information on the mechanisms through which antimicrobial peptides (AMPs) interact with phospholipid bilayers or reconstituted membranes. Depending on the specific research aims, it is possible to use either solution or solid-state NMR techniques. Solution NMR spectroscopy is widely used to determine the structure of globular proteins and the interactions of relatively small membrane-protein complexes (~30 kDa) in isotropic environments, whereas solid-state NMR spectroscopy

allows for the study of larger complexes in the presence of disordered phospholipid bilayers [134].

To determine the folding and structure of membrane proteins, standard 2D and 3D NMR experiments are commonly used. To study more complex systems such as peptide-lipid aggregates or to visualize protein assemblies, 2D experiments with double quantum filtration on labeled molecules are very useful [99] and to determine the mechanisms through which proteins are inserted into the membrane, such as the case of AMPs and pore-forming peptide [135], experiments of ^{2}H and ^{31}P are used, monitoring the orientation of ^{15}N peptides labeled during their interaction with the membrane mimetics [135], [136]. Using NMR techniques, methodologies such as isotope labeling, paramagnetic magnetization, or magnetic transfer have been developed and optimized for study using NMR spectroscopy in solution- and solid-state [110], [133], [137].

Fluorescence

Fluorescence spectroscopy has been positioned as a fundamental technique in determining structural aspects, providing information on the topology and dynamics of polypeptides. Fluorescence occurs when a substance is lightly irradiated, and its emission wavelength is higher than that of excitation. By monitoring changes in the fluorescence of certain molecules, called fluorophores, it is possible to study the mechanism through which molecular binding occurs; these fluorescence changes are generated mainly due to conformational changes of the fluorophore during the binding processes or due to modifications in its environment [138].

The use of fluorescence spectroscopy in determining interactions between polypeptides and lipid bilayers involves two main methodologies. The first approach utilizes the intrinsic fluorescence properties of certain amino acids, specifically tryptophan (Trp) and tyrosine (Tyr) found in the polypeptide chain, to gain insight into the peptide-membrane interactions and environment.

The second methodology for determining interactions between polypeptides and lipid bilayers utilizes probes that modify the fluorescence properties of the target molecule. This allows for monitoring the influence of the peptide on the membrane and providing information about the changes that occur after the interaction [133], [138].

The main advantage that fluorescence offers is its high sensitivity and specificity. Other advantages to consider are that it permits determining protein structure, conformation, and interaction mechanisms through fluorescence parameters such as intensity and decay time.

However, its major limitation is that not all peptides or proteins exhibit fluorescent properties, making them unsuitable for this method. Additionally, the use of fluorescent probes has limitations, such as short lifetimes caused by photostability, and they can be potentially toxic. Furthermore, small changes in the environment, such as pH or other properties, can cause interference in the results obtained [133], [138], [139].

In recent years, the application of fluorescence spectroscopy has played a key role in the pharmaceutical industry, contributing to the characterization and quantification of the interaction of various molecules with their target biological membranes, such as hormones, toxins, and antimicrobial peptides. Such is the case of defensins and lipopeptides, which upon insertion into cell membranes generate changes in the intrinsic fluorescence of tryptophan or other fluorescent amino acids. In addition, fluorescence can be used to study the selectivity of peptides toward model membranes containing specific types of lipids [138], [140], [141].

Conclusion

This review attempts to provide an overview of the characteristics of the main membrane mimetics used in the study of membrane proteins, as well as a summary of the biophysical techniques used to study protein-membrane interactions. It is important to note that the specific mimetic and biophysical techniques used will depend on the unique characteristics of each protein system studied and the research objectives.

Chapter 3: Aescin-lipid bicelles

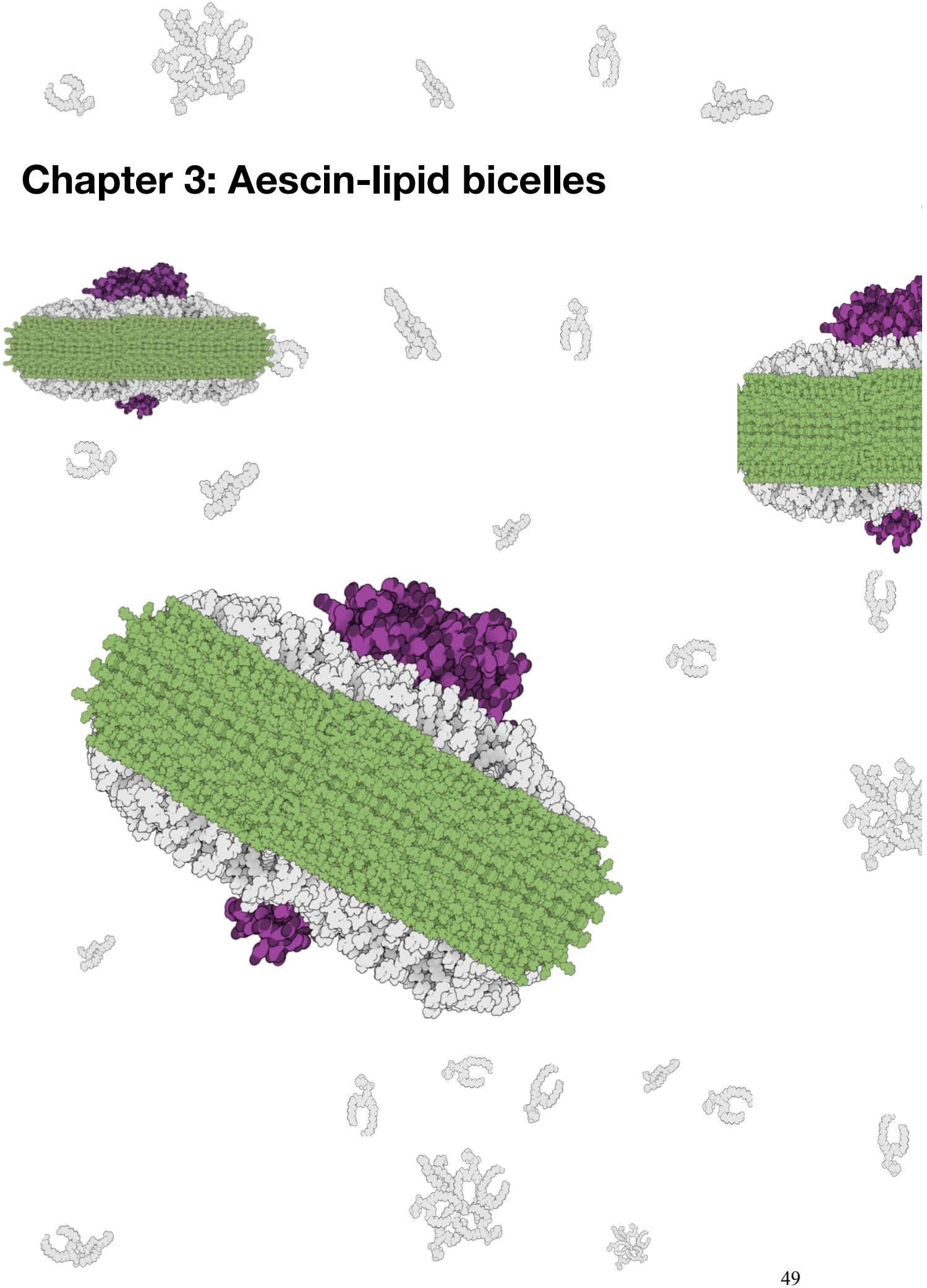

-

Chapter 3: Aescin-Lipid bicelles

This chapter reflects content of the following publication.

Characterization of size-tunable Aescin-Lipid Particles as Platform for Stabilization of Membrane Proteins

Fatima Escobedo-Gonzalez, Mohan Gospalswamy, Pia Hägerbäumer, Julian Victor, Georg Groth, Holger Gohlke, Thomas Hellweg*, Manuel Etzkorn.

status*: in preparation*

Abstract

Disc-like nanoparticles, stabilized by saponin biosurfactants, display fascinating properties, including their temperature-driven re-organization [142]. The interactions of saponins with lipids have important biological and biotechnological applications [143], [144]. β-aescin, a saponin obtained from horse-chestnut-tree seeds extract, shows strong interactions with membranes and has gained interest due to its beneficial therapeutic implications as well as its ability to form size-tunable discoidal nanoparticles [145]. Here we obtain fundamental insights into the molecular properties of aescin-lipid interactions and their temperature modulations. In addition, we demonstrate that, under defined conditions, aescin-lipid discs can accommodate medium-sized transmembrane proteins, opening the road for further applications.

Introduction

Aescin, also called Escin, is an isomeric mixture Of α- And β- Triterpene Saponins obtained from the extract of the seeds of the horse chestnut tree *Aesculus hippocastanum* [146]–[149].

The pharmacologically active component of the Aescin mixture is the β-form. It was reported that the β-Aescin has anti-inflammatory, anti-edematous, and venotonic properties, as well as antifungal, antibacterial, and anti-yeast activity. Therefore, it is used as an active component in the treatment of disorders such as heart failure, varicose veins, hemorrhoids, diarrhea, fever, cancer, and rheumatism [145], [150]–[153]. The biological

activity of β-Aescin is driven by its interaction with biological membranes and is due to its molecular structure; it consists of a head group composed of two glucose molecules and a glucuronic acid attached to a hydrophobic triterpenic backbone [142], [154]. Due to the presence of several hydroxy groups located on the same side of the principal chain, the Aescin molecule has a well-defined polar side and a non-polar side. In solution, the hydrophobic part of the Aescin molecule seeks protection from the hydrophilic environment [155]; this behavior promotes the formation of stable structures when the β-aescin interacts with phospholipids such as 1,2-dimyristoyl-sn-glycero-3-phosphocholine (DMPC). The resulting discoidal lipid structures are known as bicelles or nanodisks [26], [154], [156]. Previous studies have characterized their properties to form size-tunable discs concluding that the shape, stability, and size are correlated with the Aescin-phospholipid ratio; likewise, it was found that the interaction of β-aescin with lipid bilayers is highly dependent on the phase state of DMPC, which in turn correlates with temperature [142], [146], [154], [155]. The described characteristics of β-Aescin make it a promising candidate in the study and stabilization of hydrophobic molecules and drug delivery.

Here we provide additional NMR-based insights into these features and identify a complex occurrence of different states of Aescin-lipids mixtures at different temperatures and in the presence of different concentrations of Aescin. Furthermore, we explore the possibilities of using Aescin: DMPC discoidal nanoparticles as a new platform to stabilize membrane proteins.

Material & Methods

Chemicals

1,2-Dimyristoyl-sn-glycero-3-phosphocholine (DMPC) was purchased from Avanti Polar. Lipids. Inc (Alabaster, AL). The saponin β-aescin (>95%, CAS-number 6805-41-0, and chloroform were obtained from Sigma Aldrich (Munich, Germany).

Sample preparation

DMPC lipids in chloroform stock were dried under nitrogen flow to obtain a thin lipid film and stored under vacuum overnight for complete chloroform removal. Then the dry film was hydrated by previously prepared β-aescin solution at the desired aescin concentration

dissolved in 50mM phosphate buffer at pH 7.4 (to guarantee a constant solubility of β-aescin). All prepared samples had the final DMPC mass concentration of w(DMPC) = 15 g/L, while β-aescin concentration ranged from 0 to 30 mol% with respect to DMPC molecules amount. The samples were exposed to five freeze-thaw cycles in liquid nitrogen and warm water.

Dynamic Light Scattering

The bicelles' hydrodynamic diameter (HD) was analyzed by dynamic light scattering (DLS) using a Zetasizer Nano-ZS device (Malvern Systems, Worcestershire, UK) equipped with a laser source of wavelength λ = 633 nm. All samples were measured in 10 mm diameter polystyrene cuvettes at 25°C. The temperature was equilibrated for 1 min before each measurement. The number-average diameter results were obtained and processed in Zetasizer Software v8.02.

NMR analysis

All 1D and 2D ^{1}H spectra were recorded on a 600 MHz Bruker Avance spectrometer. The bicelles samples were measured in the same buffer conditions (50mM sodium phosphate pH 7.4 90% H_2O/10% D_2O. 1D spectra were recorded in a range of 10 to 50 °C with two degrees increments. 2D NOESY spectra were recorded with 128 scans at 10 and 40°C. All peaks were assigned by comparing with previous assignments and the Spectral Database for Organic Compounds (SDBS) for DMPC and β-aescin. All NMR data were processed using TopSpin 3.5 (Bruker) and analyzed using Sparky.

Results

Characterization of Aescin-DMPC particles

We use NMR spectroscopy, to investigate the properties of the aescin-lipid interaction and assembly in more detail. We initially recorded 1D ^{1}H spectra of the individual components, i.e., buffer solubilized aescin (Fig. 3.1a,b) and DMPC prepared in the form of SUVs (Fig. 3.1c,d). The ^{1}H spectrum of aescin is consistent with the expected chemical heterogeneity of this natural product (Fig. 3.1b). Albeit partly overlapping peaks of DMPC and aescin exist that complicate data analysis, a few clearly separated peaks between aescin and DMPC are also present. Consequently, the 1D ^{1}H spectra already enable NMR-based analysis of aescin-DMPC mixtures with molecule-specific resolution. It has been shown in previous studies that aescin-DMPC interactions are strongly influenced by the applied

molecular ratio as well as by temperature effects [151], [155]. To investigate the latter, we recorded a series of ^{1}H spectra at different temperatures starting with an increasing temperature from 10°C to 50°C followed by a decreasing temperature from 50°C back to 10°C.

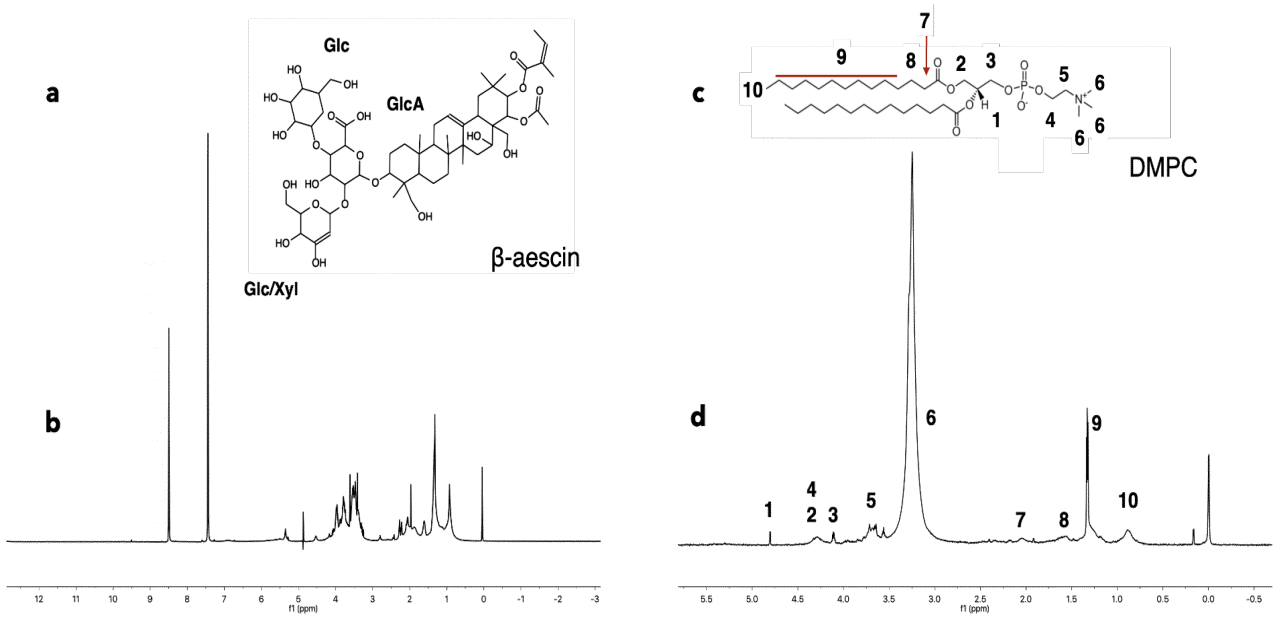

Figure 3.1 Molecular structure and NMR spectral properties of aescin and DMPC lipids. *a) Chemical structure of aescin consisting of a well separated glycone and aglycone part. The natural product contains a mixture of different chemical moieties at the indicated positions. b) 1D ^{1}H NMR spectrum of aescin, recorded at 24°C, 22,15 mM (15g/L) , 50 mM phosphate buffer, pH 7.4 buffer. c), d) Chemical structure and NMR spectrum of DMPC recorded under identical conditions as spectrum shown in b). Resonance assignments are indicated.*

Characterization of temperature induced transitions via NMR

In general, increasing measurement temperatures will lead to an increased molecular tumbling resulting in increased NMR intensities. Similarly, a temperature-induced transition of an ordered conformation into a more fluid phase, as present for the DMPC lipid phase transition, normally occurring between 20 – 30 °C, will lead to an (additional) increase in the detected ^{1}H signal intensity. Since the NMR spectra allow to separate of individual atoms in the DMPC lipids and the aescin (even in binary mixtures), following the temperature depending on changes in NMR peak intensities enables site-resolved insides into temperature-induced effects on, e.g., aescin-DMPC mixing, micelle/bicelle formation, and lipid-phase transition. The data reveal that the DMPC's hydrocarbon chains undergo a transition at elevated temperatures as compared to the head group as well as the

membrane-centered terminal methyl groups (Fig. 3.2). Interestingly, the data for the hydrocarbon chains (CH_2) indicate the presence of a more complex transition involving a 'classical' lipid phase transition as well as an additional transition potentially related to temperature depended aescin-DMPC particle rearrangements.

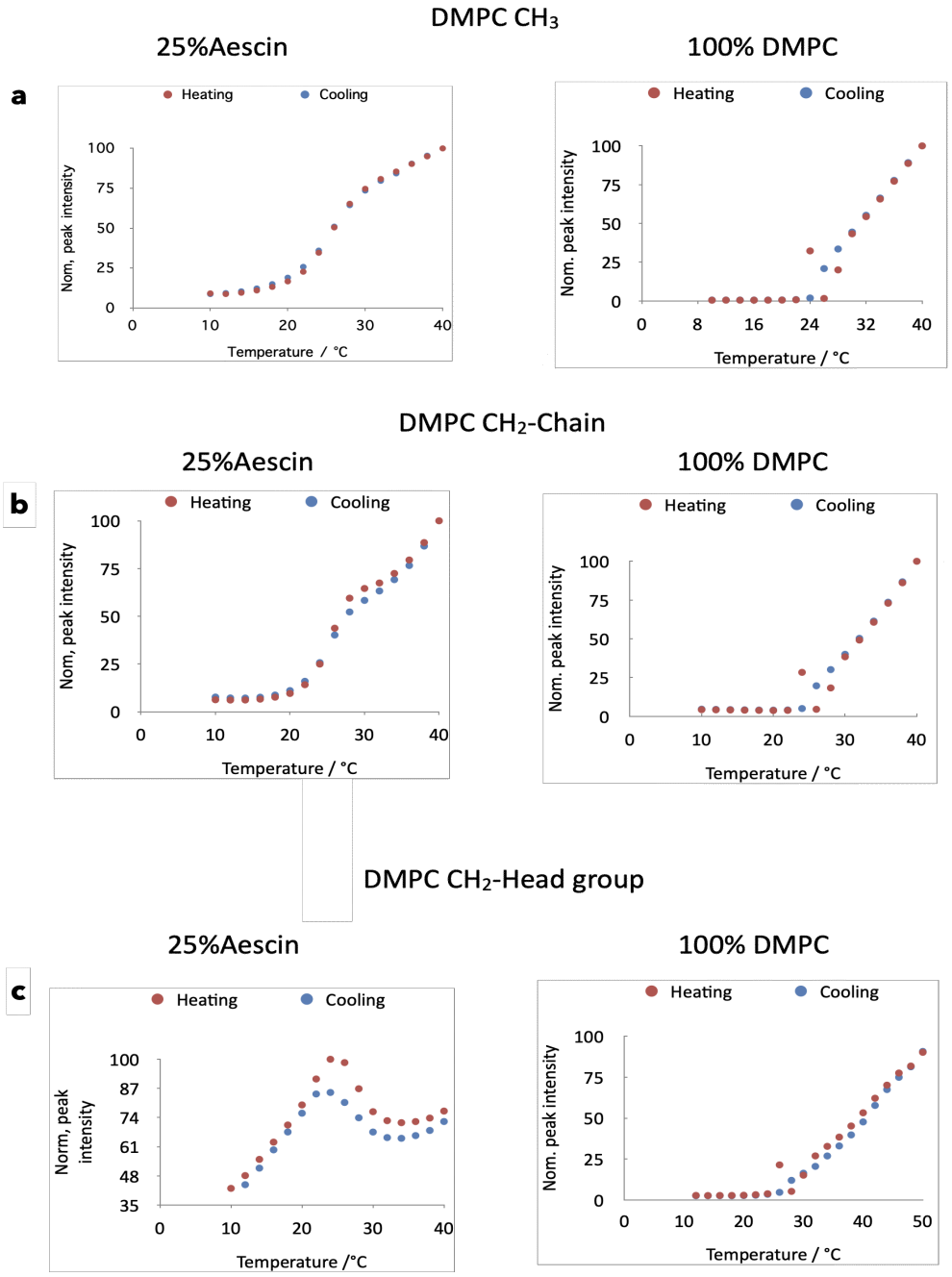

Figure 3.2 *Temperature-depended NMR-peak* intensities of different chemical groups of DMPC in DMPC:aescin bicelles (at 25 % aescin and without aescin). a*) CH_3 signal, representing the center of the lipid bilayer. b) CH_2 signal, representing the DMPC's hydrocarbon chains. c) C5 signal representing the buffer exposed head group of DMPC.*

-

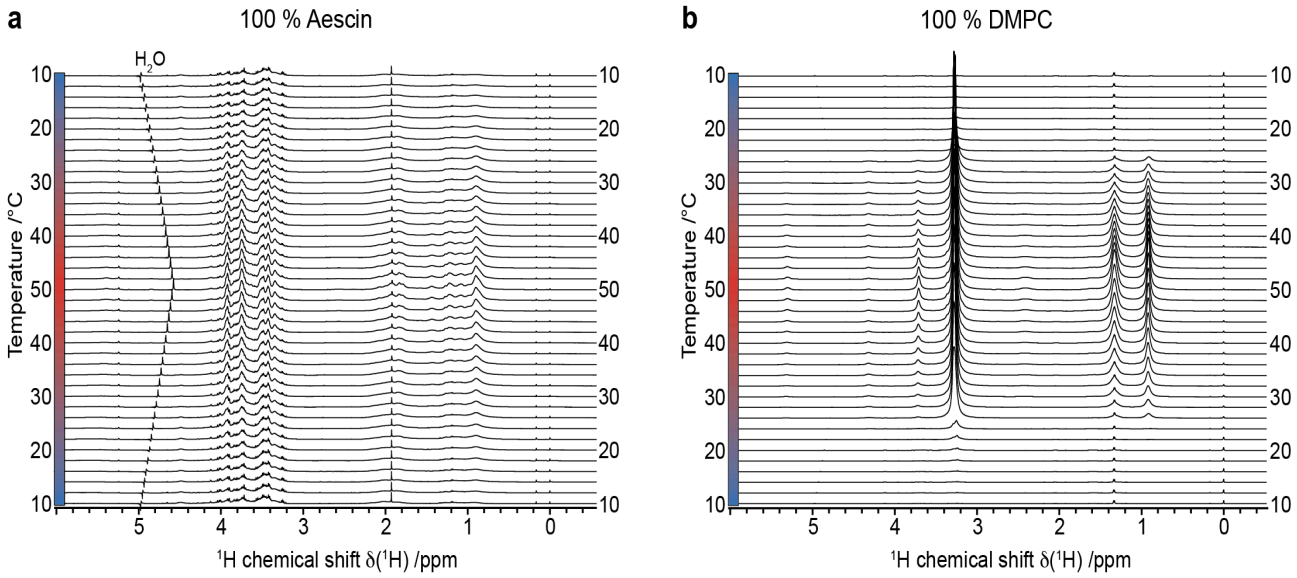

Figure 3.3 Temperature effects on ^{1}H NMR spectra of aescin (a) and DMPC (b) serving as reference for the individual compounds. Respective samples were first measured under stepwise increasing temperatures (from 10 °C to 50 °C in steps of 2 °C, followed by measurements under decreasing temperatures from 50 °C to 10 °C).

To investigate the transition in more detail and characterize the different states present in aescin-lipid mixtures at different aescin: lipid ratios and temperatures, we recorded a comprehensive set of NMR spectra in the temperature regime between 10 and 50 °C as well as at aescin: DMPC molar ratios spanning from 7 – 30 % aescin at constant concentrations of DMPC (22.15 mM). As mentioned above, initially, temperatures were increased in 2°C steps, followed by decreasing temperatures. To disentangle the effects of aescin-DMPC interactions, it is important to first have a look at the separated individual compounds. Figure 3.3 provides the respective reference data showing that the NMR spectrum of aescin is only slightly affected by temperature (figure 3.3a). Here the most pronounced effect is a moderate broadening of most NMR signals at higher temperatures indicative of conformational exchange processes in the µs to ms regime. As expected, the respective data for DMPC SUVs show a stronger temperature dependence (figure 3.3b). The observed behavior is in line with a strong increase in peak intensities due to a more fluid lipid matrix after the gel-to-lipid phase transition of the DMPC bilayer. Noteworthy, for

both isolated compounds, the heating and cooling periods have very similar effects resulting in a symmetric appearance of the shown data.

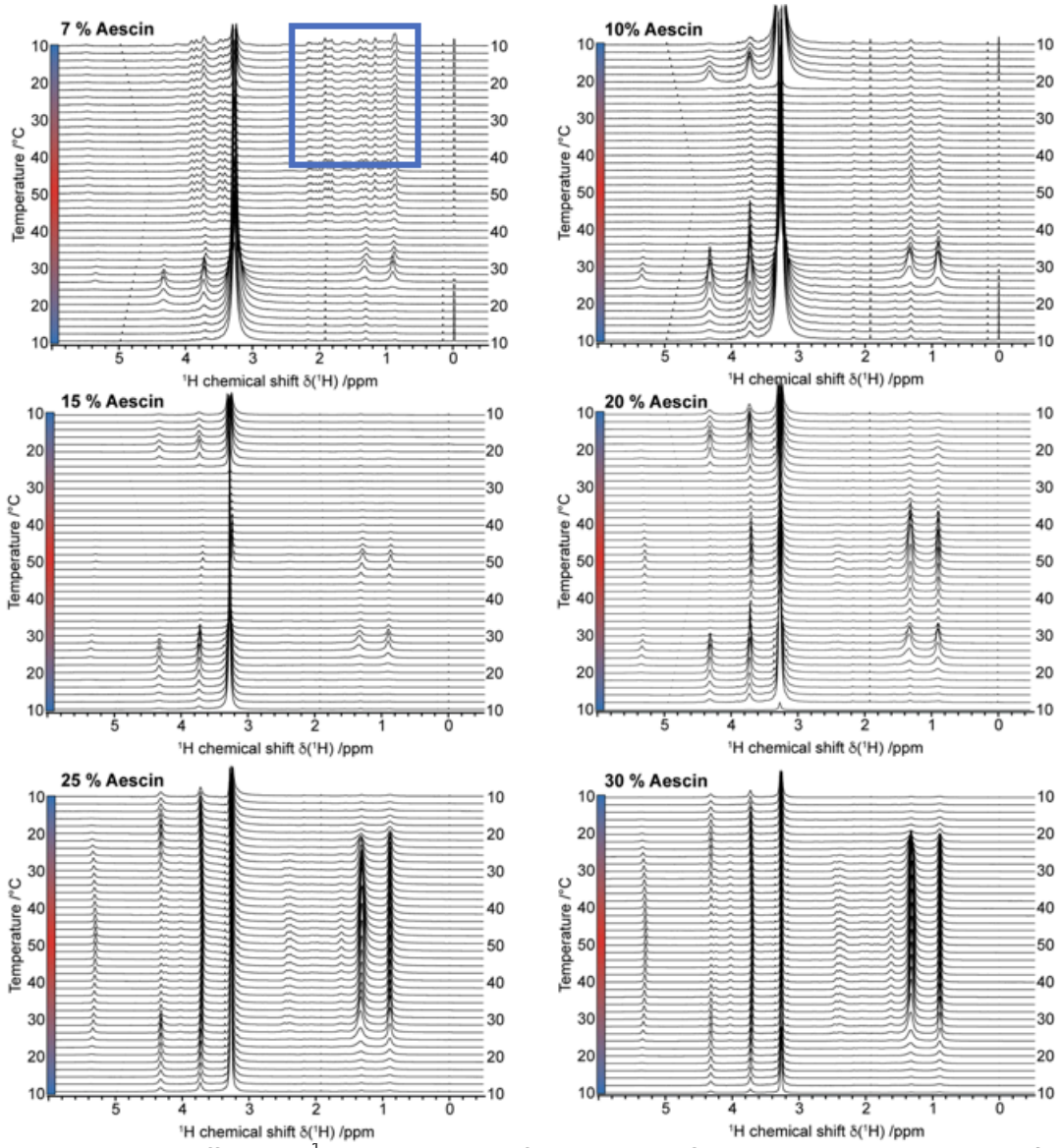

Figure 3.4 Temperature effects on ^{1}H NMR spectra of aescin: DMPC mixtures at indicated molar fractions of aescin.

Figure 3.4 shows the set of experiments for the tested aescin-DMPC mixtures confirming a complex behavior of the mixtures that is not only strongly dependent on the applied temperature but also varies considerably with the molar ratio of aescin: DMPC.

The different states that can be observed include a species with a distinct spectral appearance only found at 7% aescin after the sample was heated up to above 40°C (Fig. 3.4, 7% aescin). Noteworthy, a highly unsymmetric appearance in the data shows that this state remains dominant even after the temperature is lowered well below the initial transition temperature and is not reversible under the applied conditions. This behavior, therefore, reveals the presence of an energetically trapped state. Interestingly, the visible

NMR signals of this state appear to originate from the aescin molecules. The phase transition effects of the DMPC matrix, which are still observable during the heating period, are not observed during the cooling down period. While other explanations are possible, this behavior would be in line with a perturbation of the DMPC matrix by aescin molecules that either dissolve the lipid bilayer or are incorporated into the vesicles.

Looking at the behavior of the samples with the higher molar percentage of aescin (i.e., 25% and 30 %), the data show a symmetric appearance indicative of a single state or interconvertible states with low energy barriers. These features are only found for aescin ratios at or above 25%. The samples with ratios between 7 – 25% reveal several difficult-to-interpret features with an unsymmetric appearance, affecting different peaks different peaks (likely originating from the DMPC molecules) in different manners. The in-part, fluctuating peak intensities could originate from chemical and conformational exchange processes that can counter the expected peak intensity increase at elevated temperatures. In this respect, the data could, e.g., indicate differential interactions of the aescin molecules with the respective DMPC moieties. However, since the data also contains lipid phase transitions and likely (re-)formation of aescin-DMPC particles, it is difficult to separate the different processes from each other.

Mixing behavior of aescin with the DMPC

To better characterize interactions between aescin and DMPC molecules, we recorded a set of 2D NOESY spectra that report on through-space interactions between all ^{1}H spins in the system in the range between approx. 1 – 7 Å. Thus, these spectra are generally capable of detecting close intermolecular contacts, referred to as NOE-contacts, between aescin and DMPC. Indeed, distinct NOE-contacts could be clearly identified, confirming direct interactions of aescin with the CH_2 and CH_3 groups of the lipids Fig 3.5a. Since not all resonances and, consequently, all possible NOE correlations are resolved in the 2D spectra, it is not possible to derive an exact binding mode between the aescin and DMPC. Nevertheless, NOE contacts involving the H33 moieties of aescin identify these regions as a part of the intermolecular interactions (Fig. 3.5a). The respective correlations are only observable at aescin fractions of 25% and 30%, which is in line with the expected smaller particle sizes formed at these ratios (Fig 3.5b).

-

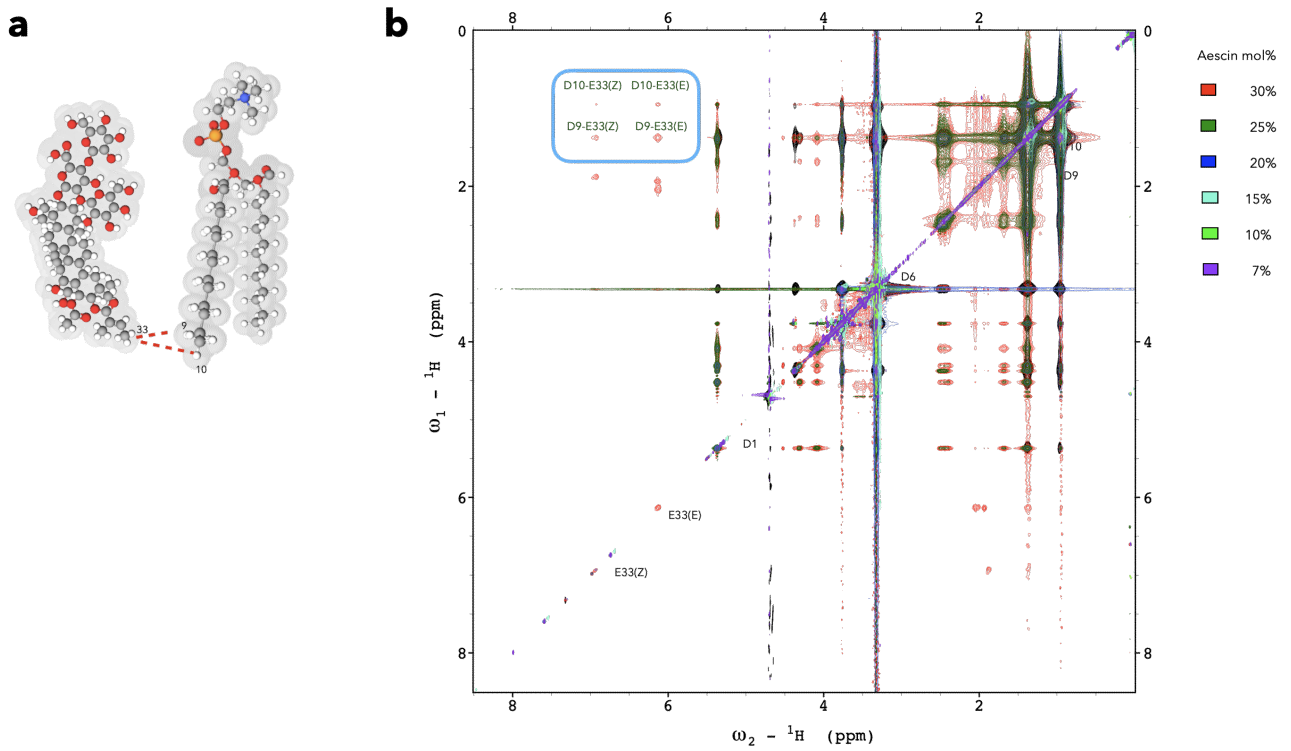

Figure 3.5 2D ^{1}H-^{1}H NOESY spectrum of aescin: DMPC *(30% aescin, 40°C) showing clear intermolecular contacts between aescin and DMPC. Resolved peaks point to interactions between* aescin's H33 *and DMPC* CH_2 *and* CH_3 *groups.*

Complementary to the detection of direct intermolecular NOE contacts, the chemical shift perturbations (CSPs) induced by changes in the molecular environment can be used as indirect probes of molecular interactions. Here, e.g., replacing DMPC-DMPC packing with aescin-DMPC interactions will lead to changes in the resonance frequency of the spins that experience a different neighbor. In this respect, the magnitude of the induced CSPs can also correlate with the fraction of the intermolecular interactions found in the ensemble of molecules in the sample. Figure 6 shows the results of a CSP analysis for distinct peaks. It can be seen that while some peaks are not affected (e.g., 1 and 2), other spins show clear concentration-dependent CSPs (e.g., 7 and 10). This data indicates that 10, 9, and 7 are involved in the aescin: DMPC interface, while 1 and 2 are not.

-

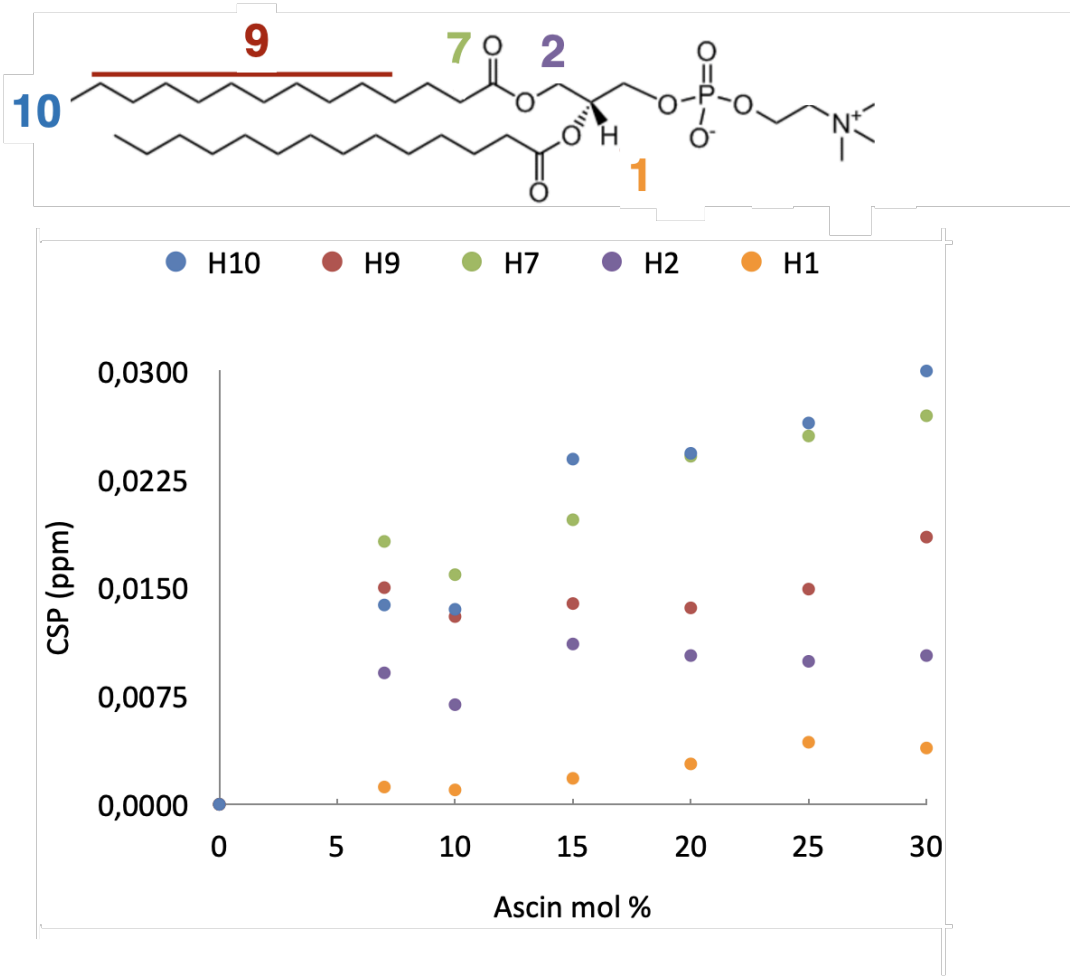

Figure 3.6 Chemical shift perturbation (CSP) analysis for indicated peaks of TMS-calibrated 1H spectra. E.g., the same spins as found in the NOESY data also show CSPs.

Interestingly, changing the aescin/DMPC ratio shows an unexpected behavior in the ^{1}H-1D spectrum, in which very prominent aescin-specific peaks start to disappear with an increasing molar fraction of aescin (figure 3.6). The reduced aescin peak intensity does neither correlate with the increasing aescin concentration nor the expected changes in particle size, which should be favored by smaller particles. The data would, however, be in line with the presence of aescin monomers and/or micelles in solution that requires a certain critical aescin: DMPC ratio to shift the equilibrium towards aescin: DMPC bicelles. The observed increase in DMPC-specific peak intensities with increasing aescin concentration supports a possible formation of bicelle-like particles. According to our data, the molar ratio that is required to (nearly) fully incorporate aescin into and/or around the lipid matrix is in the range of 1:4 (aescin: lipid) at 40°C (Fig. 3.7a). When lowering the temperature, the critical aescin: DMPC ratio is shifted to higher values (supporting Fig. 3.7b), suggesting that bicelles formation is facilitated by a fluid-phase of the lipid bilayer.

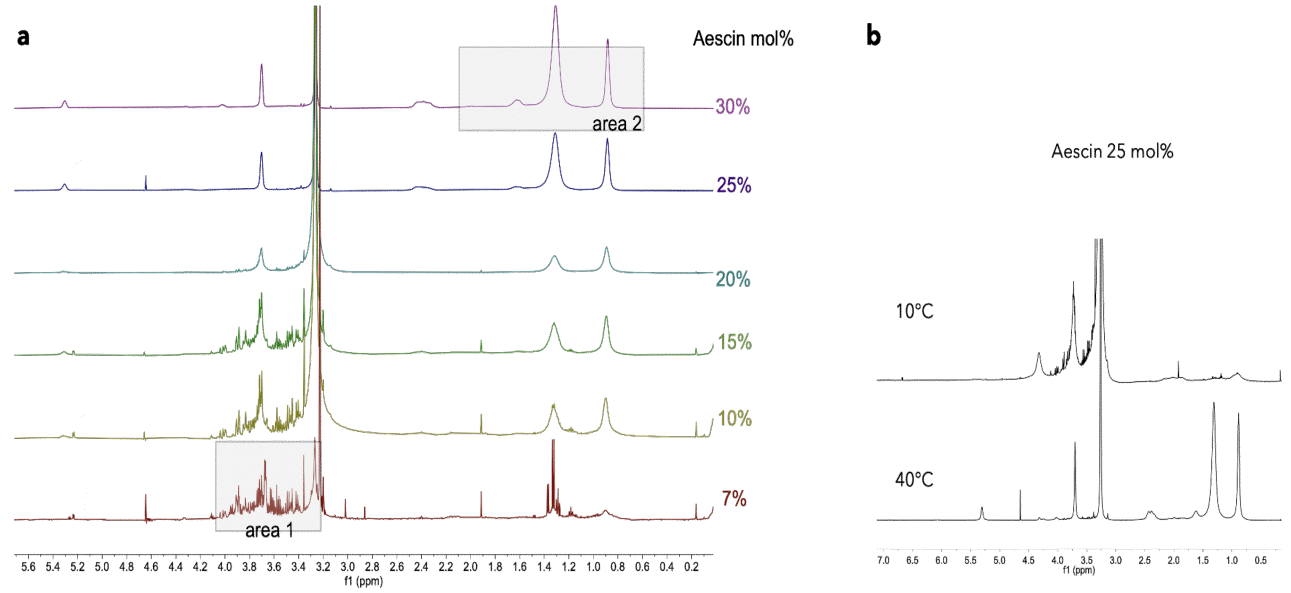

Figure 3.7 Mixing behavior of aescin and DMPC as seen by 1D ^{1}H NMR. *(a) Characteristic peaks observed at lower aescin ratio (area 1) indicate the presence of monomeric and/or micellar fractions of aescin. Increased DMPC-specific peaks (area 2) with increasing aescin concentrations indicate formation of smaller particles.*

Overall, our data confirm the attractive properties of the aescin system to tune the formation of distinct lipid-containing particles via temperature and/or varying the aescin: lipid ratio. In this respect, an unexpectedly high number of NMR-distinct states at different conditions and the presence of energy-trapped states were observed. Our data may help to identify the most suitable conditions that, e.g., are characterized by homogeneous and stable particles for various applications.

Using aescin-DMPC nanoparticles as platform to stabilize transmembrane proteins

One promising application of the aescin-lipid system is its potential capability to stabilize membrane proteins in size-tunable particles. However, so far, no successful incorporation of a transmembrane protein into aescin-lipid particles could be reported. Therefore, we set out to investigate the potential of the nanoparticles as membrane mimicking environment using the established test protein bacteriorhodopsin (BR). BR contains seven transmembrane helices, and its retinal cofactor exhibits a characteristic absorbances spectrum that can serve as a sensor of the BR's 3-dimensional structure [56], [57], [157]. In general, BR is known for its high stability and tolerance of different environments [55], [157], [158], and paired with its directly accessible sensor of 3D structure, provides an

excellent test system to assess whether medium-sized transmembrane proteins can be incorporated in aescin-lipid nanoparticles with intact 3D structure.
Following our previous strategies, cofactor-free Bacteriohopsin (BO) was expressed in a cell-free setup to ensure that no coordinated lipids would be transferred from the expressing organism [57], [159]. The resulting BO pellet was simultaneously solubilized and refolded using retinal and DDM micelles containing buffer.

We applied two strategies to transfer the BR from DDM into aescin-DMPC particles. In a first setup, we carried out a stepwise buffer exchange to substitute DDM micelles via centrifugal filters (20 kDa cutoff) by adding (detergent-free) aescin-DMPC buffer. The resulting sample still contains soluble BR that exhibits the characteristic absorption spectrum (Fig. 3.8 a). ^{1}H-NMR analysis indicates that DDM has been effectively removed by this procedure (Fig. 3.8 b).
Due to the above-characterized importance of the applied aescin: lipid ratios, we next varied this main parameter to evaluate the resulting capability to support protein solubilization and integrity as well as to assess the overall particle sizes of the respective aescin: lipid: protein mixtures. For the latter, DLS was used to determine the hydrodynamic radii. As expected, the particle size decreases with increasing aescin concentration (Fig. 3.8 c, Table 1).

-

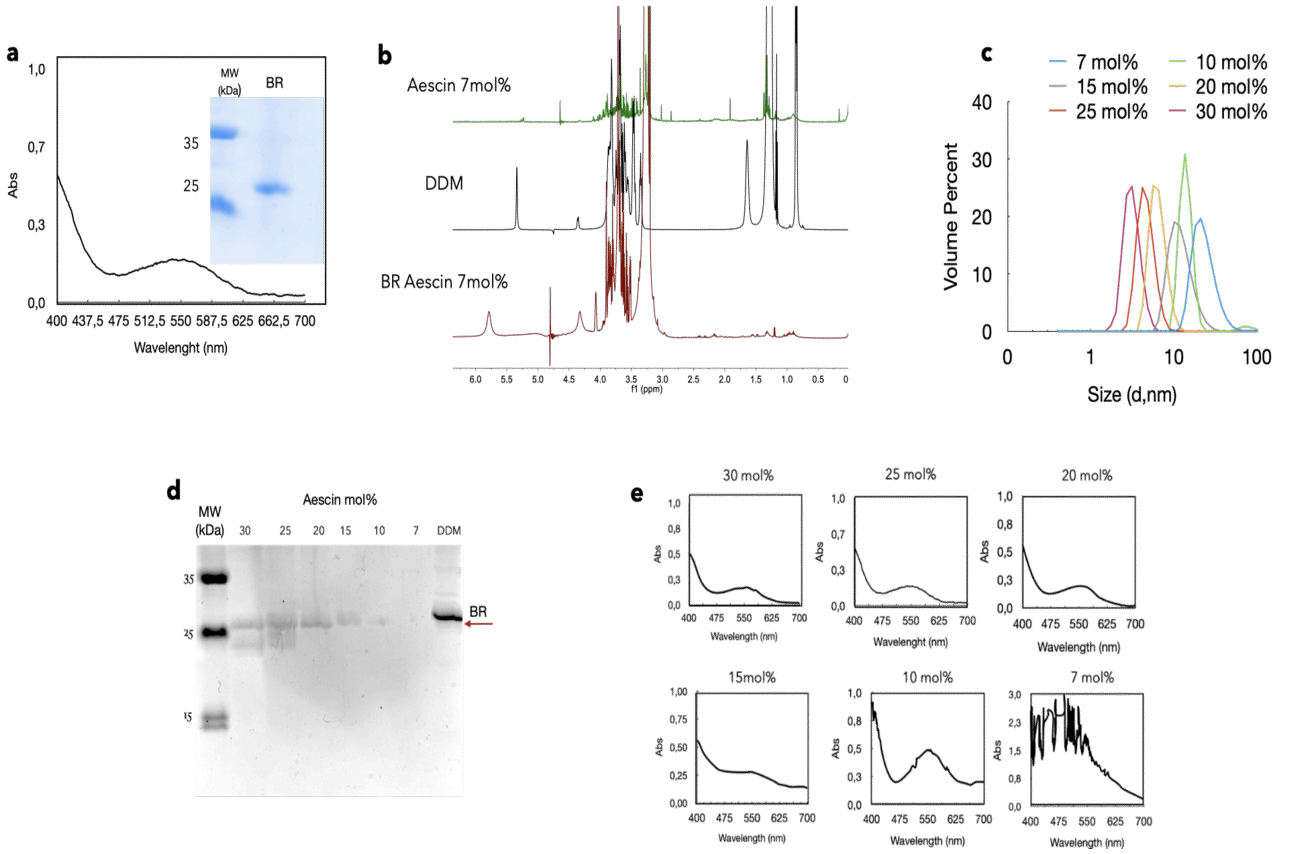

Figure 3.8 Analysis of transfer of BR from DDM micelles into aescin-DMPC particles using spin centrifugal filtration. *a) Absorption spectrum of BR after transfer from DDM micelles into aescin-DMPC particles (25% aescin at room temperature). The absorption peak at 550 nm demonstrates the presence of folded BR. The insert shows SDS PAGE results of DDM refolded BR at high purity used as starting material for the transfer into aescin-DMPC particles. b) 1D NMR spectra showing effective removal of DDM. c) DLS data of resulting particles using different aescin: DMPC ratios. d) SDS PAGE results detecting soluble fraction of BR in aescin: lipid particles at indicated aescin ratios. e) Absorption spectra of BR in respective aescin: DMPC particles.*

SDS-PAGE analysis further suggests that the solubility of BR is increased at higher aescin concentrations (Fig. 3.8 d). Absorbance data show that functional BR is found for all ratios excluding 7% aescin, which did not enable detection due to increased level of protein precipitation and low solubility (Fig. 3.8 e). While the applied sample preparation method appears to be effective for most tested conditions, it generally affects the effective aescin: lipid ratio in the resulting sample due to the different and not fully deductible effects of the centrifugal filter membrane on the dynamic exchange of aescin: lipid particles. In addition, the preparation will lead to large access of empty (i.e., not BR-containing) particles. Hence, the DLS data does not allow us to determine the size of BR containing aescin: lipid particles.

-

We, therefore, applied a second procedure to transfer BR from DDM micelles into aescin: lipid discs. We immobilized the BR in DDM micelles on Ni-NTA agarose beads to enable a more accurate exchange of the applied conditions and not accumulate empty bicelles. The resulting samples show a less pronounced decrease in particle size with increasing aescin concentrations (Fig. 3.9 a, Table 1). An explanation that would be consistent with this observation would be that the DLS data is predominantly detecting the empty bicelles included in the elution buffer. We, therefore, repeated the same setup but using an elution buffer without additional aescin (Fig. 3.9 b Table 1). The resulting particles show a large increase in particle size. This observation can be explained either by isolating only BR-containing discs and/or by reassembly of the aescin: lipid particles due to dilution of the total aescin concentration. To test a possible reassembly of aescin: lipid: BR particles, we added 4-fold excess of empty aescin: lipid particles to the respective preparations. DLS analysis shows a noticeable decrease in particle size for all tested conditions (Fig. 3.9 c, Table 3.1).

Table 3.1. Scattering Lengths of the respective aescin mol %

Aescin mol %	Hydrodinamic radius (nm)		
	Centrifugalfilter	Ni-NTA	
		w/ aescin	w/o aescin
7	19.6	24.2	18.4
10	13.52	13.5	21.0
15	6.9	10.75	23.11
20	5.61	10.8	18.0
25	4.18	11.9	15.6
30	3.61	8.1	10.6

To test whether this observation is caused by averaging effects in the DLS detection, we recorded comparable data on a two-particle system comprising fixed-size MSP-derived nanodiscs with a diameter of 8.3 nm (figure 3.9 d).

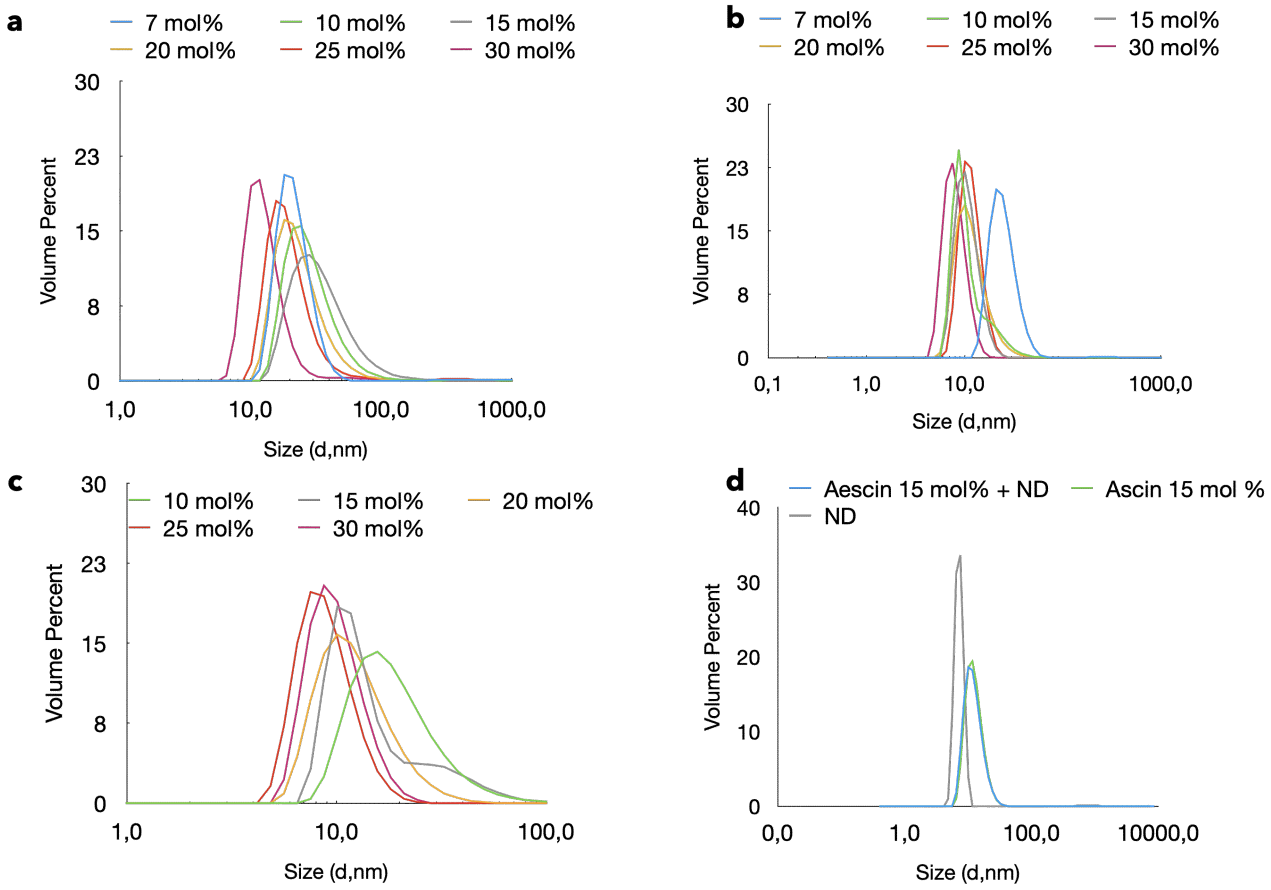

Figure 3.9 DLS profiles of resulting particles using different aescin: DMPC ratios

The data demonstrate that DLS is not capable of separating the respective particle sizes in heterogeneous mixtures. Therefore, our data on diluted ascin: lipid: bR particles suggest that DLS is predominantly detecting empty bicelles.

Conclusion

Overall, our data show that aescin: lipid particles allow stabilizing transmembrane proteins while still maintaining their intriguing properties of changing the particle size. This may open up exciting new avenues of the aescin system as a size-tunable platform for future structural and functional studies of (trans-) membrane proteins.

Chapter 4. Nanodiscs & DNP

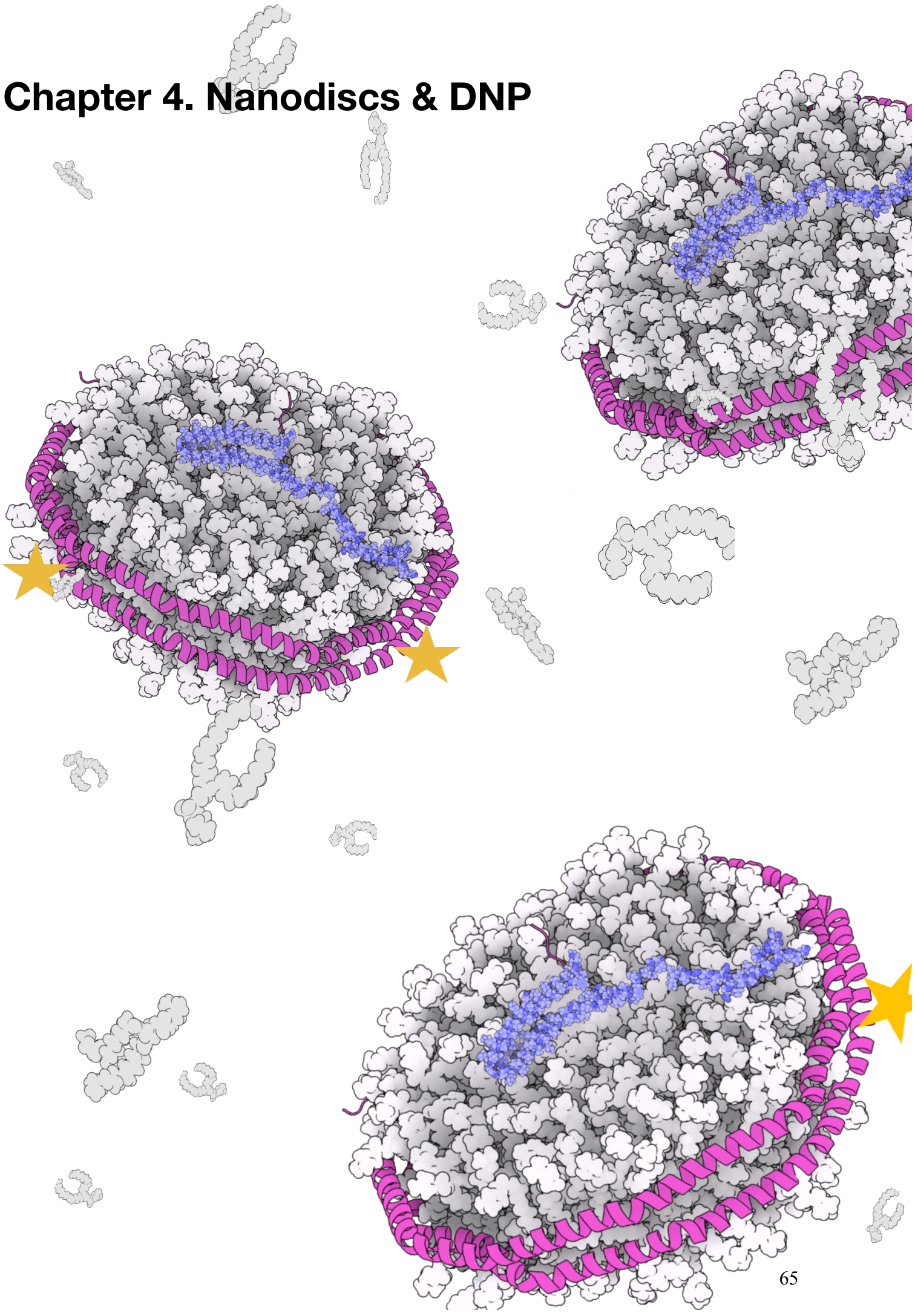

Chapter 4: Nanodiscs & DNP

This chapter reflects to content of the following publication:

Selective hyperpolarization of membrane associated systems

by:
Baran Uluca-Yazgi[#], Fatima Escobedo-Gonzalez[#], Thibault Viennet, Hamed Shaykhalishahi, Luis Gardon, Nina Becker, Chetan Poojari, Wolfgang Hoyer, Olivier Ouari, Henrike Heise, Manuel Etzkorn
(#contributed equally)

status*: in preparation*

Abstract

Interactions of proteins or peptides with membranes can modulate important biological processes. Often these interactions are transient and in equilibrium with non-membrane interacting populations of the protein or peptides in solution. For ensemble techniques, such as NMR spectroscopy, low-populated membrane-associated states are consequently difficult to characterize. Here we present a general platform to selectively investigate membrane-associated conformations in samples that contain soluble and membrane-bound proteins in equilibrium. The method relies on selective hyperpolarization of lipid-bilayer nanodiscs and is therefore also applicable without physical separation of the different species. Selective hyperpolarization is achieved via covalently attaching a modified version of the AMUPOL biradical to the scaffold proteins stabilizing the nanodisc. While, here the application of the system is demonstrated for the membrane interactions of the α-synuclein protein, which is associated with Parkinson's disease, the setup generally enables label-free investigation of a large variety of target proteins. Due to its well-defined character, it additionally enables addressing fundamental questions related to DNP-transfer mechanisms.

Introduction

Transient membrane interactions can have important implications in modulating signaling processes and/or disease-related misfolding events [21], [160]–[163]. One prominent example of the latter is the membrane interaction of the protein α-synuclein (aSyn), which can be inhibited as well as promoted via different membrane binding modes [164], [165].

Noteworthy, a membrane-induced nucleus may represent a putative starting point of the aSyn aggregation pathway. Therefore, it may be one of the most interesting states in the context of aSyn's amyloid-fibril formation. This holds true from a fundamental mechanistic interest in the process as well as from a pharmacological perspective. However, it could be established that this state can only be reliably generated in vitro in the form of a dynamic equilibrium consisting of lower amounts of membrane-attached (possibly nucleating) aSyn proteins and access to soluble (in this context, not interesting) aSyn proteins. Albeit specific insights could also be generated via freeze trapping different species after (partly) separation [166], the thermodynamics of amyloid fibril formation and the involved exchange processes will generally disfavor preparation of well-defined membrane associated species in the nucleation phase complicating conventional ensemble readouts.

In addition to distinguishing membrane and soluble species, sensitivity is frequently a limiting factor in the investigation of low-populated membrane-associated states. Dynamic nuclear polarization (DNP) has largely contributed to overcoming many sensitivity limitations in various biological systems [167]. The required polarizing agents are normally equally distributed in the sample (i.e., being soluble in the applied buffer) to enable homogenous hyperpolarization of all molecules within the sample [168]. In addition, a number of dedicated approaches to enhance the sample of interest more specifically have been introduced [169]–[177].

In general, the characterization of low-populated membrane-associated states would benefit from a combination of signal enhancement and selectivity of the membrane-bound fraction. To realize this, we designed a universal platform to direct hyperpolarization (only) to membrane-associated proteins. Via covalent attachment of a new MTSSL-modified variant of the AMUPOL biradical (Fig. 4.1, mAMUPOL) to cystine mutations specifically introduced in the Membrane-Scaffold-Protein (MSP), we show that well-defined nanodiscs containing AMUPOL radicals in the belt can be generated. Under targeted-DNP conditions, these allow to selectively hyperpolarize of the whole nanodisc system, including lipids and membrane-bound species of the target protein. The rather well-defined composition and size of the nanodisc system also allowed quantifying fundamental properties of the DNP-transfer mechanism. In this respect, we show that a single copy of biradical on the MSP protein results in considerably higher enhancements as an MSP variant containing two AMUPOLs, indicating detrimental couplings between the radicals in the given geometry. Furthermore, our data demonstrate that, under the applied conditions, one AMUPOL suffices to enhance thousands of ^{1}H nuclei.

-

Material & Methods

a-Synuclein expression and purification were carried out as previously described [178], [179] in short:

Escherichia coli *BL21 DE3* was transformed by utilizing the plasmid pT7-7. The cells were grown in LB medium supplemented with 100mg/mL of ampicillin; protein production was induced at OD 1-1.2 with 1 mM Isopropyl β-D-1-thiogalactopyranoside (IPTG) and, after 4 h at 37°C cells were harvested by centrifugation in a Beckman Avanti J25 centrifuge with a JA-20 rotor at 6000 rpm (Beckman Coulter, Fullerton, CA). The cell pellet was resuspended in 20 mM Tris-HCl pH 8.0, 1 mM EDTA, 1 mM PMSF, and lysed by multiple freeze–thaw cycles and sonication. The cell suspension was boiled for 20 minutes at 95 °C and centrifuged at 15,000 xg for 30 min. The remaining soluble aSyn was collected and subjected to an ammonium sulfate precipitation by adding saturated ammonium sulfate solution to 50% saturation at 4 °C. After 30 minutes under agitation, the solution was centrifuged at 15,000 × g and 4 °C. Precipitated protein was resuspended in 50 mL of 50 mM Tris-HCl pH 8,0 sterile-filtered, and loaded onto an ion exchange chromatography column (HiTrap Q FF, GE Healthcare), the elution was carried up using a salt gradient from 0 mM to 600 mM NaCl. A-Synuclein was eluted at 300 mM NaCl in 50 mM Tris-HCl pH 8. Elution fractions were subjected to a second ammonium sulfate precipitation and purified by SEC on a Superdex 75 10/ 300 (GE Healthcare) previously equilibrated with 20 mM sodium phosphate pH 7.4, 50 mM NaCl. Purified-protein concentration was estimated from the absorbance at 275 nm using an extinction coefficient of 5600 $M^{-1}cm^{-1}$.

Membrane scaffold protein expression and purification

Membrane scaffold protein expression and purification were done as previously reported [109], [180], [181]. Briefly, *E. coli BL21 (DE3)* bacteria were transformed with MSP1D1-wt, -G27C, or -G27C A162C plasmid DNA in the pET28a vector. Cells were grown in LB medium supplemented with 50 µg/L kanamycin. The culture was grown for approximately four hours until it reached an optical density of 0,7, induced by 1 mM IPTG, and incubated 5–6 h at 37 °C. Pelleted-down cells were resuspended in 50 mM Tris-HCl pH 8, 500 mM NaCl, 6 M Gdn-HCl, and lysed by sonication (Sonopuls MS72 probe; Bandelin, Berlin, Germany). Proteins were purified by immobilized metal ion affinity chromatography. The elution fractions were pooled and dialyzed against 100-fold 200 mM Tris-HCl pH 7.5 and 100 mM NaCl. Enzymatic cleavage was performed by adding TEV protease in a 1:50

molar ratio overnight at 4°C in order to remove the N-terminal His-tag. ΔHis-proteins were purified by reverse IMAC and concentrated to the desired molarity using a Vivaspin 20 (MWCO: 10kDa, Sartorius).

Nanodisc assembly and spin labeling

Nanodiscs were assembled according to established protocols [20], [182]. In short, in order to remove chloroform from the1-Palmitoyl-2-oleoyl-sn-glycero-3-(phospho-rac-(1-glycerol) (POPG) lipid stock (Avanti Polar Lipids, Alabaster, AL). The lipids were dried under nitrogen flow and stored under vacuum overnight. The resulting lipid film was solubilized in lipid resuspension buffer (20 mM Tris-HCl pH 7.5, 100 mM NaCl, 5 mM EDTA, 60 mM Na-cholate). ΔHis-MSP1D1-wt or single and double cysteine variants were mixed with the appropriate amount of lipids (MSP: POPG molar ratio was calculated from geometrical considerations). The mixture was supplemented with fresh 5 mM DTT per each cysteine residue in the sequence of the MSP1D1 variant. 40% w/v of previously washed Biobeads SM-2 (Biorad) were added, and the mixture was incubated overnight at room temperature. The Biobeads were then removed by centrifugation, and 40% w/v of fresh Biobeads were added. The mixture was incubated for an additional 2 h.

A buffer exchange of Single and double cysteine label Nanodiscs was performed in order to remove the reducing agent in a PD10 desalting column pre-equilibrated with 50 mM sodium phosphate pH 7.5, 150 mM NaCl. The elution fraction was dropped directly into a clean 1. 5 mL conical tube containing MTSL solution that will be used to label the protein with the paramagnetic biradical probe AMUPOL-MTSSL (1-oxyl-2,2,5,5-tetramethyl methanethiosulfonate) previously dissolved in 100% D_2O

The assembled Nanodiscs were purified by SEC on a HiLoad 16/600 Superdex 200 pg column (GE Healthcare) equilibrated with 50 mM sodium phosphate pH 7.5, 150 mM NaCl using a flow rate of 1 mL/min. Homodisperse nanodiscs were pulled down and concentrated to the desired molarity using a Vivaspin centrifugal device of 10 kDa MWCO.

A second buffer exchange was done using a Vivaspin centrifugal device of 10 kDa MWCO to get the final concentration of 6 mM NaPi pH 7.5, 10 mM NaCl in 100% D_2O; after that 60% glycerol was added.

Dynamic Nuclear Polarization (DNP) NMR spectroscopy

DNP experiments were carried out following a stabilized methodology previously described [166], [178] using a wide-bore Avance 600 MHz spectrometer (Bruker, Billerica, MA) connected to a 395.18 GHz second-harmonic gyrotron as a source of continuous microwaves. The samples were prepared from non-acetylated αS (250 μg) in the presence

of 2:1 and 64:1 molar ratios of 100% POPG NDs. The final buffer conditions in the sample were 15 mM sodium phosphate pH 7.4, 25 mM sodium chloride, 30% D_2O, 60% glycerol-d6, 10% H_2O, and 2.5 mM AMUPOL. The samples were filled into 3.2-mm sapphire rotors, and experiments were performed at a temperature of 100 K. All experiments were recorded using a recycle delay of 5 s. Two-dimensional [^{13}C-^{13}C]-proton-driven spin diffusion (PDSD) spectra with 1 s mixing time were recorded using 300 t1 increments with 48 or 64 scans. All PDSD spectra were recorded at a magic angle spinning frequency of 9 kHz. Two-dimensional ^{13}C-^{13}C double quantum/single quantum (DQ/SQ) SPC5 spectra were recorded at a magic angle spinning frequency of 8.2 kHz. The maximum evolution time was set to 1.3 ms. For all samples, ^{1}H decoupling using SPINAL-64 with a decoupling field of 104 kHz was employed during evolution and detection periods. All NMR spectra were processed with the software TopSpin 3.2 (Bruker).

Results and Discussion

Design of a lipid bilayer nanodisc platform for targeted DNP

Nanodiscs are a particularly stable and well-characterized membrane mimetic system. They come in a range of fixed diameters, have planar bilayers, and can accommodate many different lipids and lipid mixtures. We hypothesized that combining the nanodiscs system with our previously reported targeted-DNP approach [169] would create a general platform to characterize low-populated membrane-associated processes.

To validate our approach and to improve our previous targeted-DNP setup that relied on the usage of TOTAPOL biradicals, we first generated a chemically modified variant of the more potent AMUPOL biradical (mAMUPOL). The introduced MTSSL modification can be used to attach mAMUPOL to cysteine residues via established protocols. To enable selective mAMUPOL positioning in the belt of the nanodiscs, we introduced cysteine mutations on the MSPD1 protein, which otherwise does not contain any cysteine residues. Using the NMR-solution structure of the slightly shorter MSPD1d5 protein in its nanodiscs-forming conformation [183], we selected two positions in the sequence (64 and 164) that should allow positioning of in total four mAMUPOL (figure 4.1a) biradicals in each quadrant of the belt of one nanodisc with roughly homogenous inter-biradical distances. Biochemical and biophysical analysis shows that homogenous nanodiscs of the expected size can be formed using the new double mutant MSP1 construct (figure 4.1 b). Subsequent biradical labeling using mAMUPOL (figure 4.1c) resulted in the desired nanodiscs (figure 4.1d), which we will refer to in the following as hyperpolarization nanodiscs or, in short, hyperdiscs.

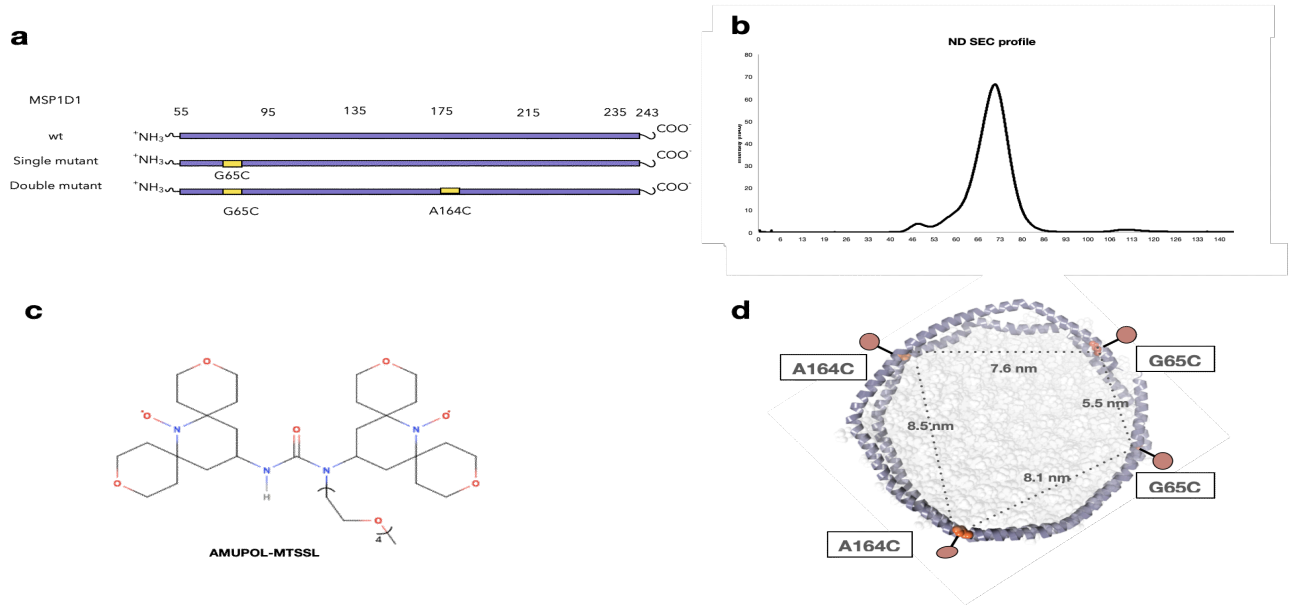

Figure 4.1 Positions of AMUPOL biradical labeling in MSP1D1 sequence **a.** Schematic of MSP1D1 sequence. Positions of introduced Cysteine residues are highlighted in yellow. **b.** SEC profile of the assembled nanodisc after biradical labeling showing homogenous hyperdiscs at the expected elution volumes. **c.** AMUPOL structure **d.** Expected relative positions of mAMUPOL according to the structure of MSP1D1 nanodiscs.

Hyperdiscs enable target-protein hyperpolarization and provide unique insights into DNP spin physics

To test the desired usage of the hyperdiscs we selected aSyn as the target protein, which shows well-characterized interactions with lipid bilayers, including nanodiscs [166], [178], [184]. In this respect, it is established that, depending on the charge and phase of the lipid matrix as well as the aSyn: lipid molar ratio, aSyn will interact with the membrane via different binding modes [166]. Since the interactions are strongest for anionic lipids in the fluid phase and applying only one aSyn per membrane leaflet, we prepared hyperdiscs with a lipid content of 100 % anionic POPG and added aSyn in a ratio of 2:1 (molar, aSyn: hyperdisc). As a reference, we additionally prepared conventional nanodiscs comprising the same lipid content to be measured in a conventional DNP setup using soluble AMUPOL [185]. To reduce spectral overlap in the (low temperature) DNP spectra, selective labeling via the previously described TEASE strategy was applied for the aSyn target protein [166], [186].

The ^{13}C cross polarization (CP) spectrum of the reference sample shows an expected strong enhancement factor ($\sum$) of the buffer (figure 4.2a; glycerol signal with $\sum$ = 150). In addition, the target protein-specific peak also shows strong enhancement (figure 4.2a;

aSyn signal with ∑ = 30). The lower enhancement of the aSyn may be related to a 'shielding effect' of the membrane-bound fraction and/or broadening effects due to the enhancement of different conformers.

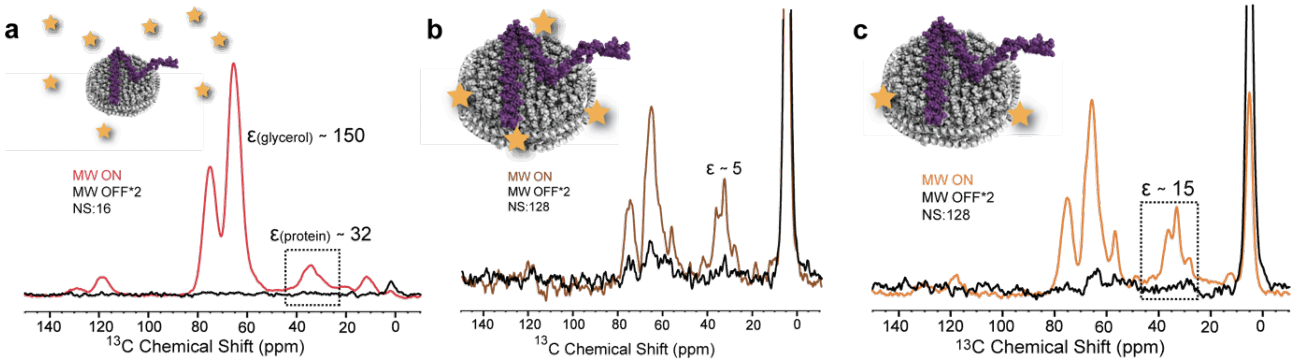

Figure 4.2 Comparison of ^{13}C CP spectra of conventional DNP approach and hyperdiscs **a.** Reference ^{13}C CP spectra using a conventional DNP approach. Red spectrum shows signal under DNP conditions, black spectrum without DNP enhancements conditions. **b.** Target DNP setup using hyperdiscs assembled using the double-mutant MSP construct resulting in attachment of up to four biradical per discs. Brown/black spectrum was recorded with/without DNP enhancement, respectively. **c.** Target DNP setup using hyperdiscs assembled using the single-mutant MSP construct resulting in attachment of up to two biradical per discs. Orange/black spectrum was recorded with/without DNP enhancement, respectively.

To our surprise, the first DNP measurements using hyperdiscs generated with the double mutant MSP construct did only show a moderate enhancement (∑ = 4), which was comparable for buffer and target protein. This enhancement is well below the values obtained in our previous targeted DNP studies on soluble proteins both in terms of absolute enhancement as well as with respect to selectivity [169]. In general, it has been shown before that at concentrations of 10 mM AMUPOL; the DNP enhancement is reduced by about 2-fold due to too close inter-biradical distances [172], [187]. At this concentration, the average inter-AMUPOL distance in the DNP-juice matrix can be calculated to be about 50 nm. Interestingly the inter-biradical distances in the double mutant hyperpolarization discs can be estimated to be in the same range. However, while in the conventional setup, this will be an average distance meaning that also less disturbed biradical contributes to the signal, the hyperdiscs provide a rather well-defined homogenous distance distribution between the biradicals. The resulting considerably stronger decrease of enhancement, therefore, may help to quantify and understand the inter-biradical quenching effects better.

We consequently hypothesized that reducing the biradical density of the hyperdiscs should lead to an increased enhancement of the target protein. To test this hypothesis, we develop a second type of hyperdiscs that are assembled using just a single cysteine

mutant at position 65 of the MSP. The DNP measurements recorded under otherwise identical conditions indeed show a much stronger enhancement of the target protein (Fig, 2 c, $\sum$ = 15). This value is similar to the value obtained for our previous targeted-DNP setup on soluble proteins [169] and only slightly lower than the one obtained in the conventional setup, albeit using about 40-fold fewer radicals in the sample. In general, it can be anticipated that usage of a single biradical per hyperdiscs may even further improve enhancement and selectivity. However, since such hyperdiscs could only be produced by mixing biradical labeled and not labeled variants, the resulting sample will contain all possible combinations of labeled and unlabeled discs, which will consequently lead to reduced enhancements as well as more difficult to interpret heterogenous polarization settings.

Overall, our results support the notion of inter-biradical couplings in the double-mutant-MSP-derived hyperdiscs that are detrimental to the enhancement of the target protein and provide additional quantitative information of on the DNP mechanism. In this respect, it should be noted that, at this point, the inter-biradical distances are only estimated based on the structure of the MSDP1d5, variant and it cannot be excluded that the positions in the used constructs differ and/or that their relative distance is variable to some extent. Still, the overall geometry and molecular composition of the system is well defined and thus allow to provide defined intervals for the possible inter-biradical distances and quantitative insights in the hyperpolarization capability under defined ratios of biradicals to nuclei. Regarding the latter, our data demonstrate that one biradical can effectively hyperpolarize about 9.000 ^{1}H nuclei. The system may also serve further studies to simulate the hyperpolarization transfer mechanism, including the distance and geometric dependence of inter-biradical couplings.

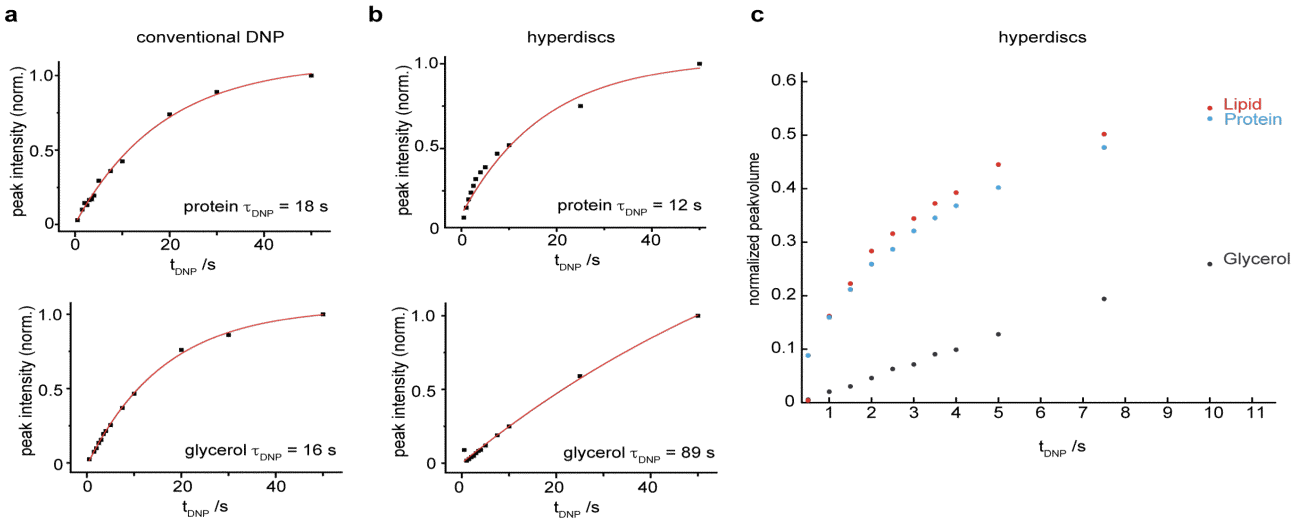

Figure 4.3 DNP buildup curves recorded using a conventional DNP setup (a) and using the (single mutation)

hyperdiscs (b). While buffer (glycerol) and protein signals experience an uniform hyperpolarization buildup in the contentian case (a), the protein signal shows considerably faster buildups, as compared to the glycerol peak, in the hyperdiscs system. (c) Comparison of the initial DNP buildup regime in the hyperdiscs system. The signal buildup of protein (blue), lipid (red) and glycerol (black) signal is shown, revealing substantial selective hyperpolarization of protein and lipids that depends on the applied DNP-polarization times.

Hyperdiscs enable selective hyperpolarization of membrane-associated processes

Next, we investigated whether the hyperdiscs can also provide the aspired selectivity that allows separating membrane-associated processes from the rest of the sample. The first indication of selectivity is the relative enhancement of the buffer (glycerol) and the target protein [169]. Our data indicate that both variants of the hyperdiscs have roughly the same enhancement factors for glycerol and target protein. The equal enhancement factors considerably differ from the selectivity obtained for soluble proteins [169]. However, when looking at the reference aSyn: nanodiscs sample (figure 2a), it is apparent that the properties of the system strongly favor the enhancement of the buffer over the target protein. In this respect, the hyperdisc changes the target-protein-to-buffer enhancement from about 5:1 to 1:1, thus, indeed, directing more hyperpolarization towards the membrane system.

To further evaluate the selectivity of the hyperdiscs, we recorded DNP-buildup curves (Fig. 4.3). The data clearly demonstrate that, while comparable buildup rates are found in the conventional setup, with τ_{DNP} = 18 s and 16 s for protein and glycerol, respectively (Fig 4.3 a), in the targeted DNP setup the polarization buildup is much faster for the membrane attached aSyn nuclei (τ_{DNP} = 12 s) as for the glycerol signals (τ_{DNP} = 89 s) (Fig. 4.3 b). When directly comparing the protein, lipid, and glycerol signal buildup (Fig. 4.3 c), it is clear that the protein and lipid nuclei experience comparable hyperpolarization, which are both considerably faster than for the glycerol signal. This data provides a clear reference for selectivity, which can be tuned via the applied DNP-transfer time.

In general, the molecular features of the buffer's glycerol differ in many aspects from the realistic target protein system. We, therefore, set out to also characterize the hyperdisc platform under more realistic conditions. To this end, we changed the aSyn: ND ratio from 2:1 to 64:1. Under these conditions, a large fraction of the target protein is not membrane attached [169]. Therefore, if the hyperpolarization is confined to the membrane-associated aSyn proteins, we would expect a drop of enhancement by about 4-fold (since all aSyn molecules will contribute to the DNP-off signal, whereas only the approximately 25% membrane-attached aSyn will contribute to the enhancement).

The resulting DNP spectra show the expected behavior for the conventional reference sample (figure 4.4 a) and, indeed, also a strong difference under targeted-DNP conditions. In addition, the relative intensities of the different NMR-active nuclei change (figure 4.4 b). The change in intensity perfectly fits the expected change in the population of membrane-attached aSyn and soluble aSyn. In other words, and since the sample state is well characterized and these conditions, the spectrum corroborates a selective enhancement of (only) the membrane-associated fraction of aSyn.

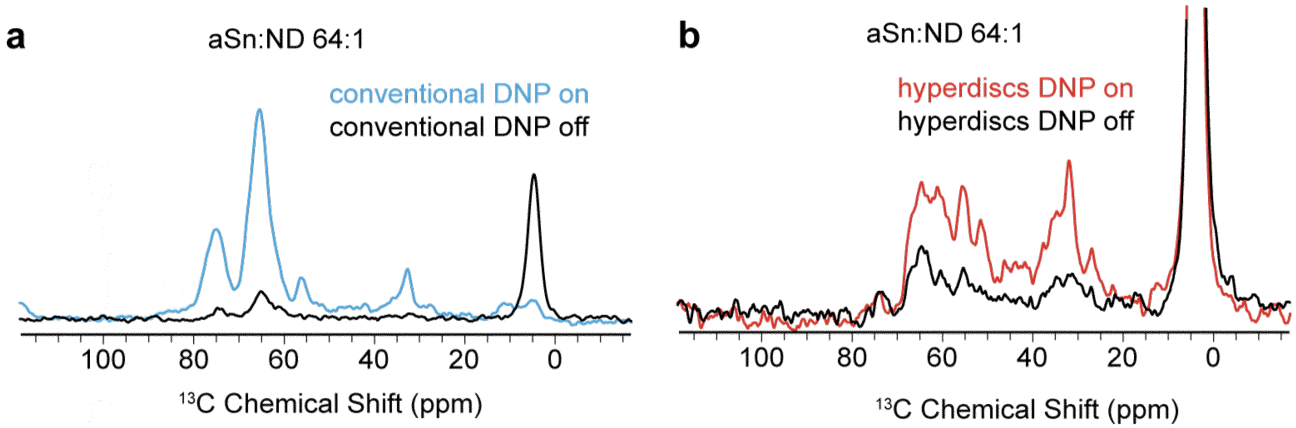

Figure 4.4 ^{13}C CP spectra at large excess of aSyn over nanodiscs (aSyn: ND ratios of 64:1). a) Conventional DNP setup shows expected enhancement comparable to data for a 2:1 ratio (figure 4.2). b) The hyperdiscs setup shows strongly reduced overall enhancement, which is in line with the expected behavior for selective enhancement of the minor population of membrane-associated proteins under this condition. Note that the buffer enhancement is further reduced under these conditions, further promoting selectivity towards the membrane system.

Selecting the membrane-bound conformation of aSyn out of an exchanging equilibrium

Interestingly, when comparing the protein-specific signal in the conventional DNP spectrum to the results obtained with the hyperdiscs, it can be seen that the latter shows a considerably increased ^{13}C linewidth in the 30-40 ppm region (figure 4.5 a). It can be speculated that the increased resolution is related to a selective enhancement of a better-defined membrane-attached conformation. Indeed, that respective frequency is consistent with an α-helical secondary structure, whereas the broad peak shape in the conventional case would be in line with the contribution from different secondary structure elements. This data corroborates that the hyperdiscs platform can indeed generate selective insights into structural features of membrane-associated states.

To further investigate this aspect, we carried out 2D DQ/SQ spectra that allowed us to better characterize the structural features of the respective states [166].

While the spectrum recorded under conventional DNP conditions essentially shows two different α-helical conformations that have been observed before [166] (figure 4.5 b, black), the targeted-DNP setup introduces a clear change in the spectrum by only showing signals for one of the two positions (figure 4.5 b, red). The same behavior is also observed in 2D PDSD spectra (figure 4.5 c). This observation strongly indicates that different conformations are present in the sample, of which only one is directly membrane-associated. We can think of two possible scenarios to explain this finding, i.e., (i) one helical conformation is directly in contact with the membrane, whereas the other one (belonging to the same aSyn protein) is completely surrounded by the buffer, (ii) membrane binding induces α-helical secondary structure in aSyn which is maintained for a while even after the aSyn leaves the membrane surface. The, in general, fast spin diffusion along the protein chain will favor the second scenario, suggesting that our approach may also enable exciting novel insights into the dynamic exchange of membrane induced structural changes and how they propagate. In this picture, the two conformations identified in the data from the conventional DNP setup would originate from the population that is currently attached to the membrane and another population that has already left the membrane but is still in an α-helical conformation, resulting in the second peak. Note that the detected secondary chemical shift for the second conformation would be in line with less pronounced helical features, thus corroborating this picture. Under conventional DNP conditions, it can be assumed that aSyn in each of the two conformations will equally contribute to the total signal [166]. Thus, the data can also provide quantitative information about the respective populations. In this respect, our data suggest that about 60% of the aSyn molecules are α-helical but not (anymore) membrane attached. This would imply that a considerable exchange process between bound and unbound aSyn exists, which is, in part, supported by previous quantitative SEC analysis [178]. Interestingly, our data also provide insights into the structural features of the involved populations, including, for the first time, the state that presumably already left the membrane surface.

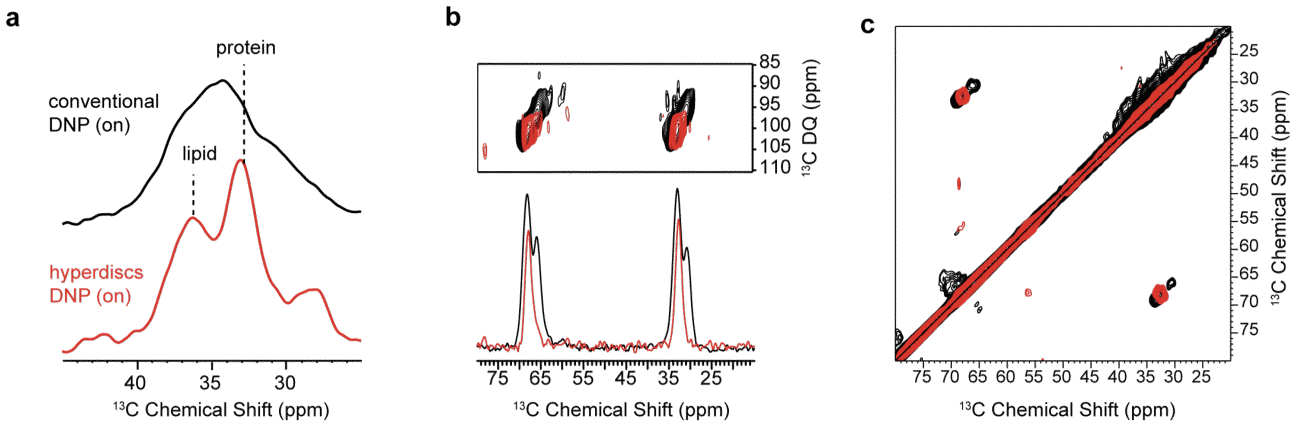

Figure 4.5 Comparison of DNP spectra. Hyperpolarization discs provide new insights into structural features of the target protein at aSyn: ND ratios of 2:1. a) Direct comparison of DNP spectra recorded with conventional setup (black) and using the hyperdiscs platform (red) (spectra are identical to DNP on data shown in figure 4.2a and 4.2c.) b) DQ/SQ spectra of conventional (black) and hyperdiscs setup (red). Lower panel shows 1D projection of relevant spectral extract. c) 2D PDSD spectra of conventional (black) and hyperdiscs setup (red).

Conclusion

We have introduced a general platform that allows us to characterize low-populated membrane-associated states by selectively directing hyperpolarization to a defined membrane system. The hyperdiscs can be used to address a broad range of open questions in structural biology as well as to provide a robust molecular framework to answer fundamental questions regarding the DNP mechanisms.

Using the aSyn system, we directly exploited the inherent benefits of the hyperdiscs platform to disentangle structural features of membrane-associated and 'membrane-released' states. Based on our data, it appears that under the applied conditions, an exchanging equilibrium is formed in which the membrane-induced alterations of the structure of aSyn have propagated to a surprisingly large degree and also to the populations that are not in contact with the membrane (anymore). This observation may have far-reaching implications in the interpretation of most applied data (CD, EPR, NMR) that only reports on the ensemble average conformations.

Overall, we anticipate that by providing new means to selectively investigate membrane-associated processes with atomic resolution, the hyperdiscs platform will resolve a number of persisting open questions in central biological systems.

Chapter 5:
Melanocortin receptor accessory proteins

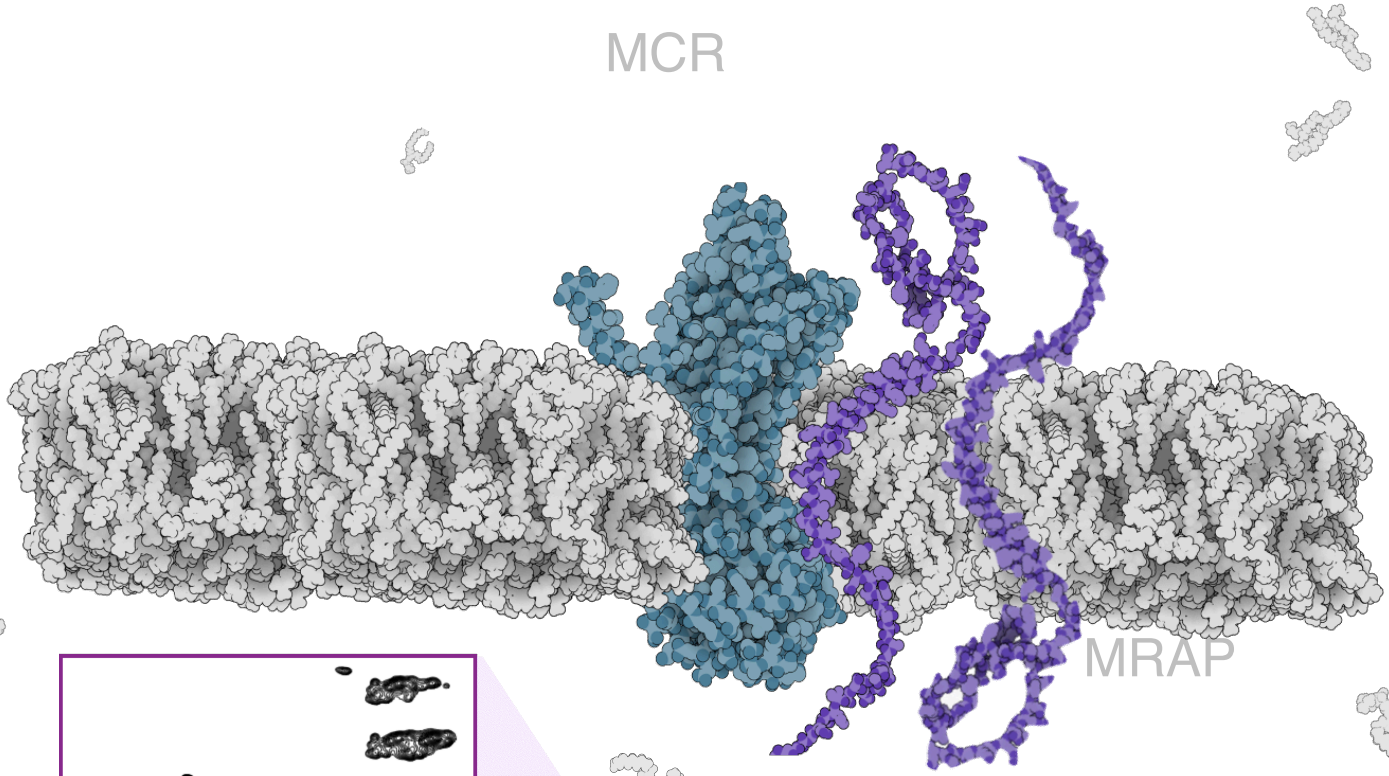

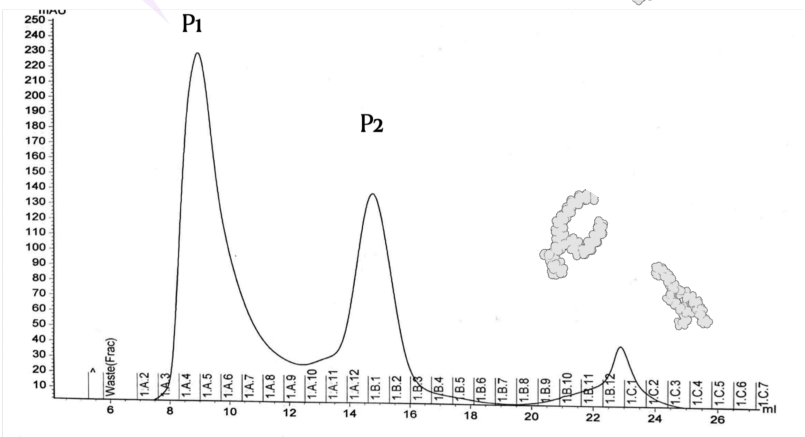

-

Chapter 5: Melanocortin receptor accessory proteins

Melanocortin Receptor Accessory Proteins (MRAPs) are poorly understood but very interesting proteins that play an essential role in promoting the proper functioning of melanocortin receptors and several other GPCRs. The MRAP family consists of two proteins, MRAP1 and MRAP2, about which very little is known so far. To understand more about MRAPs, this chapter provides a brief background of the melanocortin receptor family. It presents our new results obtained in the study of MRAP1 and MRAP2, including their optimized expression and purification using two different expression systems: cell-free expression and bacterial expression, and their reconstitution in different membrane mimetics.

Introduction

Melanocortin receptor system

The mammalian melanocortin receptor (MCR) family consists of five transmembrane G protein-coupled receptors (MC1R, MC2R, MC3R, MC4R, MC5R). These receptors are categorized within the class A (rhodopsin-like superfamily, RLF) [188]. They were primarily associated with skin pigmentation; however, they are now known to be associated with a wide variety of critical reproductive and survival functions, including energy homeostasis, appetite regulation, stress and pain response, growth, sexual behavior, response to UV radiation, and many others.

Structurally, the MCRs belong to the class A GPCRs; they have unusually short extracellular domains [189].

The melanocortin 1 receptor (MC1R), also known as MSHR, is found mainly in the skin. It is activated by its endogenous agonists ACTH and α-MSH, which stimulate melanin production in melanocytes. This receptor has a key role in skin pigmentation and hair color, as well as DNA repair after ultraviolet radiation. Genetic variants of MC1R (RHC variants) present in fair-skinned people and redheads are directly associated with an increased propensity for skin cancer and melanoma in both humans and mice [190], [191].

The MC2R, also known as ACTH (adrenocorticotropic hormone) receptor, was the first MCR to be identified. It is the only one that binds ACTH in a highly selective manner and is the smallest reported associated GPCR [189], [192]. It is abundantly expressed in the pituitary-adrenal glands. Loss or dysfunction of MC2R leads to severe ACTH resistance,

leading to familial glucocorticoid deficiency (FGD). Glucocorticoids are essential hormones such as cortisol and cortisone that regulate cardiovascular, homeostatic, metabolic, and immune functions [193]–[195].

The MC3R and MC4R are essential receptors in energy production and many other processes, including weight regulation, growth, sexual maturation, and fertility. Both receptors are expressed in hypothalamic neurons, particularly in the paraventricular nucleus (PVN), and have an affinity for the same α-MSH agonist.

Deficiency or loss of function in the MC3R is associated with reduced growth, late onset of puberty, and a high proportion of fat to body mass [196].

The MC4R deficiency provokes resistance to insulin syndrome and obesity. The primary role of MCR4 lies in regulating the equilibrium between energetical consumption and food intake, while it also has some influence on appetite control. It has been shown that the injection of its agonists α-MSH and β-MSH reduces the food intake in mice, while the antagonists increase it [197]–[199].

MC5R is expressed in high concentrations in the adrenal glands, as well as in the sebaceous, apocrine, and eccrine glands of the skin, among others. Functionally, it is involved in the secretion of sebum throughout the body. Mutations in this receptor reduce sebum production, weakening the skin's protective barrier, and impairing skin maintenance and thermoregulation. Additionally, MC5R has been implicated in the recovery of skin cells following injuries caused by UV radiation [200].

The MCR system has endogenous agonists, antagonists, and inverse agonists, which makes it especially peculiar among GPCRs. The main agonist ligands for members of the MCR family are melanotropins, peptides found in the pituitary gland derived from the proopiomelanocortin (POMC) gene. MCRs could be activated by the binding of melanocyte-stimulating hormone (α-MSH, β-MSH, γ-MSH, and δ-MSH) and adrenocorticotropin hormone (ACTH), except for MC2R, which is specifically activated by ACTH. MSH ligands retain the core sequence –M–X–H–F–R–W– adopt a β-turn secondary structure required for [201] receptor activation [195]. The natural inverse agonists of the MCR system include agouti protein, agouti-related protein (AGRP), and agouti signaling protein (ASIP). AGRP is an orexigenic peptide consisting of 132 amino

-

acids whose expression occurs predominantly in the adrenal gland and the hypothalamus and, at lower levels of expression, is found in the testes, lungs, and kidneys.

Both agouti and AGRP proteins contain a C-terminal domain composed of ten cysteines, six of which form a structural motif through disulfide bonds known as a cysteine knot. Some studies suggest that the mechanism of agouti proteins regulating food intake also involves interaction with calcium channels due to the presence of the same structural motif in invertebrate toxins. By antagonizing the anorectic effects of the peptide ACTH and other agonist ligands, AGRPs are also involved in the regulation of metabolic rate and food intake. Overexpression of AGRP has been shown to produce hyperphagia and obesity in mice [198], [201]–[203].

The activity of most MCR is further modulated by a family of proteins called melanocortin receptor accessory proteins (MRAPs), which generally promote proper localization of the receptors on the cell surface. Malfunctions of MCR or their accessory proteins that interact with them can trigger serious degenerative diseases, including eating disorders, obesity and anorexia, diabetes, sexual dysfunction, heart disease, cancer, and disorders of skin [201], [204]. Therefore, the study and understanding of the melanocortin receptor system and the MRAP family hold great promise for the development of possible therapeutic targets.

Melanocortin accessory proteins

Accessory proteins are small transmembrane proteins whose function is to modulate the signaling and activity of G protein-coupled receptors. These proteins are found in a wide variety of species, from nematodes to mammals [205], and their selectivity varies greatly; they can act specifically on one receptor or on a wide variety of receptors.

After studying a great diversity of vertebrate species, it was concluded that the orthologs of the MCR family require the presence of an accessory protein for their activation, function, and transit to adrenal cells. This family of proteins is known as MRAPs (melanocortin receptor accessory proteins) [206].

The MRAP family is composed of two unique transmembrane proteins; MRAP1 and MRAP2. Both MRAP1 and MRAP2 can modulate the operation of MCRs [197]. These accessory proteins have very peculiar structural and functional characteristics, such as the formation of antiparallel homodimers when inserted into the cell membrane; that is, they

-

are found in both orientations, both N_{in}/C_{out} and N_{out}/C_{in}. This dual topology is so far an exclusive feature of the MRAP family (figure 5.1).

Both structurally and functionally, MRAPs are unique proteins. They modulate the activation of several G protein-coupled receptors, not only within the melanocortin family but also outside of it. Their activity is not limited to interaction with different families of receptors, as they sometimes act as enhancers and other times as inhibitors.

Melanocortin receptor accessory protein 1 (MRAP1, M1)

MRAP1 in humans has two isoforms, hMRAPα containing 172 amino acids, and hMRAP1β formed by 102 residues. Both α and β MRAP1 are abundantly expressed in adrenal tissue and have a high degree of homology to each other at their 37 and 23 amino acid N-terminal and transmembrane domains, respectively. They differ only in part farthest to the C-terminus. Both MRAP1 isoforms have an LKANKHS and LDYI motif. Regarding the topology, MRAPs show unusual behavior, forming homodimers or higher oligomers in which the N- and C-terminal ends of MRAPs face outwards, contrary to the predictions in which a N_{in}/C_{out} orientation was forecasted. MRAPs are the first eukaryotic-transmembrane proteins and the only ones known until 2007 that form dimers with an antiparallel orientation [207]. This dual topology of MRAPs is due to the presence of a positively charged region near the transmembrane domain, the LKANKHS motif. It is known that when this motif is modified, MRAP1 inserts only in the N_{out}/C_{in} orientation. Furthermore, the LDYI motif not only directs the topology it is also essential for receptor signaling [208].

Functionally, MRAP1 plays a fundamental role in the correct expression and activation of the MC2R; it is associated with the trafficking of the MC2R receptor towards the plasmatic membrane as well as in its signaling. Both MC2R receptor deficiency and mutations in the MRAP1 sequence produce abnormalities in ACTH uptake, resulting in FGD type 1 and type 2 glucocorticoid deficiency, respectively. MRAP1 deficiency is also associated with adrenal disease. MRAP1 is the first known GPCR accessory protein whose malfunction is the cause of human diseases [189], [208].

-

Melanocortin receptor accessory protein 2 (MRAP2, M2)

MRAP2 is predominantly expressed in the cerebrum, hypothalamus, cerebellum, and brainstem of a wide variety of mammals [209]. Structurally, MRAP2 has an amino acid identity with its counterpart MRAP1 of almost 40% in the N-terminal and transmembrane domains [197]. However, MRAP2 does not have the LDYI motif seen in MRAP1. That is why its activity was not initially related to binding to the ACTH ligand. Two shorter variants of MRAP2 have recently been identified: hMRAP2b (154aa) and hMRAP2c (128aa). All MRAP2 variants share identical amino acid sequences in an N-terminus and transmembrane domains (TMD), and they differ in their C-termini [210]. Although much remains to be understood about the activity of MRAP2, it is known that it plays a crucial role in the trafficking of MC2R to the plasma membrane through the formation of the MC2R/MRAP2 complex. The presence of this complex drastically decreases the affinity of the MC2R towards ACTH. Additionally, MRAP2 is also associated with ACTH and MC2R signaling.

The activity of all members of the MRAP family is still unclear. Until now, a peculiarity has been identified between their functions since members of the same family have opposite activities, i.e., MRAP1a and MRAP2c significantly increase cell surface expression of MC3R while MRAP1b decreases it, and MRAP2a and MRAP2b do not effect it [210], [211].

Similarly, MRAP2a has activity as an enhancer of the melanocortin-4 receptor, of the orexin receptor 1 OX1R, in energy homeostasis and glucose homeostasis. In addition, it also acts as an inhibitor of the MC5R receptors and prokinetic receptors 1 and 2 (PKR1, PKR2) whose stimulation, like MC4R, decreases food intake.

Despite its apparent promiscuity to modulate different families of receptors, MRAP2 exhibits a great selectivity toward its targets. For instance, the MC3R receptor, despite belonging to the melanocortin receptor family, does not seem to be included in its molecular targets. However, the mechanisms that govern the selectivity of MRAP2 are not yet known.

MRAP2 deficiency or malfunction is associated with several syndromes and diseases, such as familial Addison's disease, familial glucocorticoid (FDG) deficiency, obesity syndrome in mice and humans, as well as glucose intolerance and insulin resistance.

-

Reasons like its unique structure, its unknown mechanisms towards different families of GPCR, the high selectivity towards its ligands, and its dual role as enhancer and inhibitor make MRAP2 an interesting target for scientific investigations. However, so far, no characterization of any MRAP construct could be reported. Therefore any contribution to the clarification will provide important advances in the understanding of the crucial GPCR accessory proteins in various biological processes, undoubtedly fundamental for the development of new therapeutic applications [192], [194], [195], [212].

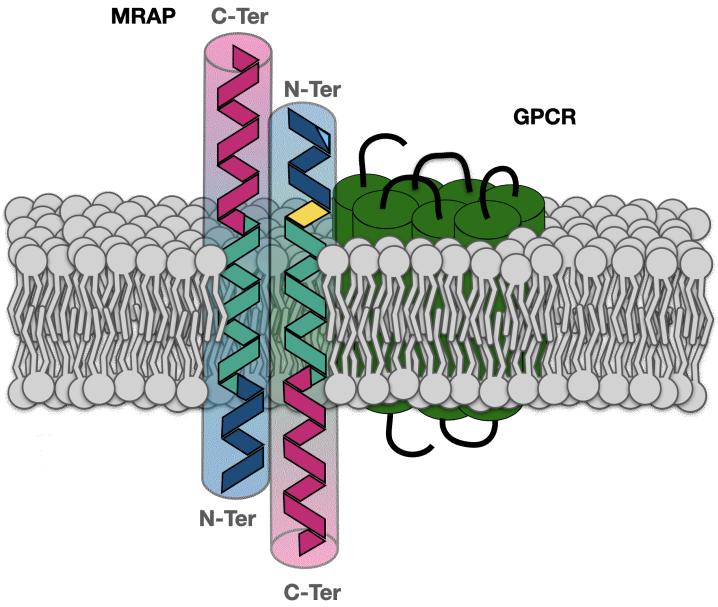

Figure 5.1 General scheme depicting MRAPs' dual topology. These accessory proteins are the first only transmembrane proteins known to date to have two transmembrane orientations (N_{in}/C_{out} and N_{out}/C_{in}).

Material and Methods

Material

IPTG (Gerbu, Gaiberg,Germany),
15N Ammonium chloride (Cambridge Isotopes, Cambridge, USA)
POPG, DMPC lipids (Avanti polar lipids, USA)
Bacto Agar [Becton, Dickinson and Company]
Bio-Beads SM-2 Adsorbent Media [BioRad]
Protino Ni-NTA Agarose [Macherey-Nagel]
Äkta Pure [GE Healthcare Life Sciences]
HiLoadTM 16/600 SuperdexTM 200pg [GE Healthcare Life Sciences]
SuperdexTM 200 10/300 GL [GE Healthcare Life Sciences]
Jasco J-715 Spectropolarimeter [Jasco]
Eppendorf centrifuge 5804R [Eppendorf]

-

NanoDrop 2000 Spectrophotometer [Thermo Fisher Scientific]
Eppendorf centrifuge 5415R [Eppendorf]
Gel-Documentation-System, Universal Hood III [BioRad]

Eppendorf Thermal cycler, Mastercycler epgradient S [Eppendorf]
Beckman coulter Avanti J-26XP centrifuge [Beckman]
Rotors:
JLA 10.500 [Beckman] ▪ JA 20.1 [Beckman]

Media for *E. coli* cultivation All media were autoclaved before use.

Luria Bertani (LB) for **1 L**

Tryptone	10 g
Yeast extract	5 g
Sodium Chloride	5 g

2YT Media for **1 L**

Tryptone	16.0 g
Yeast Extract	10.0 g
Sodium Chloride	5.0 g

M9 Minimal Medium for **1 L**

H_2O	940 mL
SBMX stock solution	40 mL
"S" stock solution	1 mL
"TE" stock solution	2 mL
Thiamine	1 mL
Vitamin stock solution	1 mL
Glucose	2 g
NH_4Cl	1 g

25x SBMX (Stock solution) for **500mL**

K_2HPO_4	87,5 g
KH_2PO_4	16,15 g
NaCl	18,25 g

S" stock solution for **100 mL**

K_2SO_4	4,8 g

"TE" stock solution for **500 mL**

$MgCl_2$ $6H_2O$	28.8 g
$FeCl_2$ – stock solution	10 mL

FeCl2 – stock solution for **100 mL** in 50% EtOH

Vitamin stock solution for **1 L**

-

HCl concentrated	10 mL
$FeCl_2 * 4H_2O$	5 g
$CaCl_2 * 2H_2O$	184 mg
H_3BO_3	64 mg
$MnCl * 4H_2O$	40 mg
$CoCl * 6H_2O$	18 mg
$CuCl_2 * 2H_2O$	4 mg
$ZnCl_2$	340 mg
$Na_2MoO_4 * 2H_2O$	605 mg

Biotin (vitamin B7)	2,2 mg
Folic acid (vitamin B9)	2,2 mg
PABA (para-aminobenzoic acid)	220 mg
Riboflavin (vitamin B2)	220 mg
Pantothenic acid (vitamin B5)	440 mg
Pyridoxine HCl (VitaminB6)	440 mg
Thiamine(vitaminB1)	440 mg
Niacinamide(vitaminB3)	440 mg

Buffers and solutions

Buffer for MRAPs purification by IMAC and SEC

Buffer A	
NaPi	20mM
NaCl	50mM

Buffer B	
NaPi	20 mM
NaCl	50mM
Urea	6 M

Buffer C	
NaPi	20 mM
NaCl	50mM
Urea	6 M
Imidazole	10mM

Buffer D	
NaPi	20 mM
NaCl	50mM
Urea	6 M
Imidazole	20mM

Buffer E	
NaPi	20 mM
NaCl	50mM
Urea	6 M
Imidazole	300mM

Buffer for MSPs purification and ND assembly

Buffer I	
Tris-HCl	50 mM
NaCl	500 mM
Urea	6 M

Buffer II	
Tris-HCl	50 mM
NaCl	500 mM
Triton X-100	1%

Buffer III	
Tris-HCl	50 mM
NaCl	500 mM
Triton X-100	1%
Na-cholate hydrate	60 mM

Buffer IV	
Tris-HCl	50 mM
NaCl	500 mM
Triton X-100	1%
Imidazol	20mM

Buffer V	
NaCl	500 mM

Buffer VI	
Tris-HCl	50 mM

-

Triton X-100	1%	NaCl	500 mM
Imidazole	20mM	Triton X-100	1%
		Imidazole	250mM

Lipid-Resuspension buffer

Tris-HCl pH 7.5	20 mM
NaCl	100 mM
EDTA	1 mM
Na-cholate hydrate	60 mM

Methods

Cloning, MRAP1, MRAP2, MRAP22

The human mrap1α, mrap2, and mrap22 (a double MRAP2 construct) genes were ordered as a DNA fragment (Thermo Fisher). They were amplified and incorporated into the vectors Pivex-2.4d and pET-28a using the designed primer pair. The accuracy of the cloned genes was confirmed by sequencing.

MRAP1 and MRAP2 were expressed following two different strategies I) *E. coli* expression and II) Cell-free protein expression. In both cases, the respective fusion protein constructs comprise a 10x N-terminal His-tag followed by a SUMO cleavage tag and the MRAP sequence. In the special case of M22, the fusion construct continues with an additional TEV cleavage site followed by a second MRAP2 sequence see (figure 5.2).

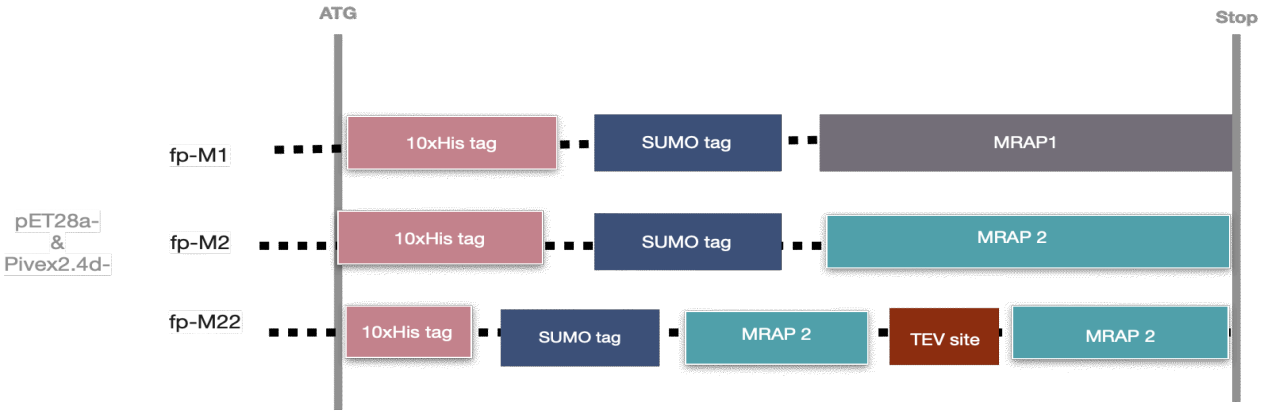

Figure 5.2. Constructs of the fusion protein (FP) that generates M1, M2 and M22. The Pivex-2.4d and pET-28a vectors were used to express the three proteins in a cell-free and bacterial expression system, respectively. FPs are conformed of a 10 His tag, a sumo recognition site, and the respective MRAP sequence.

-

I) Bacterial expression

Transformation

For *E. coli* expression, the three construct genes were cloned in the expression vector pET-28a (+). 50 µL of electrocompetent *E. coli* cells were transformed using 1 µL of plasmid (60ng/µL) in a 2 mm electroporation cuvette. After electroshock, cells were incubated in 1 mL in a fresh Eppendorf tube for 1 h at 37°C with gentle shaking. After the incubation time was up, 200 µL of transformed cells were transferred onto an LB plate supplemented with appropriate antibiotics. The plate was incubated at 37°C overnight.

Expression test

To optimize the expression of the recombinant proteins and the culture parameters, different bacterial strains, culture media, and temperatures (27°C and 37°C) were tested.

E. coli Rosetta (DE3), BL21, C41, and C43 strains were tested to determine the most appropriate bacterial strain to express the target proteins. 5 mL of sterilized 2YT medium was inoculated with bacteria from a single colony on the agar plate and incubated overnight at 37 °C. The next day 50 mL of fresh medium was inoculated with the preculture. The culture grew at 27 °C for 12 h. The cell pellets were harvested by centrifugation. The pellet was resuspended in 1 mL of lysis buffer. The crude extracts were analyzed by SDS -PAGE so that the best strain was identified. Several expression media were also evaluated. Assays were performed using nutrient-rich media such as LB and 2xYT and nutrient-deficient media M9 (details of media optimization are in chapter 6).

MRAPs overexpression and purification

All used media were autoclaved before use and supplemented with the antibiotics (50 µg/mL kanamycin, additionally, when expressed in the Rosetta strain, 30 µg/mL chloramphenicol was also added).

In the expression test, a preculture of the selected strain, was incubated overnight at 37°C and 120 rpm. The main 3L M9 media culture was inoculated from the preculture at an optical density (OD600) of 0,05. After approximately 4h of incubation at 37°C and 120 rpm, the expression culture density reached an optical density of 0.7-0.9. Hence, protein production was induced by adding IPTG to reach a final concentration of 1 mM. The expression was carried out at 27°C and 120 rpm for a duration of 12 hours. The cell pellet

-

was harvested after 10 min of centrifugation at 6000·g at 4 °C. The cell pellet was stored at -80°C or directly resuspended for protein extraction and purification.

Protein solubilization and purification

The MRAPs were purified from the inclusion bodies (IBs) as follows. First, lysis was performed without adding any chaotropic agent to remove contaminating proteins. Harvested cells were resuspended in a 5-fold wet-pellet weight of Buffer A supplemented with a Protease Inhibitor cOmplete Mini (Roche) cocktail tablet and 5 µg/mL DNase I. The lysis was performed by single-pass high-pressure homogenization (HPH) at 2400 bar. The soluble part was separated from the cell pellet by centrifugation at 18000g for 30 min. After centrifugation, the soluble fraction was discarded, and the remaining insoluble fraction was resuspended in buffer B containing an EDTA-free protease inhibitor cocktail and supplemented with 6M urea to solubilize the proteins. The solubilization of MRAPs was performed using the high-pressure homogenizer and the same pressure condition as previously described. The soluble protein was separated from cell debris by pelleting at 18,000 g for 45 min at 4 °C. After centrifugation, the solubilized protein was transferred to a fresh reaction vessel, and imidazole was added to reach a final concentration of 10 mM (buffer C) to minimize the unspecific binding. The protein was incubated for 30 min at 4°C and using gentle agitation with 2 mL of Ni-NTA resin previously equilibrated with buffer C. The lysed and resin mixture were poured into a 10-mL purification column allowing the resin to settle by gravity. The resin was washed 5 times with 2 CV of buffer C and 5 times with 2 CV of wash buffer D to remove contaminating proteins. The MRAP was eluted from the agarose by adding 5 CV of elution buffer E, and it was later stored at 4°C until its purification by SEC.

A gel filtration column (HiLoad 16/600 Superdex TM 200 pg (GE Healthcare)) was equilibrated with buffer B (20 mM sodium phosphate, pH 7.4 and 50 mM NaCl, 6M urea). Afterward, the MRAP was injected into the column using an Äkta pure device running at 1 mL/min flow rate. Elution was monitored by UV absorption at 280 nm. Elution fractions of 2 mL each were pooled and concentrated using Vivaspin 20 (MWCO: 10 kDa, Sartorius). The collected peaks were analyzed via SDS-PAGE.

The concentrated fusion proteins of MRAPs were stored at -80°C.

***II) C*ell-free protein synthesis**

-

The genes of the three constructs were cloned into the expression vector pIVEX2.4d. The expression of the MRAPs constructs was optimized starting from previously established protocols for cell-free expression systems based on *E. coli*. [70] During optimization, different concentrations of T7, tRNA, amino acids, and cell extract were tested. Likewise, cell extracts from different bacterial strains (*A19* and *BL21 (DE)*) were also examined.

The expression was carried out in a continuous-exchange cell-free system (CECF) in the absence of additives. 50 µL of the reaction mixture were prepared and dialyzed against the feeding mixture in a ratio of 1:10 using 20 KDa MWCO Slide-A-Lyzer^{TM} MINI Dialysis Devices (Thermo Scientific) in sterile 48-well BD falcon cassettes (Beckton Dickinson, Falcon). The cell-free synthesis was performed for 12-16 h at 28°C and 100 rpm. After the reaction time, the RM was centrifuged at 12000·g for 10 min. The supernatant was discarded, and the resulting protein pellet was washed twice with buffer A (20 mM NaPi, 50 mM NaCl pH 7.4). Then the proteins were solubilized in buffer B (20 mM NaPi, 50 mM NaCl, 6M urea pH 7.4). Finally, the soluble proteins were purified by IMAC using Ni-NTA agarose.

Enzymatic cleavage reaction

Purified fusion proteins were thawed on ice water and 50% diluted with NaPi buffer to reach a final concentration of 3 M Urea; afterward, 1 mM Dithiothreitol was added. For M1 and M2, Ulp1-SUMO protease was added in a ratio of 1:50 and incubated for 24 hours at 4°C with shaking. For M22, the cleavage reaction was performed using TEV protease in a 1:30 ratio incubated overnight at 4°C with 1 mM DTT. In all cases, reverse IMAC was employed to separate the ΔHis-MRAPs from the sumo or TEV protease, His-tag, and the uncleaved fusion protein. The flowthrough containing the ΔHis-MRAPs was concentrated using a Vivaspin concentrator of 10 kDa MWCO and stored at -80°C until further use. The efficiency of cleavage reactions was monitored by SDS-PAGE.

Western-Blotting

Sample fractions were analyzed by western blot. For this, the samples of interest were resolved by SDS-PAGE. Subsequently, a polyvinylidene difluoride (PVDF) membrane (GE Healthcare Europe GmbH, Freiburg, Germany) was activated by washing it in methanol for one minute. The activated membrane and 6x Whatman paper were equilibrated with blotting buffer for 10 min.

-

At the bottom of a horizontal gel electrophoresis chamber (Bio-Rad), 3 layers of Whatman paper were placed, followed by the PVDF membrane, SDS gel, and finally, another three layers of Whatman paper. Air bubbles were carefully removed between each layer. The transfer was performed using a standard 25 V, 0.1 A for 30 min. Once the transfer was complete, the PVDF membrane was blocked with 5% milk powder in TBS-T buffer (20 mM Tris/HCL pH 7.5, 250 mM NaCl and 0.1% Tween 20) for 30 min at room temperature on the roller shaker. The membrane was washed 3 times for 10 min with TBS-T buffer and then incubated in a 1:5000 dilution of rabbit anti-M2 antibody (Abcam) in TBS-T for 3 h at room temperature or overnight at 4 °C with gentle shaking. The next day, the membrane was washed 3 times for 5 min with TBS-T and subsequently incubated with a secondary antibody diluted 1:10,000 (Goat Anti-Rabbit IgG (H+L)-HRP) in TBS-T for 1 h at room temperature. The PVDF membrane was then washed 3 times with TBST and incubated with Super Signal West Pico PLUS chemiluminescent substrate (Thermo Fisher Scientific) for 1 min. The signal was detected using ChemiDoc XRS (Bio-Rad Laboratories GmbH, Munich, Germany).

Membrane Scaffold Proteins (MSP) overexpression and purification

To overexpress MSP1D1 and MSP1D1ΔH5 proteins, *E. coli BL21 (DE3)* cells were transformed using 1 µL of the appropriate plasmid DNA in vector pET-28a (+). The transformation procedure was performed following the same procedure described previously. The expression was done in sterilized 2YT medium supplemented with 50 µg/L kanamycin. The culture was grown for approximately four hours until it reached an optical density of 0,7. Then the over-expression of the MSP was induced by 1mM IPTG. The culture was incubated for 5 h at 37 °C. Cells were pelleted down by centrifugation at 6000 x g for 10 min.

The cell pellet was resuspended in buffer I supplemented with a Protease Inhibitor cOmplete Mini (Roche) cocktail tablet and 5 µg/mL DNase I and lysed by ultrasonic pulses (60% amplitude, 3s on, 3s off, 20 minutes) (Sonopuls MS72 probe; Bandelin, Berlin, Germany) on ice and then centrifuged at 18000 g for 30 min (Beckman J2-21 rotor JA-20.1). The cleared lysate was also incubated with previously equilibrated 2mL of Ni-NTA resin for 30 min to bind His-tagged fusion protein. The resin was washed 4 times with 1 CV of buffer II (1% Triton X-100), 4 times with 1 CV of MSP buffer III (60 mM Na- cholate), 4 times with 1 CV of buffer IV, and 4 times with 1 CV of Wash buffer V. The MSP was eluted

-

by adding 5 times, 1 CV of buffer VI. The eluted MSP was dialyzed against 100-fold NaPi buffer (20 mM NaPi, pH 7.4, 50 mM NaCl, 1 mM Dithiothreitol) using 10K MWCO Snake-Skin™ Dialysis Tubing (Thermo Scientific) to remove urea and imidazole. Enzymatic cleavage was performed by adding TEV protease at a 1:50 molar ratio and incubating overnight at 4 °C. ΔHis-MSP were purified by reverse IMAC and concentrated using Vivaspin 20 (MWCO: 10kDa, Sartorius).

Detergent solubilization

Detergent solubilization of MRAP2 was tested using a detergent screening. The buffer exchange was performed using a PD10 desalting column following the established gravity protocol. Briefly, the MRAP2 sample contained in urea buffer was applied to a desalting column previously equilibrated with buffer A supplemented with either 20 mM sodium dodecyl sulfate (SDS), 100 mM dodecyl phosphocholine (DPC12, Cube Biotech), N, N-100 mM dimethyldodecylamine N-oxide (LDAO, Cube Biotech), or 196 mM n-dodecyl-β-D-maltoside (DDM, Cube Biotech); and eluted from the PD10 column using the same equilibration buffer. The eluted fraction was concentrated with a Vivaspin 10 kDa MWCO concentrator, and 2 mM DTT was added.

MRAP2 reconstitution in lipid bilayer nanodiscs

The MRAP2 and ΔHis-Scaffold Protein (MSP1D1 or MSP1D1ΔH5) were mixed in a ratio of 1:2, respectively. 70- or 50-fold DMPC (1,2-dimyristoyl-sn-glycero-3-phosphocholine) lipids (Avanti polar lipids) were solubilized in 60 mM Na-cholate in 20 mM NaPi, 50 mM NaCl, 2 mM DTT, 1 mM EDTA. When the lipids were completely dissolved, they were incorporated into the protein mixture and incubated for 10 min. After incubation 40% w/v of previously washed Biobeads SM-2 (Bb) were added. The assembly reaction was incubated at room temperature for 1h, the Bbs were then removed by centrifugation and, 20% w/v of fresh Bb were added. The reaction was incubated for 2 hours with gentle agitation. Biobeads were removed once again and the assembled nanodiscs were purified by IMAC using 1mL of Ni-NTA agarose and by SEC on a HiLoad 16/600 Superdex TM 200 pg (GE Healthcare) column, using a ÄKTA pure device running at 1 mL/min

UV-Vis characterizations

All UV-Vis absorption spectra were acquired using an Agilent 8453E UV-Vis double-beam spectrophotometer (Agilent Technologies). UV absorption was measured from 200 µL of

-

protein samples using a 1 cm quartz glass cuvette. Data were collected from 200 to 800 nm in 1 nm increments. All spectra were blank-corrected using the buffer contained in each sample.

Results and discussion

Cloning, MRAP1, MRAP2, MRAP22

The sequencing results confirmed that the cloning was successful in both plasmids pET-28-a and Pivex 2.4d.

MRAP expression in *E.coli*

To evaluate the feasibility of in vitro characterization of MRAP1 and MRAP2, expression tests were performed using a pET-28a expression vector and *E. coli BL21(DE), Rosetta, C41,* and *C43* strains. The best results for the expression of the fp-M2 construct in the bacterial system were obtained from the Rosetta strain at a temperature of 27°C for 16 h using an induction concentration of 1 mM IPTG. The expression of fp-M2 was monitored by SDS-page, where an overexpression band of approximately 45 kDa was observed (figure 5,3); however, the theoretical mass expected for the fusion protein of MRAP2 is 36 kDa. This behavior, called `gel shifting,´ in which the protein appears to be larger, is observed in certain membrane proteins [213], [214]. The band that appears at 45 kDa corresponds to fp-M2. This fact was confirmed by Western blot; however, a second band of approximately 30 kDa was overexpressed in all the tested strains; this band is probably resulting in a degradation of the principal band, as seen in figure 5.3.

-

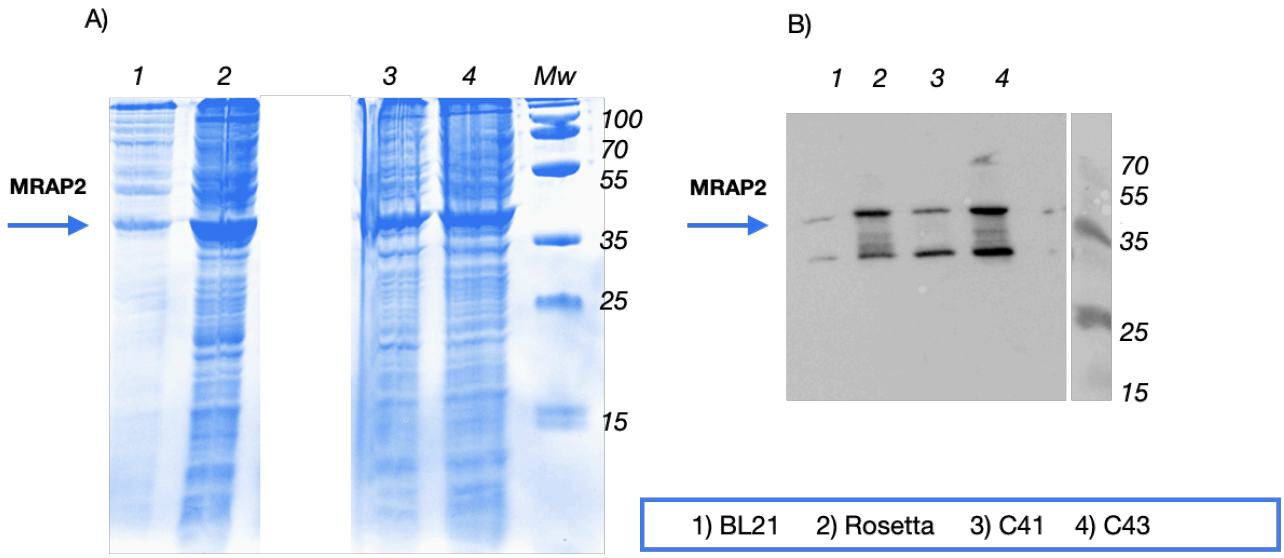

Figure 5.3 SDS-gel of expression test of MRAP2. The expression test of M2 was performed using four different E. coli strains in lane 1: BL21 2: Rosetta 3: C41 and 4: C43. The expression was monitored by A) SDS-page and western blot B).

In the next step, it was confirmed that the protein fp-M2 was expressed both in rich media LB and YT as well as in the minimal M9 medium, which is ideal for the expression of the isotopically labeled proteins, necessary when performing NMR studies. It was also surprisingly observed that in the M9 media, higher production of fp-M2 was obtained (figure 5.4), suggesting that the presence of some of the components of the minimal medium stabilized and improved the production of MRAP2. This fact will be discussed in chapter 6. It was determined that the highest production yield for recombinant unlabeled and ^{15}N-labeled MRAP2 was achieved using Rosetta strain and M9 medium.

-

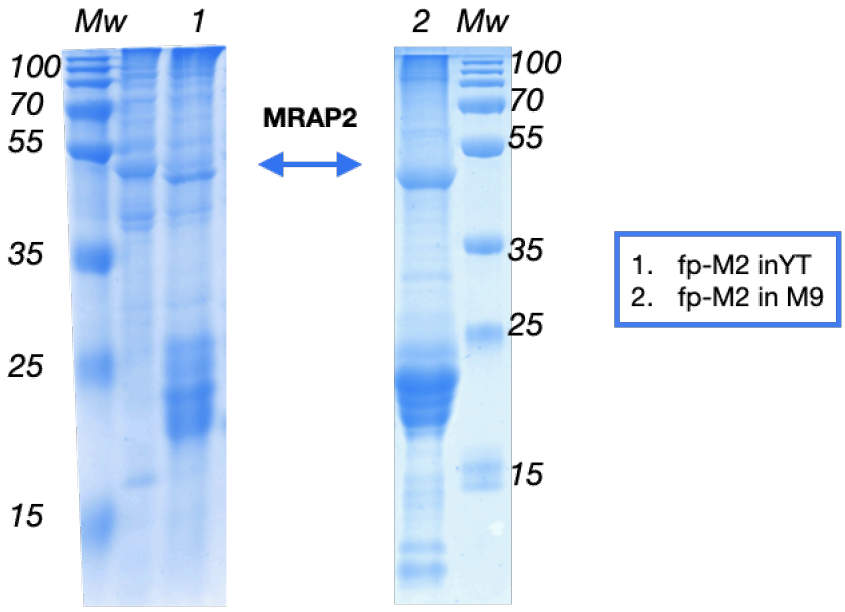

Figure 5.4 MRAP2 expression in 2YT and M9 media. The intensity of the overexpressed M2 band (around 40 kDa increased considerably.

Purification of MRAP2

MRAP2 is a membrane protein, and its overexpression in the insoluble fraction was not surprising due to its nature. To improve protein purification, lysis was first performed in NaPi buffer to remove many soluble proteins. The insoluble fraction containing fp-M2 was separated by centrifugation, and subsequently, fp-M2 was successfully recovered from the insoluble fraction using for that a buffer supplemented with 6M of urea. Fp-M2 was purified by IMAC through several washing steps with different concentrations of imidazole (figure 5.5 A lanes 1,2), and the protein was eluted with a 300 mM imidazole buffer (lane 3). Despite extensive washes, the eluted fraction was not completely pure: it contained two overexpressed bands. Due to their size difference, the IMAC eluted fraction was then injected into a gel filtration column. The sample elution was followed via measuring the absorbance at the wavelength of 280 nm, which is where the maximum absorption of the aromatic rings of the amino acids appears. The chromatogram obtained from the purification by size exclusion shows two protein peaks at 9 and 15 mL of retention volume and an imidazole peak at 33 min of retention time (figure 5.5 B). According to the column calibration standards, the retention volume for the first peak would be similar in mass to the ferritin (440 kDa) and peak 2 to carbonic anhydrase-ribonuclease A (29-13 kDa) molecular mass. The fractions corresponding to each peak were pooled and analyzed by

-

SDS-PAGE (figure 5.5 C) and Western blot (figure 5.5 D and E). As shown in the western blot, the protein purified in the first peak has an affinity to anti-His- and anti-M2-antibodies; it was confirmed that the protein of interest was contained in the first peak despite the unusual retention volume. Both in Coomassie gel and in Western blot, the presence of a band at higher molecular weights of more than 130 kDa is observed. The presence of these higher-order oligomers of fp-M2 coincides with the unexpected retention time for fp-M2.

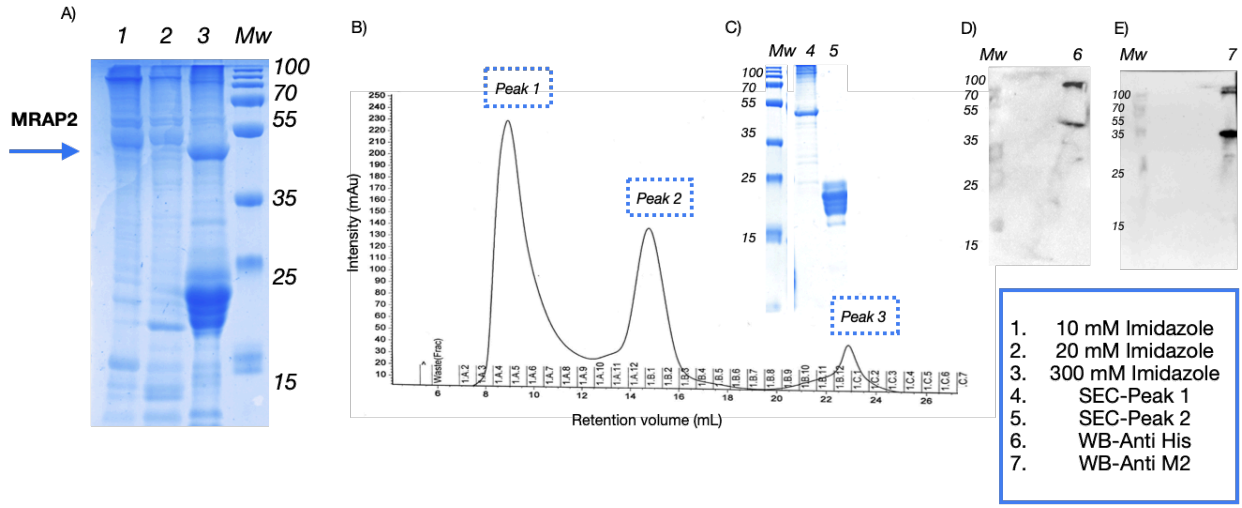

Figure 5.5 Purification of M2. Ni-NTA IMAC performed the first step of purification. The efficiency of purification was monitored by SDS-page A) After several washing steps with 10 mM imidazole (lane1) and 20 mM imidazole (lane 2) the protein was eluted using 300 mM imidazole (lane3); despite the washing steps the Fp-M2 (45 kDa) was not completely pure. SEC was performed to remove the contaminant proteins. The chromatogram B) shows 3 peaks. These peaks were collected and analyzed by SDS-page. P1 and P2 was loaded in lane 4 and 5 respectively. The first peak corresponds to the pure fp-M2. The sample in lane 4 was analyzed by western blot using D) anti His- and E) anti M2-antibody. Positive results of the western blot in lane 6 and 7 confirm that the purified protein contain the His-tag and that is indeed the fp-M2. In all gels it is appreciable the presence of M2-oligomers at higher molecular weights >100kDa; this fact coincides with the unexpected retention volume observed for fp-M2.

To reduce these oligomers, six aliquots of fp-M2 were taken, and different reagents, including SDS, DTT, TCEP, βMe-ETOH, or a higher concentration of 8M urea, were added, respectively. In the SDS gel, it is observed that oligomers from samples to which TCEP, DTT, or βMe-EtOH were added were successfully reduced (figure 5.6).

-

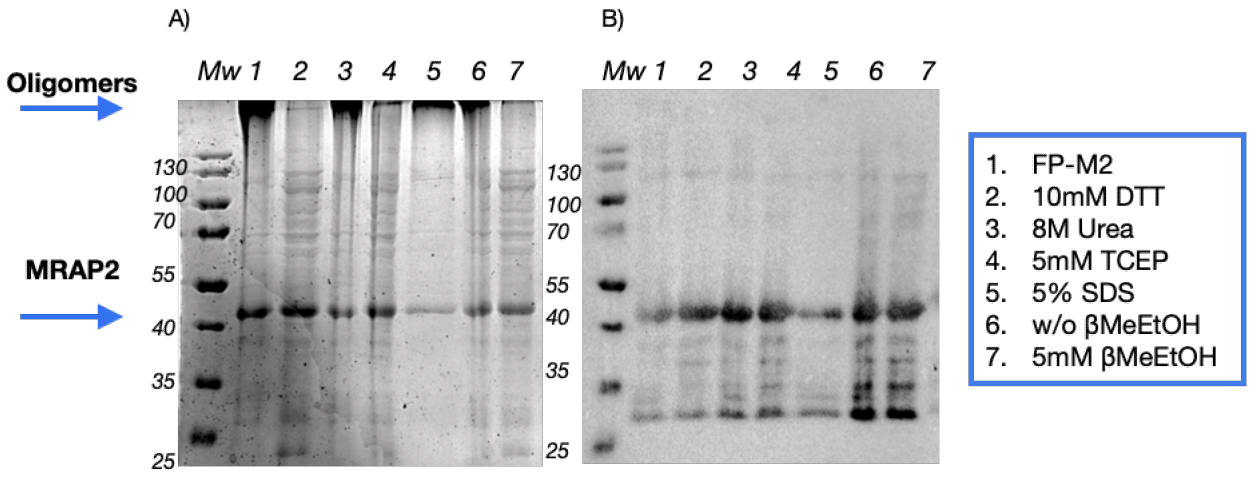

Figure 5.6 Reduction of M2-oligomers. To reduce the oligomer formation different chemical substance was added to FP-M2 (lane 1), DTT (lane 2), 8 M Urea (lane 3), TCEP (lane 4), 5% SDS (lane 5), Loading buffer without β-mercaptoethanol (lane 6), and with 5 mM β-mercaptoethanol (lane 7). The reduction of the oligomers was monitored by A) SDS-page and B) Western blot anti M2. The oligomer´s band higher than 130 kDa disappears almost completely using DTT (lane 2) and TCEP (lane 4) the band also decrease using β-mercaptoethanol (lane 7) and the oligomers remains in the samples which contained urea (lane 3) and SDS (lane 5). This fact suggests the high stability of the oligomers, which are formed by disulfide bonds.

The expression and purification of fp-M1 and fp-M22 were also performed using the same conditions optimized for fp-M2. Figure 5.7 A), B) and C) shows the SEC profiles obtained for the three constructions M1, M2 and M22, respectively.

-

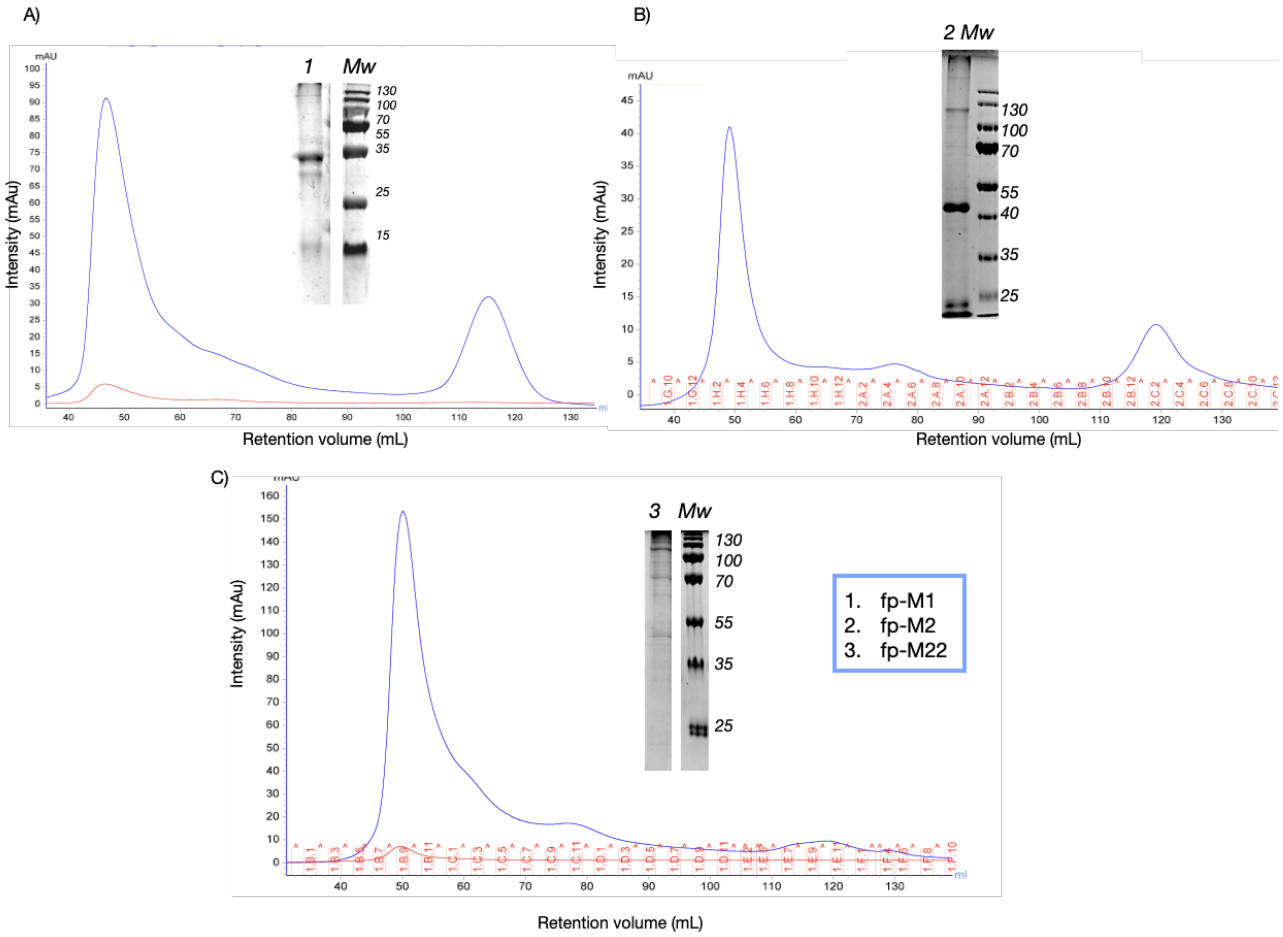

Figure 5.7 Purification of fp-M1, -M2 and -M22. All three constructs were expressed and purified using the same conditions. The SEC profiles A) M1, B) M2, and C) M22 show an intense peak at 50 mL of retention volume, exhibiting the same behavior in the three proteins regarding the formation of higher-order oligomers. In the SDS gels, it is possible to observe the band corresponding to fp-M1 (lane 1) around 33 kDa, fp-M2 (lane 2) at 45k Da and fp-M22 (lane 3) around 70 kDa. The oligomer bands at the top of the gels are also present in all three constructs.

Enzymatic cleavage of M2 and M22

Enzymatic cleavage was performed to separate the M2 sequence from the fusion protein. Cleavage was performed on fp-M2 using sumo protease and TEV protease for fp-M22. To avoid the precipitation of M2, the cleavage was performed using 3 M urea, which is the minimum concentration necessary to keep the M2 soluble without significantly affecting the activity of the enzymes. Subsequently, M2 was separated from the remaining fusion tag and protease by reverse IMAC. Figure 5.8 shows this process for the two constructs, M2

-

and M22. Lane 1 shows the fusion protein of M22 (70 kDa) before the enzymatic reaction with the sumo protease. Lane 2 shows the cleavage mixture after 24 hours of reaction. Here, the complete disappearance of the band corresponding to fp-M22 (70 kDa) is observed, as well as the appearance of a band of around 60 kDa corresponding to the M2-Tev-M2 construct; the corresponding band of the sumo protease is also observed around 28 kDa and finally the fragment corresponding to the his-sumo tag (13 kDa). The emergence and vanishing of these bands indicate that the cleavage reaction was carried out effectively. In lane 2, the reaction mixture is observed after 12 hours of cleavage reaction of M22, but this time with TEV protease. The fp-M22 band disappeared, and the band corresponding to fp-M2 (45 kDa) appeared. The bands that correspond to the protease TEV (27 kDa) and M2 (23 kDa) can also be seen, even if they overlap. Lane 4 shows the M2 once purified from the rest of the reaction mixture by reverse IMAC. Lane 5 shows the His-tagged proteins retained on the nickel resin, corresponding to TEV protease and fp-M2, one of the cleavage products of fp-M22 with the TEV protease. Lane 6 shows the fp-M2 (45 kDa) before the cleavage reaction with sumo protease. In lane 7, cleavage is observed after 12 hours of reaction of M2 with sumo protease. Here, as in the previous cases, it is observed how the fp-M2 band (45kDa) completely disappears, and the bands of the sumo protease (28 kDa) and M2 (23kDa) are also overlapped. Additionally, the band's emergence corresponding to the His-sumo tag (13 kDa) is observed. In lane 8 is the M2 band after purification by reverse IMAC. Lane 9 corresponds to the reverse IMAC eluted fraction. It also shows the sumo protease and the his-sumo tag. By comparing the bands of M2 in lane 4 (product of M22 cleavage with TEV protease) and lane 8 (product of M2 cleavage with sumo protease), it is observed that both appear at the same height. This confirms once again the obtaining of M2 through two different ways.

-

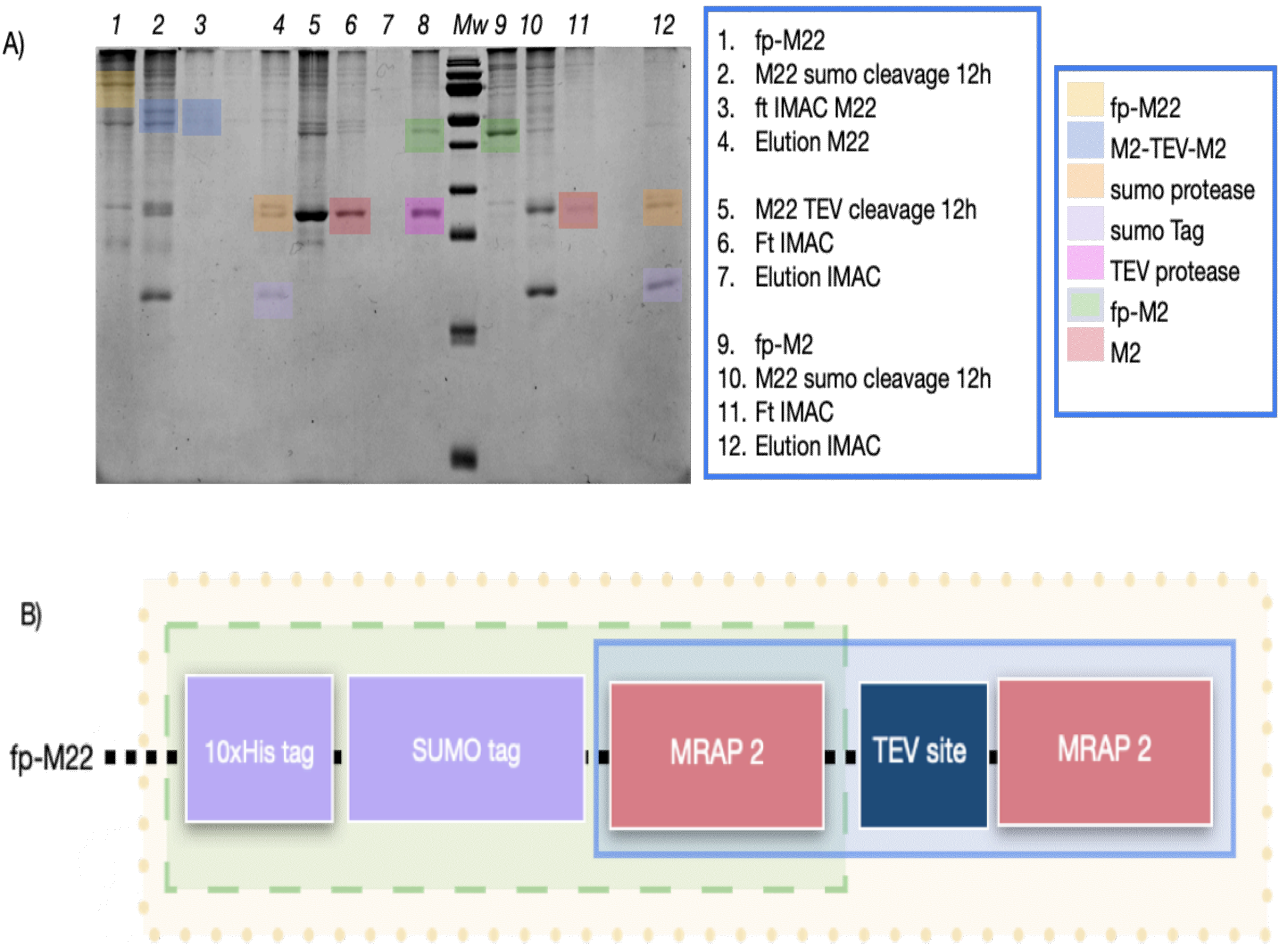

Figure 5.7 Enzymatic cleavage of fp-M2 and fp-M22. A) SDS-PAGE of the fusion protein cleavage, fp-M22 highlighted in yellow (lane1), was cleavage using Sumo protease for 24h at 4°C after incubation time; the fading of the fp-M22 band and the emergence of a 60 kDa band are noticeable, highlighted in blue (lane 2), the same band there is in the flowthrough after reverse IMAC (lane 3). Lane 4 shows the elution fraction after reverse IMAC. The sumo protease is highlighted in orange, and the sumo tag is highlighted in lilac. In lane 5, the reaction mixture of fp-M22 with TEV protease is shown. Lane 6 contains the flowthrough after reverse IMAC; the M2 free of tags is highlighted in red. The elution fraction of reverse IMAC was loaded in lane 8. The fp-M2 is highlighted in green, and the TEV protease is in pink. Purified fp-M2 (lane 9) was cleavaged with sumo protease. In lane 10, it is the cleavage reaction after 24h, the intensity of the fp-M2 almost disappeared, and two bands emerged corresponding to M2 in red, purified by reverse IMAC (lane 11). Sumo protease (orange) and sumo tag (lilac) was retained and eluted from the Ni-NTA column. B) Schematic overview of respective constructs using the same color code.

-

Cell free expression

M1, M2 and M22 expression in a Cell free system.

To improve expression yields obtained in the *E. coli* system, a cell-free system using the Pivex2.4d vector was used. The M1, M2, and M22 proteins were successfully expressed (figure 5.8); however, the expression yield was low. To increase the yield, an optimization of the fp-M2 expression was performed. Varying different parameters, such as the bacterial strain from which the cell extracts were prepared (*BL21* and *A19*), the concentration of different components such as T7 polymerase tRNA, and the amount of amino acid mixture added to the cell-free system, among others, it was possible to obtain the optimal conditions for the expression of the fp-M2 (figure 5.8). The optimal conditions were achieved using A19 cell extract and increasing the concentration of T7 polymerase. These conditions served to also express M1 and M22, attaining a large increase in the expression of the three constructs as seen in figure 5.8 C). The expression of bacterioopsin (BO) served as a reference.

Our data show that cell-free expression also offers the possibility to produce all three constructs. However, in the following, we will focus on the *E. coli system, as the* expression yield was still limited in the cell-free system, and handling and scale-up are more straightforward in the *E.coli* system.

-

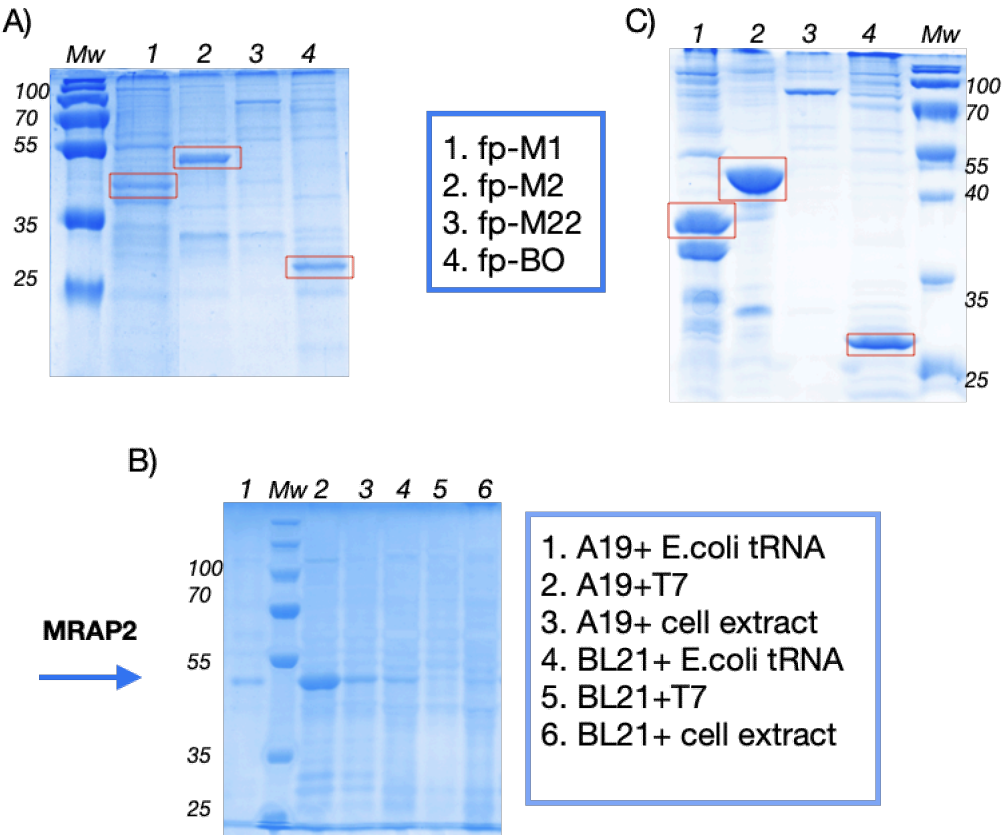

Figure 5.8 Cell free expression of M1, M2, M22 and BO. The expression of M1 (lane 1), M2 (lane 2), M22 (lane 3), and BO (lane 4) was performed in an *E. coli*-based cell-free system and was analyzed by SDS-page A). The expressed protein bands appear in the same molecular weight as the protein expressed in the E. *coli* system. Optimization of the fp-M2 expression was performed by varying the strain from which the cell extract was made and the concentration of *E. coli* tRNA and T7. The results were monitored on SDS-page B). The best condition was found using the *A19* cell strain and adding T7 (lane 2). C) The results of the expression for all four proteins using the optimized conditions are shown.

Once the expression conditions were optimized both in the bacterial and cell-free systems, the search for the optimal conditions for the reconstitution of the MRAPs using different membrane mimetics began.

M2 reconstitution

Detergent micelles

In order to find the optimal conditions to carry out a future structural characterization by nuclear magnetic resonance, different membrane mimetics were tested. The first step was to carry out a detergent screening. Buffer exchange in which the urea was replaced for different detergents via a desalting PD10 column. As shown in figure 5.9, the fp-M2 protein

-

remained soluble in both DPC12 (lane 4) and DDM (lane 3) and to a lesser extent in DPC 16 (lane 6) and SDS (lane 7) detergents after completely removing the urea, which did not happen when detergents such as LDAO (lane1) or IGEPAL (lane 2) were used. The difference in intensity of the protein bands between the sample in urea (lane 5) and these detergents is only a dilution effect since no precipitate was observed. The band corresponding to fp-M2 is still visible after the buffer exchange in both lipids.

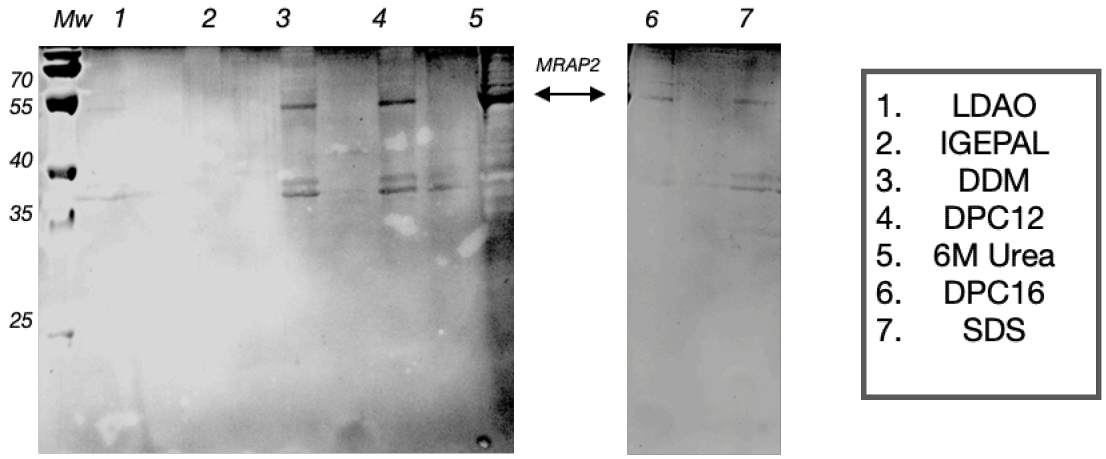

Figure 5.9 SDS-page of solubilization test of fp-M2 in a detergent screening. Seven different detergents were tested to keep fp-M2 soluble after removing the urea in the stabilization buffer. MRAP2 keeps soluble in DDM (lane 3), DPC12 (lane 4), and less in DPC16 (lane 6) and SDS (lane 7).

NMR

To characterize the properties of MRAP2 in DPC12 micelles, we acquired a TROSY 2D NMR experiment, for which the protein was labeled with ^{15}N. In the experiment, it is observed that there is a limited dispersion in the signals, which indicates that the protein is not completely folded. As time passes, weak signals indicative of protein degradation are observed, indicating low stability (figure 5.10).

-

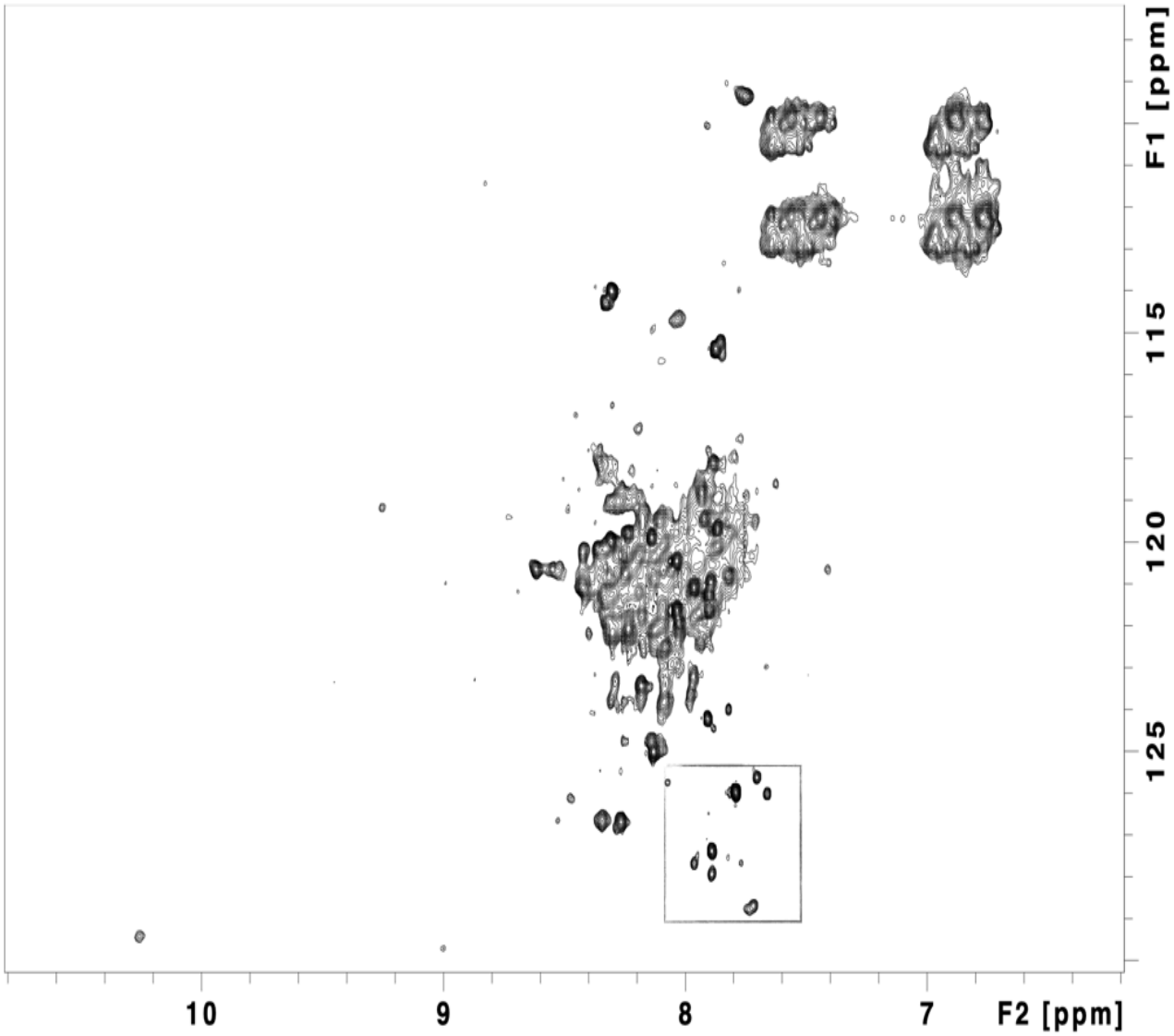

Figure 5.10 2D TROSY-HSQC spectra of fp-M2 in DPC12. The very few signals that appear in the TROSY spectrum do not allow NMR characterization. The highlighted area shows degradation fragments.

Due to the poor stability of fp-M2 in detergent micelles, its incorporation into lipid nanodiscs was carried out.

Lipid bilayer nanodiscs

Another way to stabilize the protein was by its reconstitution into nanodiscs. For this study, different assembly conditions were tested. The assembly of the nanodiscs was carried out

-

using DMPC lipids, and as scaffold proteins, MSP1D1 or MSP1D1ΔH5 were used. In order to improve the yield and the quality of the nanoparticles, different detergent removal techniques were tested. This step is essential for the correct self-assembly of the scaffolding protein and to avoid the precipitation of MRAP2. Following the procedure described above, it was possible to reconstitute the fp-M2 within the nanodiscs successfully. The nanodiscs containing M2 were separated from the empty ones by IMAC. During assembly, almost no precipitation of fp-M2 was observed. M2-NDs were purified by SEC on a HiLoad 16/600 Superdex™ 200 pg column (GE Healthcare). The SEC profile (figure 5.11A) shows that homogeneous nanodiscs were assembled. The SEC fractions containing M2-ND were pooled together and concentrated. In figure 5.11 B, the SDS gel shows in lane 1 the empty nanodiscs assembled, and in lane 2 the nanodiscs formed using the MSP1D1ΔH5 as scaffold proteins, the presence of the MSP1D1ΔH5 (17 kDa) is observed, as well as fp-M2 (45 kDa).

-

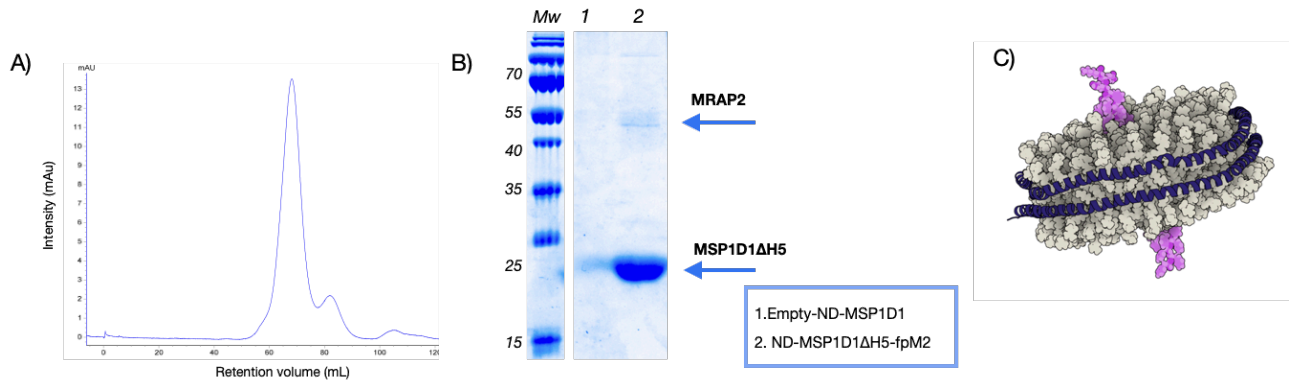

Figure 5.11 Reconstitution of fp-M2 into nanodisc. A) The SEC profile of reconstituted fp-M2 into nanodiscs using as scaffold protein MSP1D1ΔH5. The SEC profile of the assemble MSP1D1-ND shows homogenous particles at 70 min of retention time. The SDS-page B) confirm that the generated particles contain the fp-M2 and the MSP1D1. C) Schematic model of the reconstitution of M2 in the nanodisc.

In conclusion, the results of our study demonstrate the successful expression of M1 and M2 using either *E. coli* or a cell-free system and highlight the utility of nanodiscs for preserving protein solubility and stability. Our study is pioneering, and these findings may have important implications for future research and applications in the field.

Chapter 6: MRAPs as metalloproteins

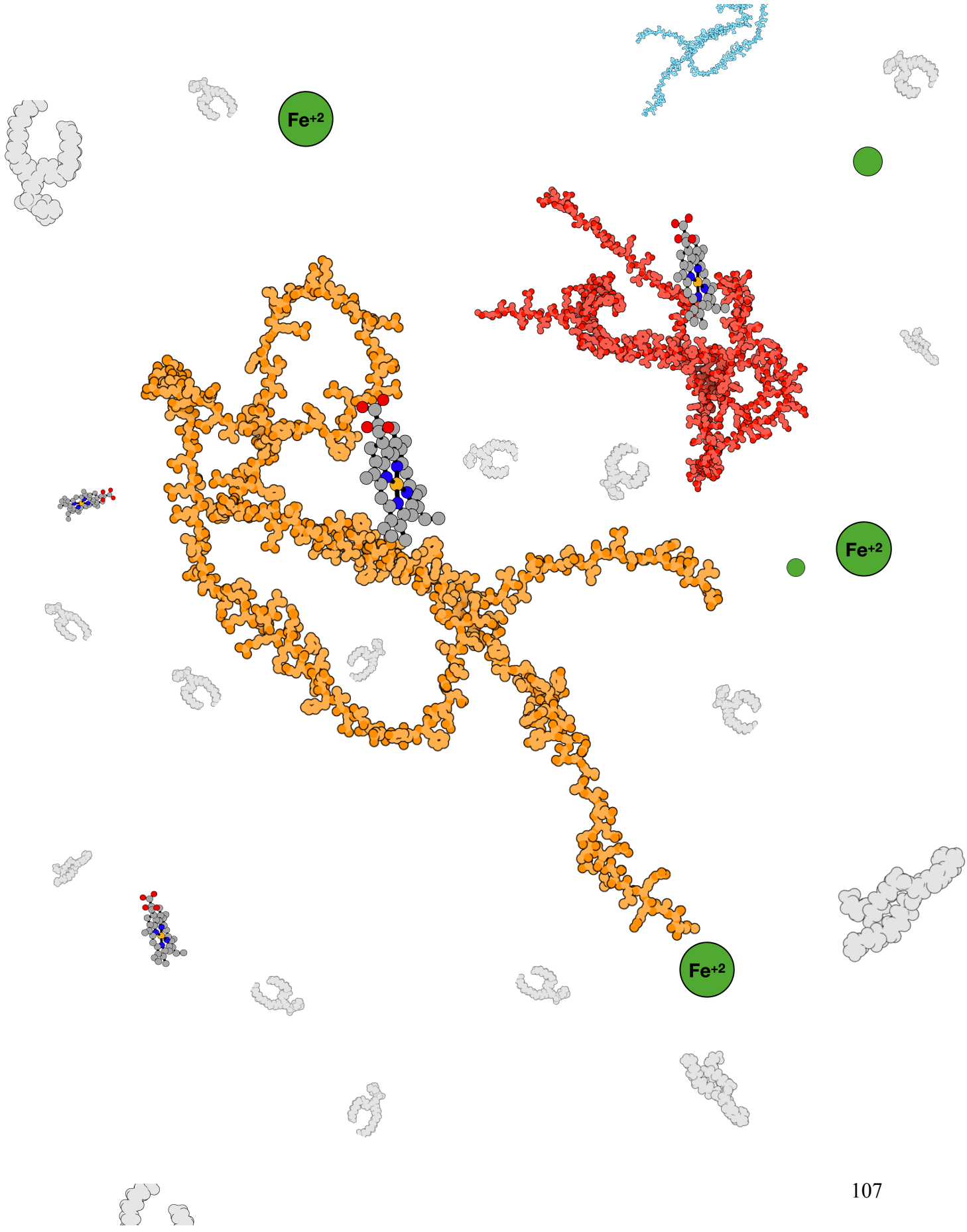

Chapter 6: MRAPs as metalloproteins

As mentioned before, the production yield of MRAP2 increased significantly when it was produced in minimal medium M9, because of that, an exploration of the principal components of this medium was carried out. The results showed that the concentration of metals, specifically iron, is responsible for the increased production yield. This chapter will give an introduction to metalloproteins, and the characterization, for the first time, of MRAPs as iron-binding proteins.

Introduction

Metalloproteins in nature

It is estimated that almost 50% of all proteins in nature have the ability to form complexes with metal ions, and more than half of all enzymes require the presence of metal ions to carry out their functions [215], [216]. These proteins, known as metalloproteins, are found in all living organisms. They are generally proteins with specific highly-conserved amino acid sequences in their primary structure through which the metal binding occurs. This binding can be either temporary or permanent, but it is usually highly stable and specific.
Metalloproteins are involved in several essential biological processes including respiration, nitrogen fixation, and photosynthesis. These processes are carried out by redox reactions, which is why metal ions play a fundamental role in these energetic processes. In addition, metal ions increase the stability of the proteins with which they form complexes [217].

Although all metal ions have redox properties, electron transfer processes in nature are governed mostly, but not only, by 12 essential metals for almost all species (Na, K, Mg, Ca, Fe, Cu, Mn, Mo, Zn Co, Ni, and V) which generally interact with certain atoms (S, N, O) of amino acid side chains such as Cys, His, Thr or Ser among others (figure 6.1). Metals play roles either as cations or as components of macrocyclic cofactors, as in heme and chlorophyll [216], [218], [219].

-

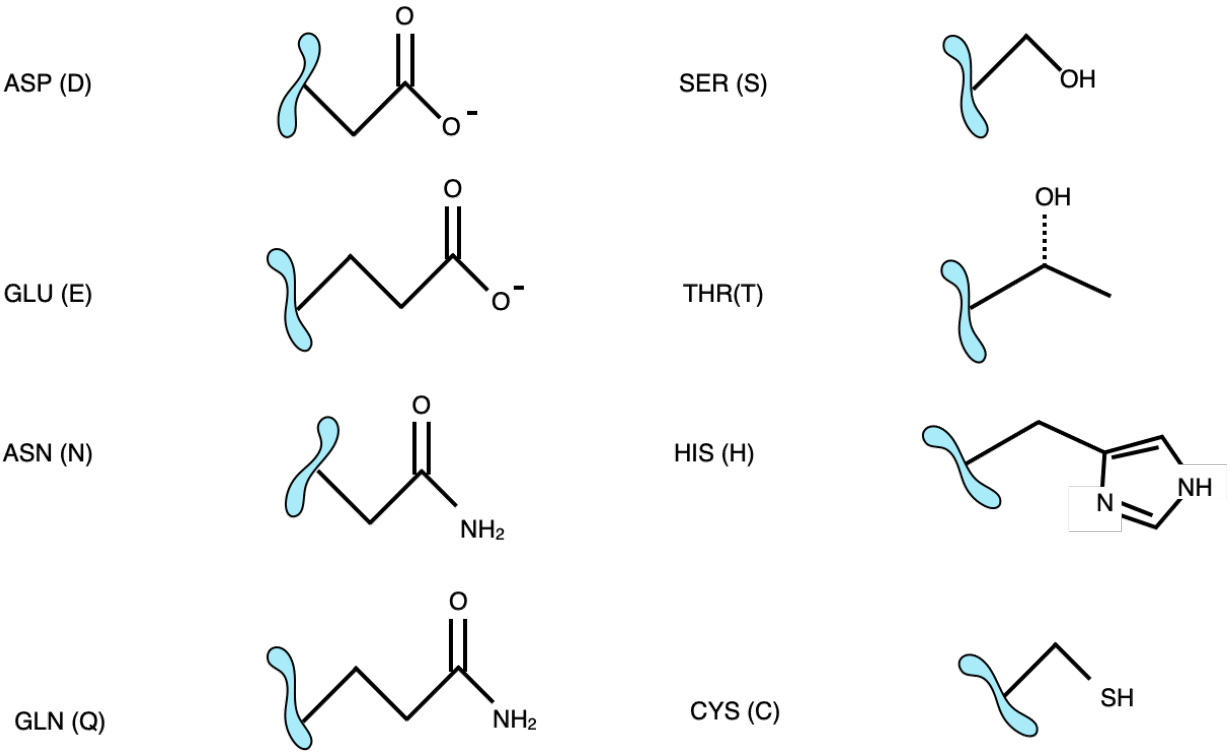

Figure 6.1 Possible sites of interaction of amino acid side chains with metal ions. Metal ions are frequently coordinated to donor atoms N, O and S from side chain of amino acids.

Due to the importance of metalloproteins in life, the detailed characterization of their union with the metallic center is essential to understand their functional mechanisms. Techniques such as mass spectrometry, nuclear magnetic resonance (NMR), X-ray crystallography, and cryo-EM are frequently used in the functional study and characterization of metalloproteins [220].

Iron binding proteins

Iron-binding proteins can be classified into two main categories based on their function. Group I is formed by Hemo-proteins, which depend on iron binding to carry out their main activity (hemoglobin, myoglobin, cytochromes, and enzymes). Group II consists of the proteins that supply the iron atoms to the Hemo-proteins. This second group of proteins can be functionally divided into two categories, proteins involved in transport and those dealing with iron storage; transferrin and ferritin belong to these two groups, respectively [221].

Hemoproteins can be both soluble and transmembrane proteins. They play an essential role in many physiological, metabolic, and energetic processes, such as oxygen transport

(hemoglobin), electron transfer, apoptosis (cytochromes), detoxification of reactive species of oxygen (peroxidase), etc. [218], [222].

Cytochromes are hemoproteins characterized by the covalent and/or non-covalent attachment of one or more heme groups to the protein backbone. There are four types of heme groups, which vary from each other in their axial ligands. Heme group is generally known as the complex formed by the macrocyclic tetrapyrrole called protoporphyrin IX, whose center is an iron atom bound to pyrrolic nitrogen atoms. The oxidation-reduction characteristics from the iron atom of the heme groups give the cytochromes the ability to act as electron carriers [218], [223], [224]. Cytochromes are classified according to the nature of their ligands in classes a, b, c, d, f, and o. Figure 6.2. These differences cause each type of cytochrome to have unique UV-Vis absorbance spectra, which can be differentiated from each other by analyzing the typical absorbance peaks (figure 6.2) [218], [225] .

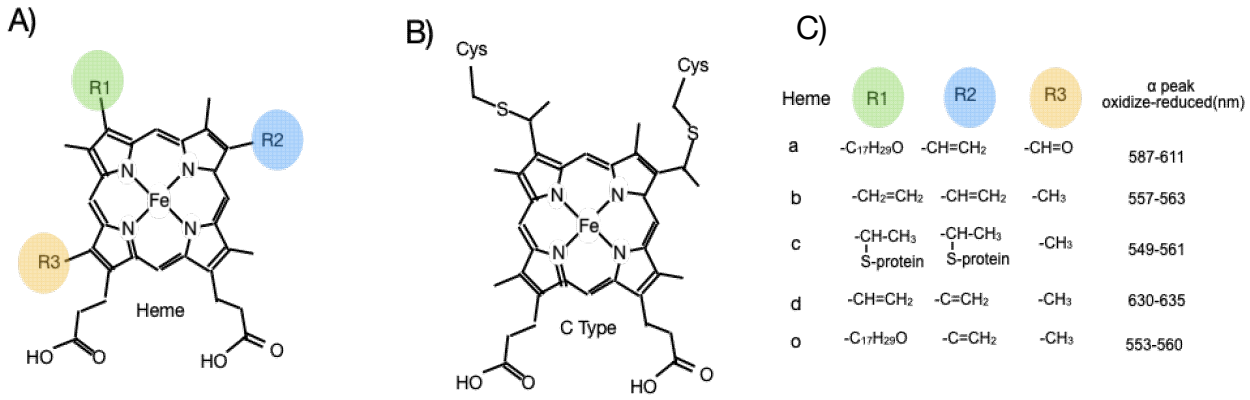

Figure 6.2 Chemical structure of a cytochrome. A) The structure of protoporphyrin IX macrocycle is the basic structure of all types of cytochromes. The different types of heme groups vary in the nature of their axial ligands in positions R1, R2, and R3. B) Chemical structure of a Cytochrome c [218], [226].

Cytochrome types

- Cytochrome type “a” has a heme-a group. This type of heme has a hydroxyethylfarnesyl side chain at position 2 of the porphyrin ring and a formyl group at position 8. The cytochrome “a” type in its reduced form has a maximum absorbance value at 605 and 444 nm wavelengths.

- Cytochrome “b” has a heme-protoheme IX type. The ligands of this heme type are methyl groups at positions 1, 3, 5 and 8, two vinyl groups at positions 2

-

and 4 and two propionates at positions 6 and 7. Protoheme Type IX is the precursor of hemes “a” and “c,” and it is characterized by its absorption bands at 557, 528, and 424 nm.

- Cytochrome “*c”* is characterized by covalent thioether binding of the vinyl groups at positions 2 and 4 of the β-pyrrole of heme “b” with Cys residues (heme c). Its characteristics will be more detailed later in this same chapter.
- Cytochrome “d” (heme d) has two cis-hydroxyl groups as ligands at positions 5 and 6 of β-pyrrole. This type of cytochrome has an absorption band of around 630 nm.
- Cytochrome “f”. The heme is pretty similar to type “c”. However, in the f-type cytochrome, the second axial ligand is the NH_2 group of a Tyr. It has an asymmetric peak from 553 to 555nm with a shoulder around 550nm [218], [225].
- Cytochrome “o” type is commonly found in bacteria. It is a b-type heme group that functions as cytochrome oxidase. The CO complex of cytochrome o shows small α and β bands at 557-567 and 532-537 nm and a γ band at 415-420 nm.

Cytochrome c

Eukaryotic cytochromes c generally contains ~100-120 amino acids and have a degree of identity of 45 to 100% in their amino acid sequence. Unlike type b cytochromes, in which the heme group is non-covalently bound to the apoprotein, type c cytochromes are characterized by covalent binding of the heme group. The heme-protein complex is almost always formed by the covalent attachment of two Cys residues of the protein to the porphyrin ring via the highly conserved amino acid sequence C-X-X-C-H- (X = any amino acid except cysteine), in which the histidine residue serves as the first axial ligand for heme iron. The second axial ligand is variable and can often be a Met or His residue at a variable distance from the motif in the amino acid sequence [226]. Although the functional advantages of covalent binding to the heme group for a type c cytochrome are still not entirely clear, it has been proposed that it improves protein stability by preventing heme loss by dissociation, [218], [223], [224].

The UV-Vis spectrum of a Cyt “c” in the reduced state exhibits three characteristic absorption bands: an intense band at ~410 nm called the Soret or γ band and two weaker

signals at 551 and 521 nm, the α and β bands (respectively) with a ratio between them of 1.87 (figure 6.3). This profile is generated, as well as in the other types of cytochromes, by transitions allowed by porphyrin π → π* mixing with interelectronic repulsions. In the oxidized state, the intensity of the α and β bands decreases. They become diffuse until they disappear, in the same way the intensity of the γ band decreases and moves towards the violet region of the spectrum [227].

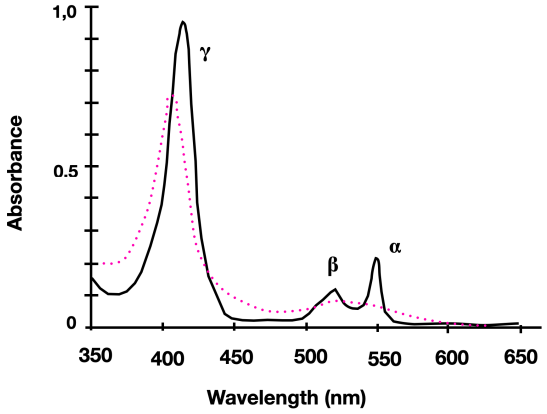

Figure 6.3 UV-Vis spectrum of Cyt c in the reduced state. The UV-Vis spectrum of Cyt "c" has three characteristic bands α, β, and γ at 551, 521, and 410 nm, respectively. In the oxidized state, only two bands are visible (dotted red line) since the α and β bands appear to overlap, and the intensity of the γ band decreases. The figure was taken from [226].

Cytochromes "c" can be classified into four main classes. Class I Cyt "c" include small (8-120 kDa) soluble proteins that contain a single heme group. Their domains are characterized by the presence of the CXXCH heme motif at the N-terminus. The presence of the His residue, through which the heme group binds to the protein, is highly conserved.

Although the CXXCH motif is the most common one, several cytochromes with different heme motifs have also been identified. In general, the number of residues separating cysteines can vary in the range from 2 to 17. Contractions of these binding motifs (i.e., CXCH or CCH) are uncommon in nature, however, they can be found in all bacterial and archaeal domains [228]**.** Some other less common heme binding sites are: Ala (Ala/Gly)-Gln-Cys-His (AQCH) found in some parasites and Leishmania [218] Cys-Lys-Cys-His (CKCH) from the anammox bacterium Kuenenia stuttgartiensis. Very atypical heme-binding motifs have also been found in nature; one of them is the AXXCH motif. This motif was found so far only in protozoa-mitochondrial cytochromes. Different studies on the unusual AXXCH variant of the heme-binding motif suggest that the loss of the thioether bond in this variant has a minimal effect on the stability of the cytochrome [224], [229]. The heme group would be attached through a single covalent bond in this particular motif.

This type of structure has been reported in cytochromes C557 and C558 of the flagellate, *Crithidia oncopelti,* and *Euglena gracilis* respectively [229], [230].

Results

UV-Vis characterization

The best expression in M9 suggests an essencial role of the metal ion. The UV spectrum was taken to check if there was a noticeable peak characteristic of metalloprotein: The spectrum indeed shows characteristic peaks for both MRAP1 and MRAP2 with a maxim at 410 nm (figure 6.4). This kind of profile is characteristic of the Fe-binding proteins and is observed in different types of hemoproteins or certain protein-Fe clusters. For this reason, a more detailed study was carried out.

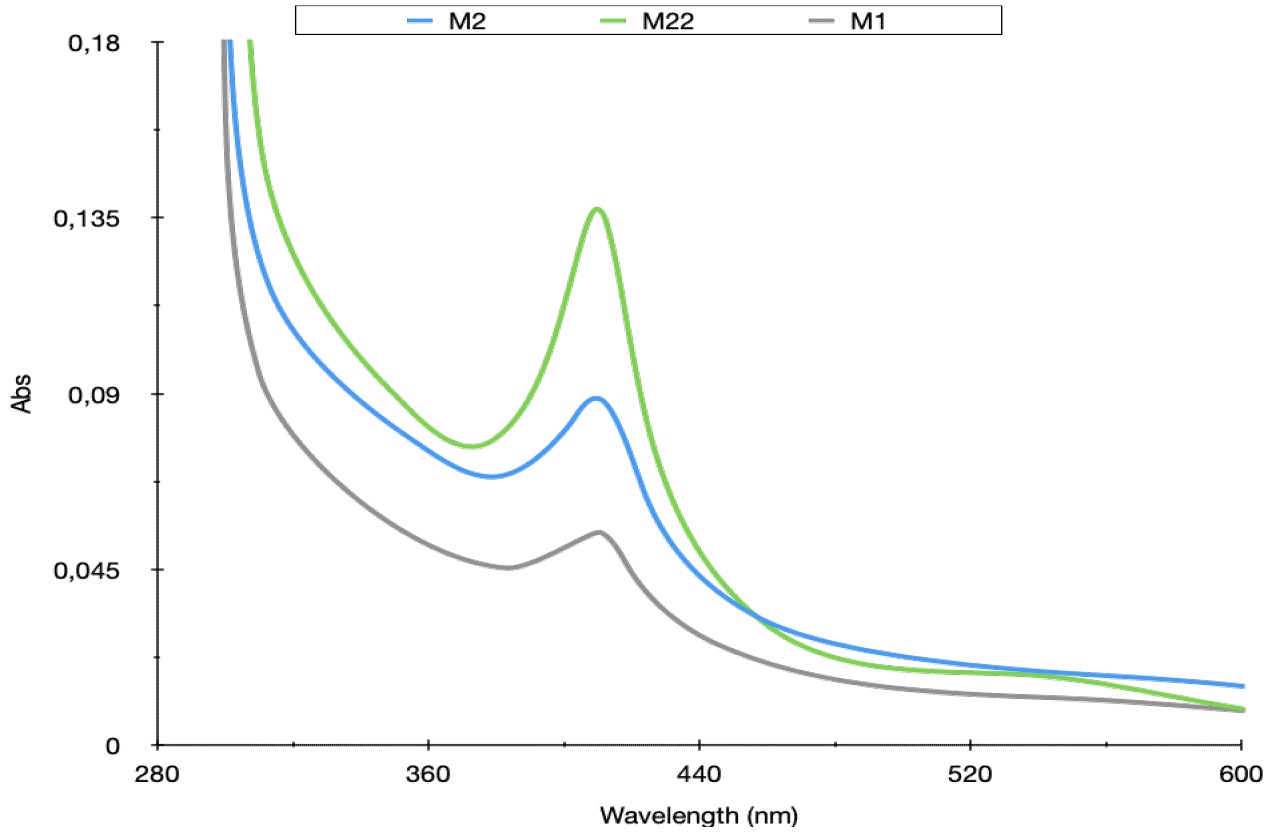

Figure 6.4 UV-Vis spectrum of MRAP1, MRAP2, and M22. All three constructs have a characteristic UV-Vis spectrum for an iron-binding protein with an intensity maximum at 410 nm.

Expression and optimization

Based on previous results, which show that the presence of trace metals increases M2 production, it was evaluated whether this effect was consistent in other culture media.

-

Hence, LB, 2YT ,and TB media were supplemented with trace elements at the same concentration used for the preparation of the M9 medium (figure 6.5).

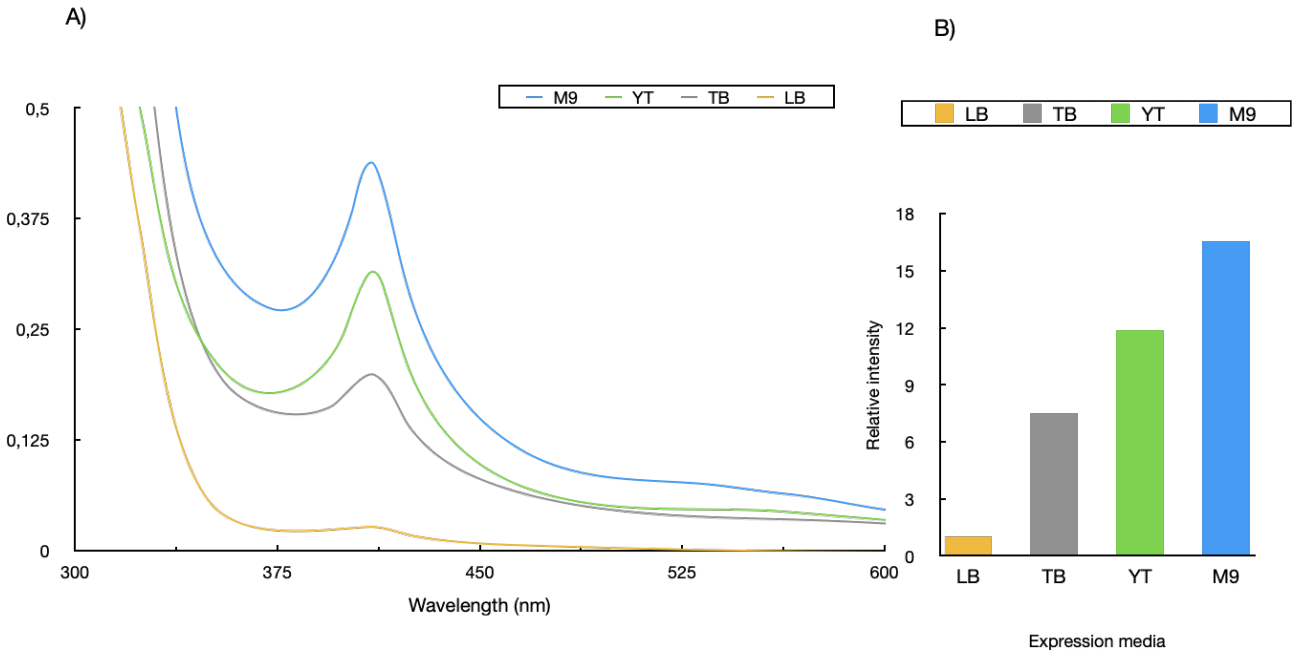

Figure 6.5 Expression of fp-M2 in different culture media. A) UV-Vis spectrum of fp-M2 expressed in 1L of LB (yellow), TB (grey), YT (green), and M9 (blue). The intensity changes of the peak at 410 nm are correlated with the expression yield obtained using each media. B) Bar diagram of the relative intensity of the maximum at 410 nm. It is observed that the expression in medium M9 produces 17-fold the amount obtained using LB medium.

It was also desired to specifically evaluate the effect of iron on the production of MRAP2. For this, an extra condition was analyzed in which a mixture of trace metals that did not contain iron was added to the different expression media (LB, TB, 2YT, and M9). In the second test, the media was supplemented with iron alone, with no additional trace metals. The results observed were consistent for the LB and the 2YT medium; in both media, the protein was better expressed when adding the mixture of trace metals (TE) compared to the media without any additives (figure 6.6). A decrease in MRAP2 production was noted when the trace metal mixture lacked iron (TE-Fe), and the highest expression rates were observed when only iron was added directly to the medium (LB+Fe and 2YT+Fe).

The same conditions as in the previous cases were evaluated in the M9 medium. It is important to mention that in the case of the minimal medium M9, the medium already contained trace metals, so completely removing them is impossible since this would prevent the cells from growing. Four conditions were tested: Normal medium (M9),

medium without iron (M9-Fe), medium with double concentration of mixture of trace metals (M9+2TE), and finally medium without trace metals but supplemented with iron (M9-TE+FE). The results show that the expression where iron was removed from the mixture of trace elements is the one that produced the least amount of MRAP2 protein. Similar expression rates were obtained when using normal M9 as well as using M9+2TE with double concentration of trace elements, which indicates a saturation in the rate of production of MRAP2 (figure 6.6).

-

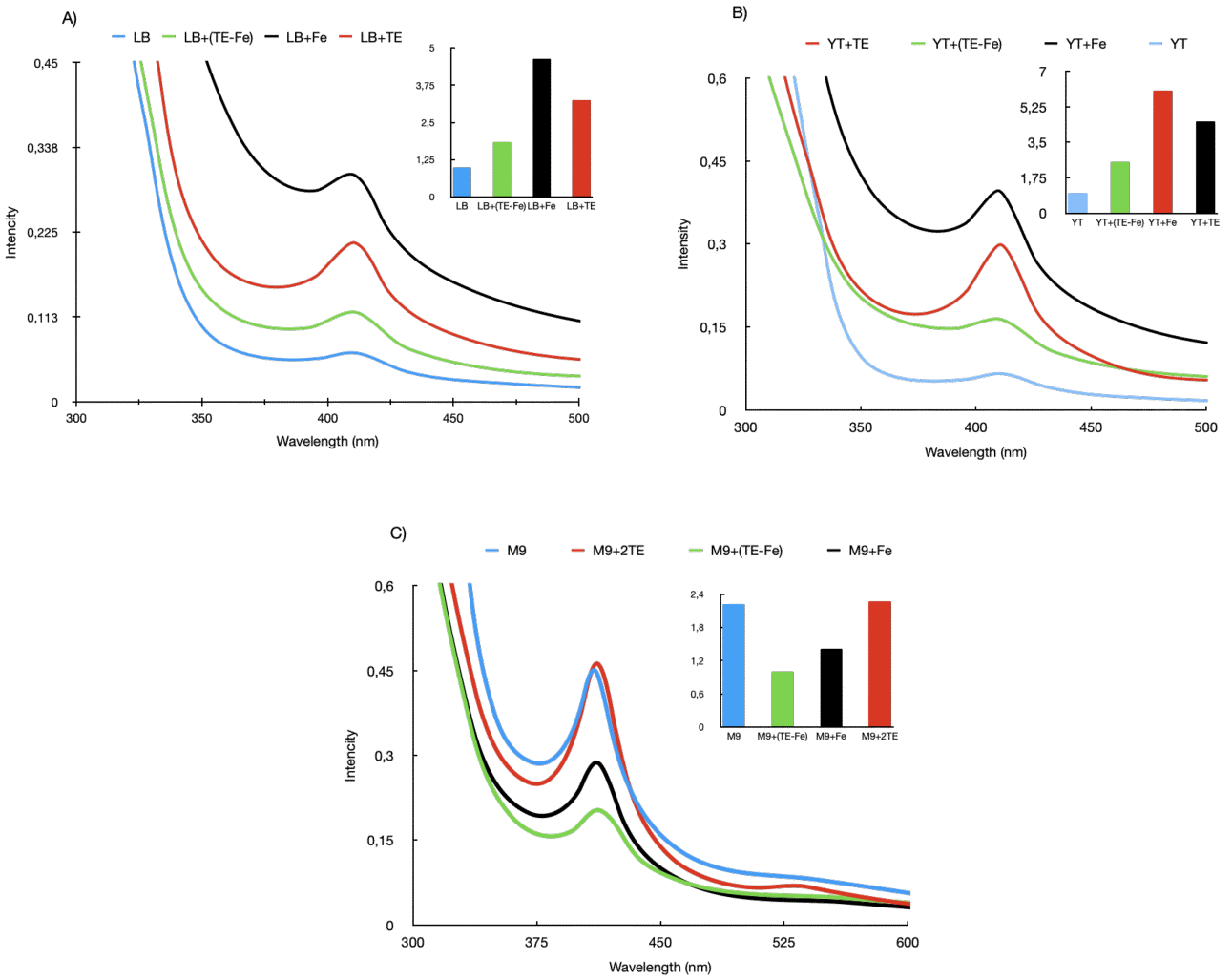

Figure 6.6 Influence of trace metals in the expression of fp-M2. The UV-Vis spectra of fp-M2 expressed in different media A) LB, B) 2YT, C) M9 supplemented with TE (red), TE-Fe (green), Fe (black), and without additives (blue). In both rich media LB and 2YT, a higher yield was obtained when iron was added. This fact confirms the role of iron as the main component that influences the stabilization of M2. On the other hand, since M9 is a minimum medium, the absence of the rest of the trace metals considerably affects the protein expression yield. Here it is also observed that adding twice more trace elements does not considerably improve the expression of M2, so it is thought that the concentration of iron initially used is sufficient to saturate the metal-coordination sites.

Effect of urea concentration in Fe-Protein interaction

Metal-protein interactions are highly stable. As mentioned in other reports [231], the iron binding interaction shows high stability even in denatured conditions such as 8 M of urea. It was also reported before that the Heme site could be resistant to Tryptic digestion [232]. These behaviors are also observed for MRAP2. To corroborate the stability of the MRAP2-iron binding, the UV-Vis spectra of MRAP2 were acquired in buffers containing different concentrations of urea. The results show that as the amount of urea decreases, the Soret

band of the heme group increases in intensity, suggesting that the heme group remains stable at 6 M urea despite being slightly affected by the presence of the chaotropic agent (figure 6.7 A). Figure 6.7 B shows the UV-Vis spectra after substituting urea for DPC12. In the presence of detergent, a decrement in absorbance is shown in the Soret band. This effect where detergents induce the loss of heme group has also been shown in other reports [233]. Therefore, we considered it unnecessary to remove the urea in future assays, which were mainly carried out at 6 M Urea.

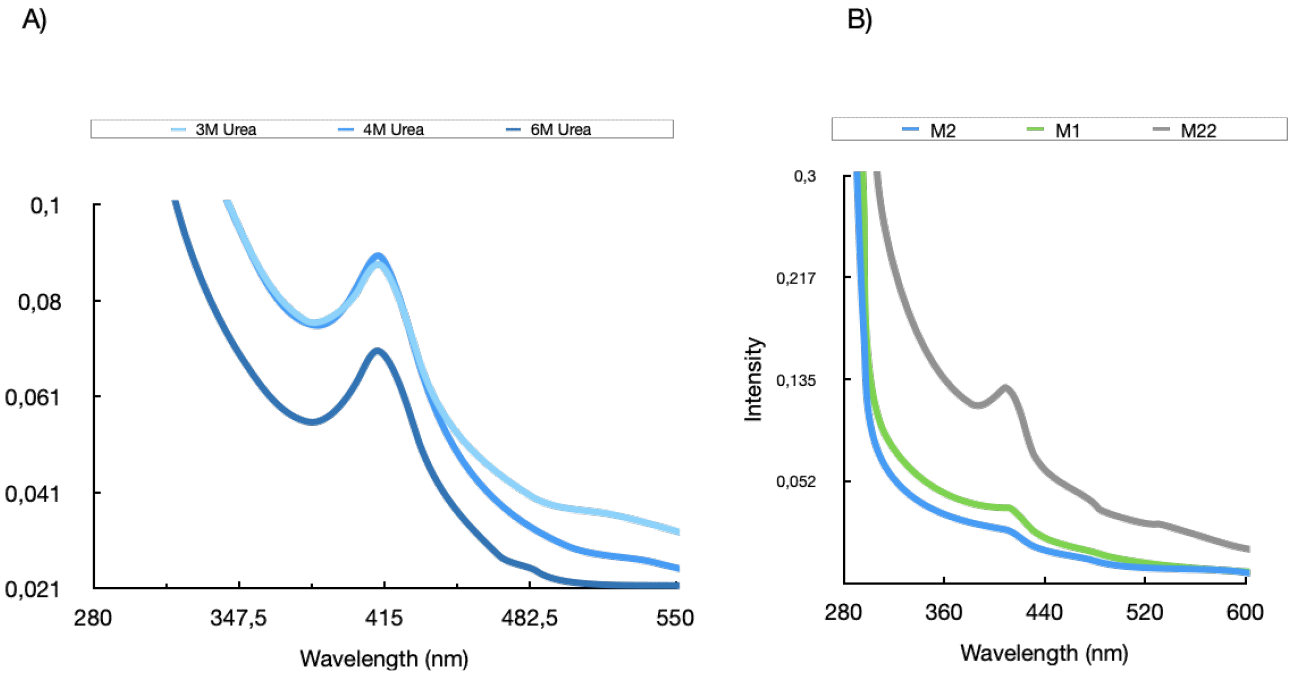

Figure 6.7 Effect of urea concentration on the iron binding. To analyze the influence urea concentrations on the stability of the iron-protein complex, the UV-Vis spectrum of fp-M2 (34 μM) was acquired at different concentrations of urea. In the spectrum, A) the maximum intensity at 410 nm increases as the urea concentration decreases. However, as reported in the literature, the iron-protein complex remains stable at 6 M urea. Spectrum B) shows the UV-Vis profile for the three constructs in DPC12 after completely removing urea.

Location of the possible iron binding site in the primary and tertiary structures of MRAPs

Once the presence of iron was confirmed via UV-Vis spectroscopy, the amino acid sequence of both members of the melanocortin accessory protein family was compared with the sequence of proteins known to bind to iron ions, looking in the amino acid sequence for the presence of a characteristic iron-protein binding motif. To our pleasant

surprise, the presence of the CXXCH motif in the MRAP1 sequence was identified (figure 6.8 A).

As previously said, the CXXCH peptide motif is characteristic of c-type cytochromes, which bind the heme group to the protein through two thioether bonds formed between the vinyl groups of the heme and the sulfides of the cysteines [234] (figure 6.8 B). Despite not having found the same motif in the MRAP2 sequence, the presence of the iron-MRAP2 bond has been verified experimentally. This suggests the presence of an iron-binding motif yet to be characterized.

Metal-binding site location based on topological and structural prediction

The results obtained from the TMHMM protein topology predictor [235] show that the heme motives are in the intracellular domain figure 6.9 A and C. However, it must be considered that MRAPs form antiparallel homodimers so that the iron-binding motif would be found both intracellularly and extracellularly.

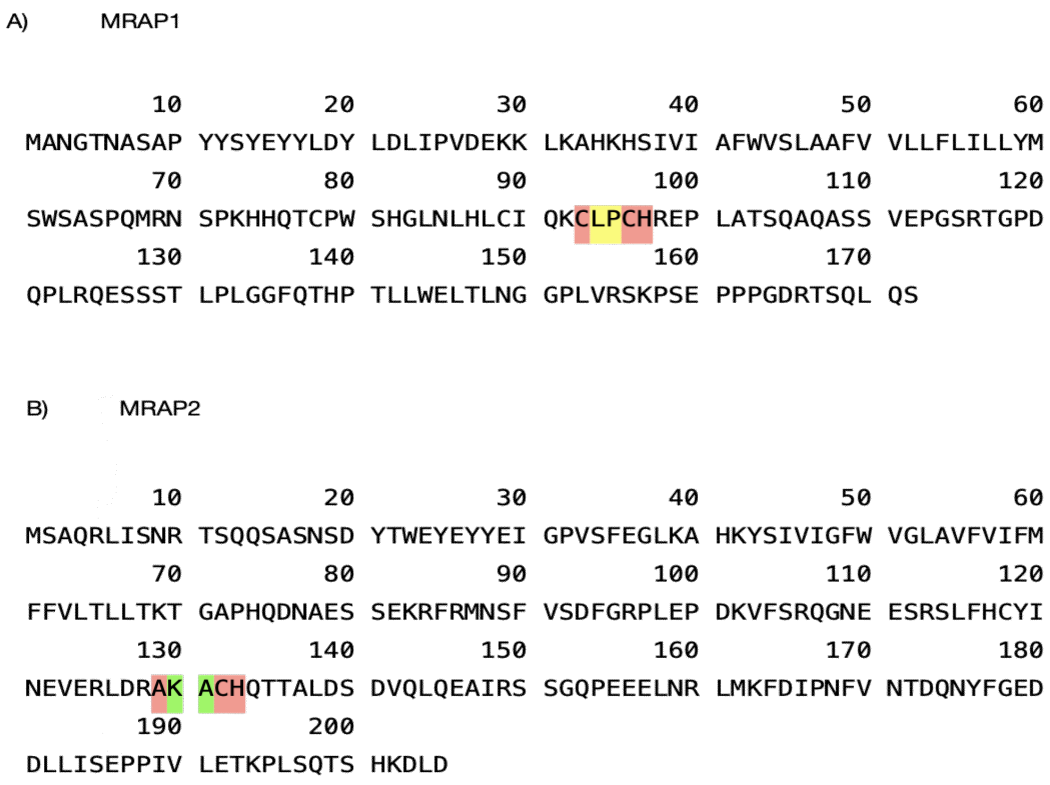

Figure 6.8 Location of iron-binding motif in the primary structure of MRAP1 and MRAP2. A) A classical C-type heme-binding motif CXXCH was identified in the sequence of

-

MRAP1. B) In the sequence of MRAP2, quite an unusual heme motif was found. The motif AXXCH was previously identified only in parasites and protozoa.

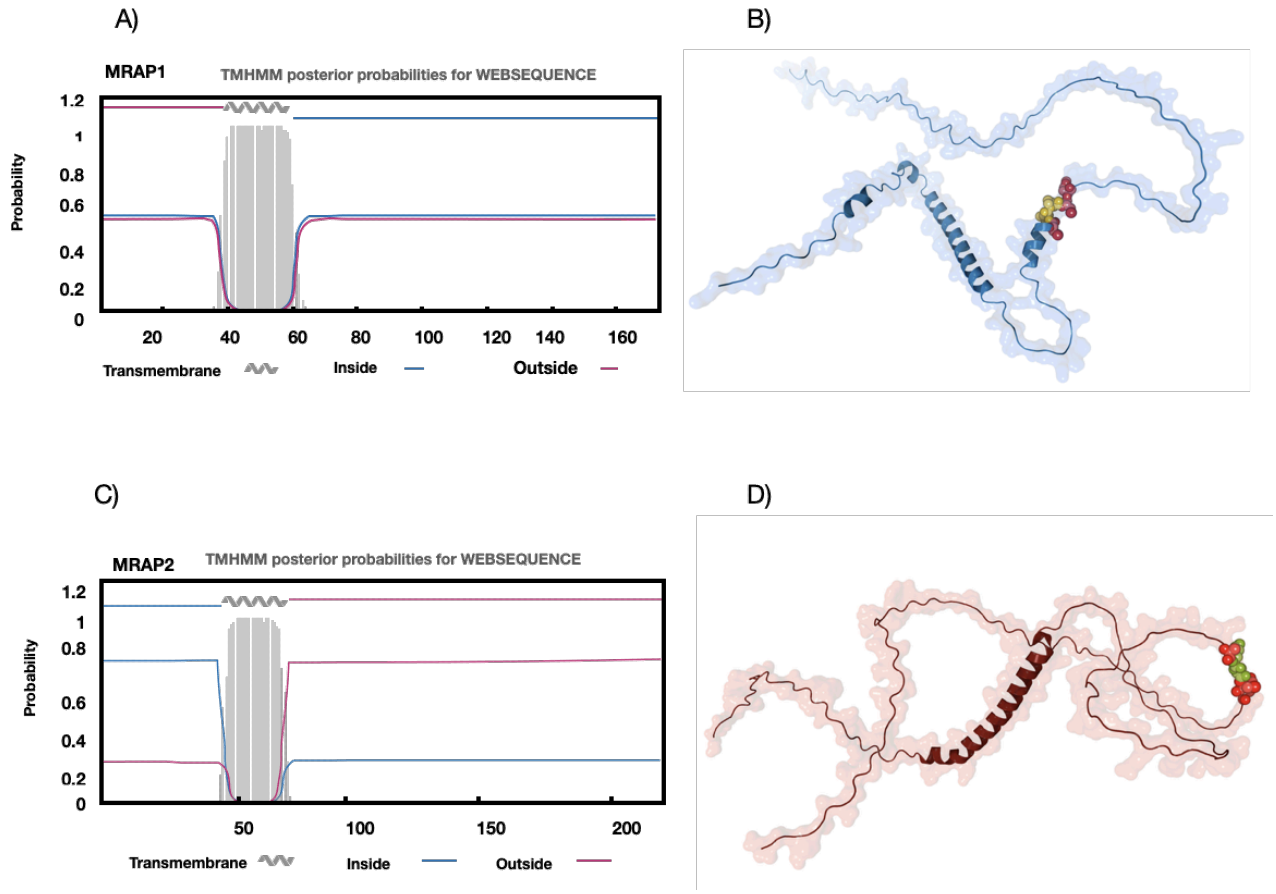

Figure 6.9 Topology and structure predictions of M1 and M2. Topology predictions of A) M1 and C) M2 were made using the online server from DTU Health Tech. According to the topology prediction, the heme-binding site would be found on the inner side of the membrane; however, because MRAPs form with reverse topology, the locations would be on both sides of the membrane just after the TM domain. The Cartoon representation of the 3D structures of B) M1 and D) M2 were predicted by alphafold reported in UniProt (Q8TCY5 and Q96G30). According to these models, MRAPs have several unstructured regions linked to a folded trans membranal domain, from 35 to 70 amino acids for M1 and 27 to 65 for M2. The iron-binding sites are highlighted in both representations.

Heme-group reduction

One way to corroborate the suspected and, so far, never reported MRAP2-Fe binding is through the reduction of the iron. Iron reduction-oxidation assay was carried out to corroborate this new characteristic of the binding of a metal ion from M2.

-

It has been observed that iron bound to metalloproteins can be reduced by adding specific reducing agents such as DTT or Na dithionite [236]. These assays consist of a titration where by adding the reducing agent, Fe^{3+} is reduced to Fe^{2+}, passing through the intermediate state Fe(II)-O_2 (figure 6.10 A) [237]. A shift in the absorption characteristic bands of the metal binding to MRAP2, Soret band (also called gamma band), can be observed at 410 nm shifts to 425 nm. In addition, the reduction caused an increase in both intensity and resolution of the beta and alpha bands that overlapped before reduction at 530 nm split after reduction to 559 and 529 nm, respectively. By adding DTT and Na dithionite to MRAP2, the characteristic shifts of the Soret band from 410 nm to 436 nm were observed, as well as the splitting of the alpha and beta bands from 530 to 529 and 559 nm, respectively (figure 6.10 B).

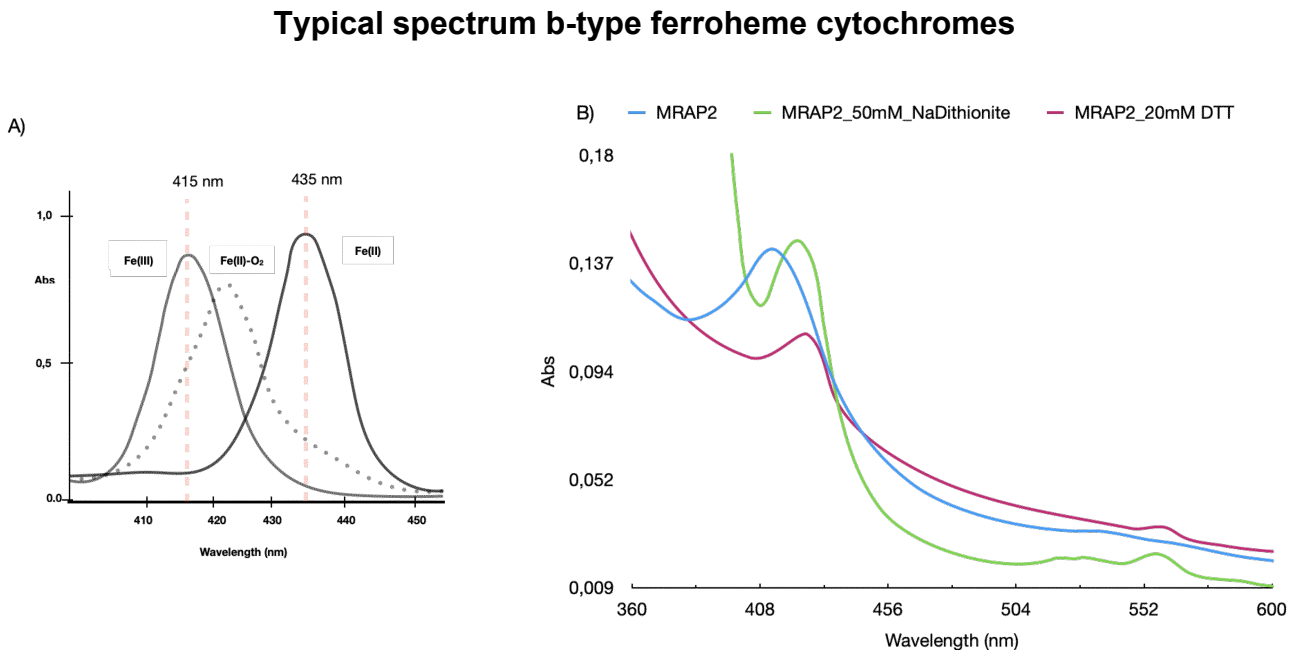

Figure 6.10 UV-Vis spectrum of heme reduction. A) UV-Vis spectrum of cytochrome c under reducing conditions, taken from [226], [237]. B) UV-Vis spectrum of MRAP2 under oxidizing conditions (blue) and reducing conditions using DTT (red) and TCEP (green) as reducing agents. The Soret band shift in oxidize state from 410 nm to 425 nm in reduced conditions. The addition of reducing agents produces an increase in both the intensity and the resolution of the α and β bands. Sodium dithionite reduction had a stronger effect on the resolution of these bands (see figure 6.12.)

In Figure 6.11, we can observe the shift of the Soret band to shorter wavelengths. Additionally, the overlapping of the alpha and beta bands once again shows the characteristic Fe (III)-protein binding spectrum.

-

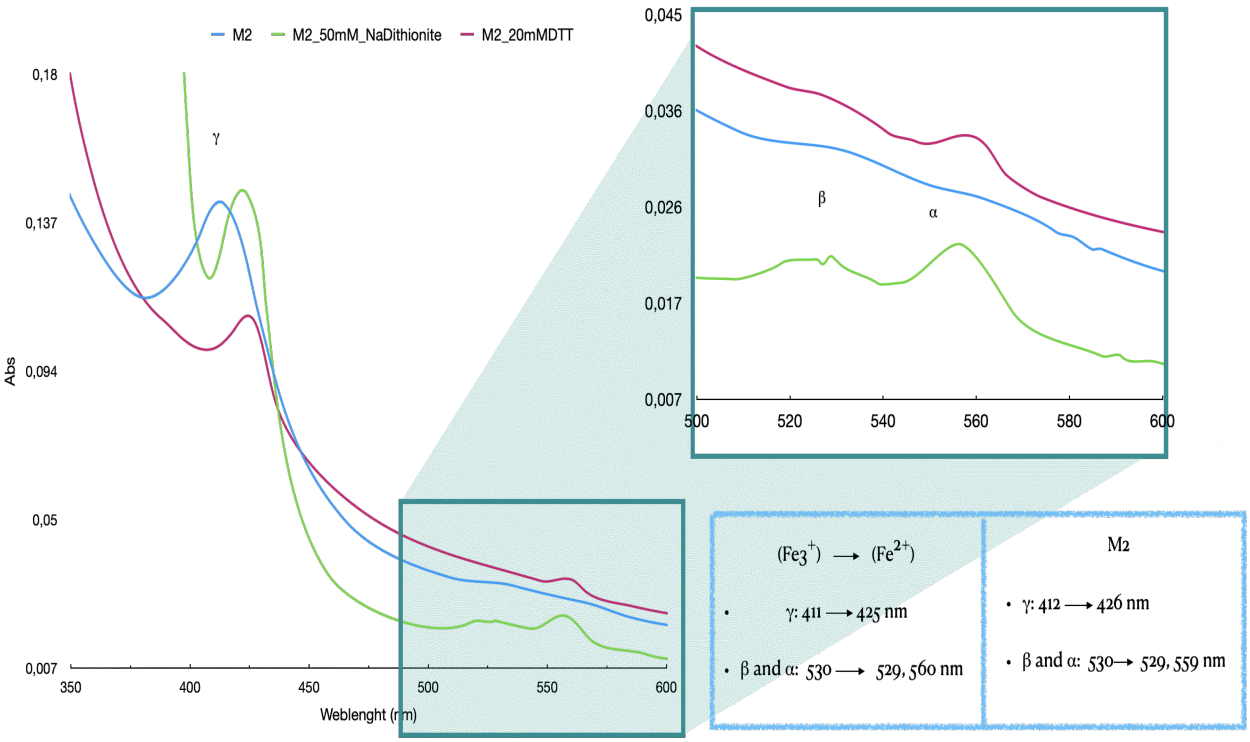

Figure 6.11 Heme reduction bands. A close-up view of the increase in both the intensity and resolution of α and β bands due to the addition of a reducing agent. The box shows the expected theoretical and experimental values obtained in the reduction of the heme group from M2.

Based on these results, we suggest that both MRAP1 and MRAP2 are (under the conditions studied) able to bind iron since they present a characteristic UV-Vis profile similar to that of other hemeproteins such as cytochrome, a characteristic never reported before for these proteins [222].

Achievements and Outlook

With the successful completion of the objectives outlined above, we have achieved significant advancements in our understanding of membrane-interacting proteins and the development of new tools for studying them.

The main achievements obtained in the research on the development on the development of escin bicelles include (chapter 3):

- The feasibility of forming DMPC-aescin bicelles whose size can be regulated by modifying the aescin concentration was confirmed.
- The Aescin-DMPC interaction was characterized by NMR.
- It was found that bicelles whose aescin concentration is equal to or greater than 25% can stabilize a transmembrane protein such as BO.

The results of this research provide a valuable new platform to study the structure and function of membrane proteins using Aescin-DMPC particles as size-tunable membrane mimetics. This opens up exciting new avenues of the aescin system as a size-tunable platform for the future structure and functional studies of (trans-)membrane proteins.

In terms of developing a new platform for the selective study of cell membrane-associated proteins, the following significant achievements were obtained (chapter 4).

- A methodology has been developed to specifically analyze membrane-associated protein conformations in samples containing both soluble and equilibrium membrane-bound proteins.
- Through the application of the hyperpolarization system, it was able to characterize membrane-associated protein using nanodiscs selectively labeled with the mAMUPOL biradical.

In terms of achievements related to the study of Melanocortin Receptor Accessory Proteins, the following stand out (chapters 5 & 6):

- MRAP1, MRAP2, and M22 were successfully expressed using a bacterial system as well as in a cell-free system for the first time.

-

- A methodology to reconstitute MRAP2 using detergent micelles and nanodiscs was successfully developed. The results suggest that nanodiscs are the most effective membrane mimetic for keeping M2 stable.
- It was found that iron ions play an essential role in the MRAPs´ stabilization.
- A heme-binding site was identified by homology in the primary structure of both MRAP1 and MRAP2.
- It was identified that MRAP1 has a heme-binding motif typical for Cyt c, and MRAP2 has an unusual heme-binging site reported before only in protozoa.

-

General conclusion

Membrane proteins play key roles in many essential life processes, including structural functions, signal transduction, cell-to-cell communication, energy production, immune responses, and even the regulation of transport between intracellular and extracellular compartments of a wide variety of drugs and compounds. Due to their influence on all these essential processes, it is not surprising that almost 60% of all FDA-approved drugs target membrane proteins.

In-vitro production of membrane proteins, as well as their characterization is challenging, even though recent decades have brought significant improvements in the expression and purification of recombinant proteins; additionally, the development of biophysical techniques allows the increasingly detailed study of their structures and interactions. One of the greatest challenges in the in vitro study of membrane proteins remains to find an appropriate mimetic system that keeps them stable and, in turn, resembles as much as possible the characteristics of their native environment. That is why the development of membrane mimetics is a recurring and challenging topic in research worldwide.

This work discusses the advantages and disadvantages of the main membrane mimetics used in protein reconstitution (Chapter 2). The use of saponins in bicelle formation to stabilize transmembrane proteins such as BO was presented as a potential membrane mimetic with flexible size adaptative (Chapter 3).
We were able to characterize low populated membrane-associated states, via selectively directing hyperpolarization, using nanodiscs as a membrane system (Chapter 4).
The MRAP1 and MRAP2 proteins were successfully expressed by two expression systems: using a bacterial and a cell-free system offers the first characterization of both proteins were found to have an iron-binding motif in their primary sequence. In the case of MRAP1, the characteristic CXXCH motif of Cyt c was identified. In the case of MRAP2, the unusual AXXCH motif identified so far in cytochromes belonging to protozoa was identified. This fact reveals information that could be crucial to understand its hitherto unknown mechanisms of action (Chapters 5 & 6).

-

List of Publications

The following manuscripts are associated with the different projects presented in this thesis:

Chapter 2:

- Fatima Escobedo Gonzalez#, Ci Chu#, Manuel Etzkorn: The interplay of macromolecules with lipid membranes: Methods and insights. (in preparation, invitation for BBA- Biomembranes).

Chapter 3:

- Fatima Escobedo Gonzalez, Mohan Gospalswamy, Pia Hägerbäumer, Julian Victor, Georg Groth, Holger Gohlke, Thomas Hellweg, Manuel Etzkorn: Characterization of size-tunable Aescin-Lipid Particles as Platform for Stabilization of Membrane Proteins. (in preparation).

Chapter 4:

- Baran Uluca-Yazgi#, Fatima Escobedo Gonzalez#, Thibault Viennet, Hamed Shaykhalishahi, Luis Gardon, Nina Becker, Chetan Poojari, Wolfgang Hoyer, Olivier Ouari, Henrike Heise, Manuel Etzkorn: Selective hyperpolarization of membrane associated systems. (in preparation).

Chapter 5+6:

- Fatima Escobedo Gonzalez, Lora Denson, Manuel Etzkorn: In vitro characterization of the melanocortin accessory proteins identifies unexpected metal ion binding properties (in preparation).

# contributed equally

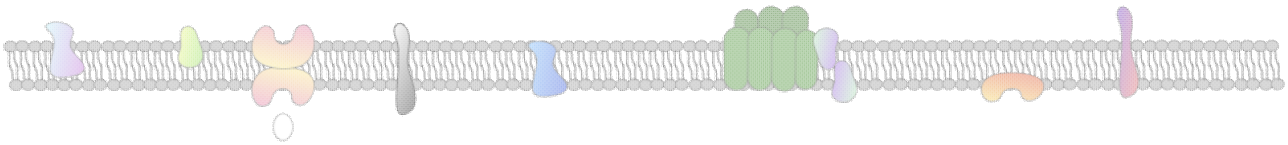

Supporting Material

Vector map **pET-28-a** vector

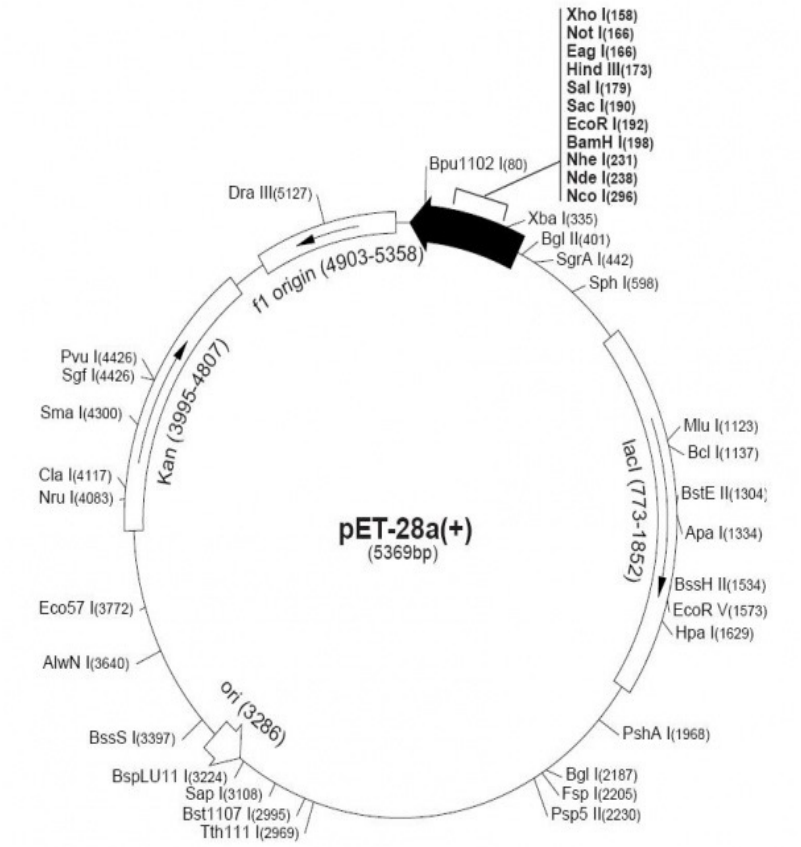

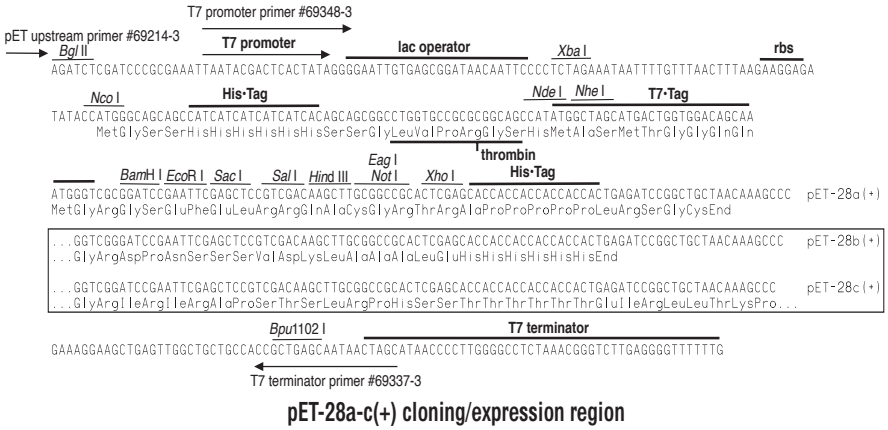

pET-28a-c(+) cloning/expression region

-

pIVEX2.4d vector

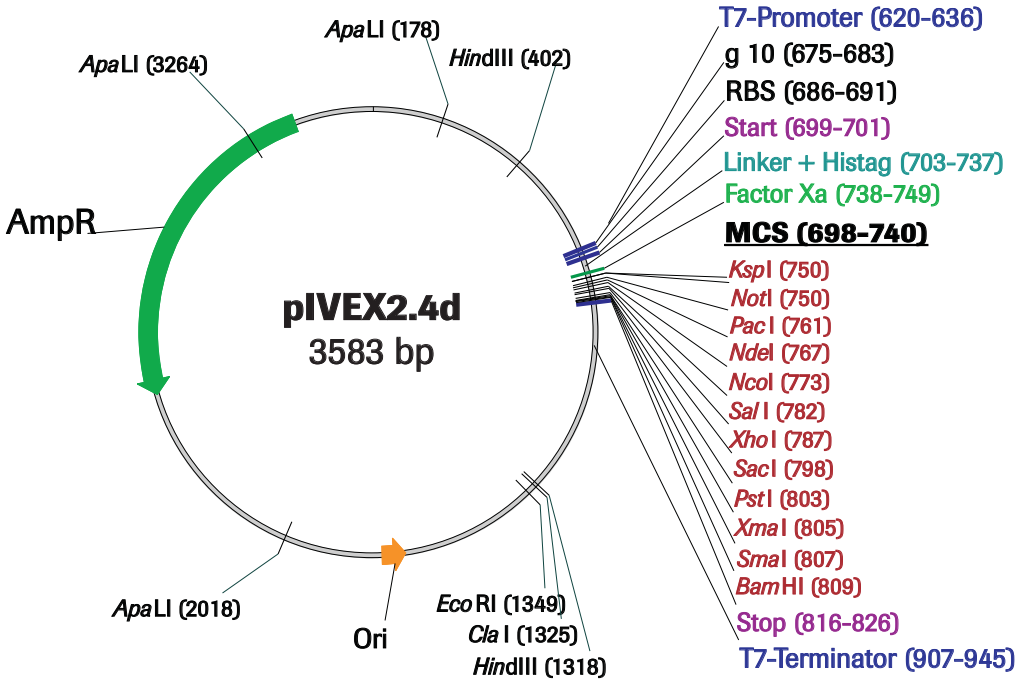


```
                                  T7-Promoter
601   GATCTCGATC CCGCGAAATT AATACGACTC ACTATAGGGA GACCACAACG
      CTAGAGCTAG GGCGCTTTAA TTATGCTGAG TGATATCCCT CTGGTGTTGC

                                    g10 ϵ       RBS
651   GTTTCCCTCT AGAAATAATT TTGTTTAACT TTAAGAAGGA GATATACCAT
      CAAAGGGAGA TCTTTATTAA AACAAATTGA AATTCTTCCT CTATATGGTA
                                                          Me

                                                       KspI
       Linker + Histag                            Factor Xa NotI
701   GTCTGGTTCT CATCATCATC ATCATCATAG CAGCGGCATC GAAGGCCGCG
      CAGACCAAGA GTAGTAGTAG TAGTAGTATC GTCGCCGTAG CTTCCGGCGC
      tSerGlySer HisHisHisH isHisHisSe rSerGlyIle GluGlyArgG

           PacI       NdeI     NcoI       SalI XhoI    SacI   PstI
751   GCCGCTTAAT TAAACATATG ACCATGGCAA GTCGACTCGA GCGAGCTCTG
      CGGCGAATTA ATTTGTATAC TGGTACCGTT CAGCTGAGCT CGCTCGAGAC
      lyArgLeuIl eLysHisMet ThrMetAlaS erArgLeuGl uArgAlaLeu

         XmaI
         SmaIBamHI
801   CAGCCCGGGA TCCGGTAACT AACTAAGATC CGGTAAGATC CGGCTGCTAA
      GTCGGGCCCT AGGCCATTGA TTGATTCTAG GCCATTCTAG GCCGACGATT
      GlnProGlyIle Arg*** * ** ***
```

-

DNA sequence

MRAP1 DNA sequence

MRAP2 DNA sequence

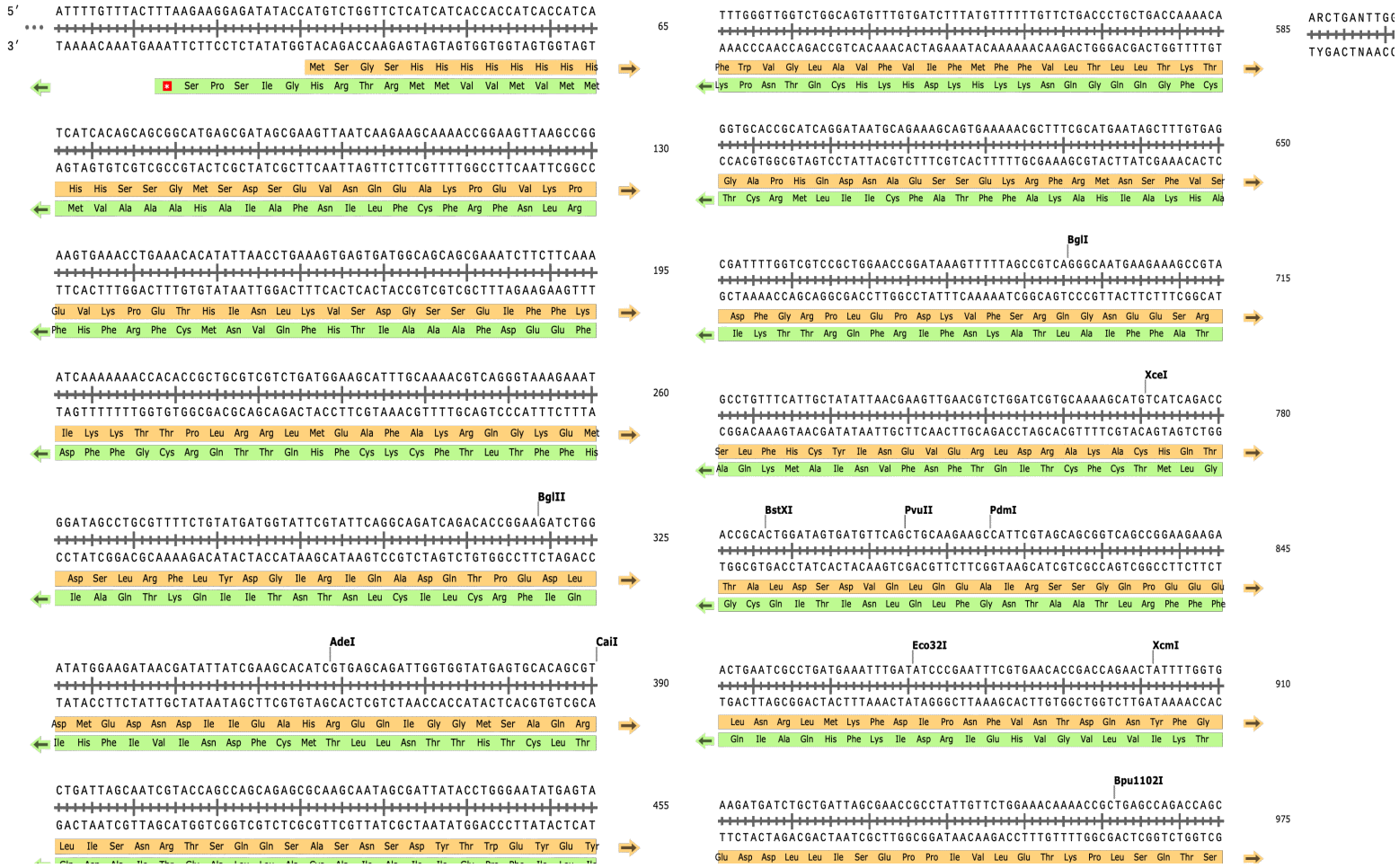

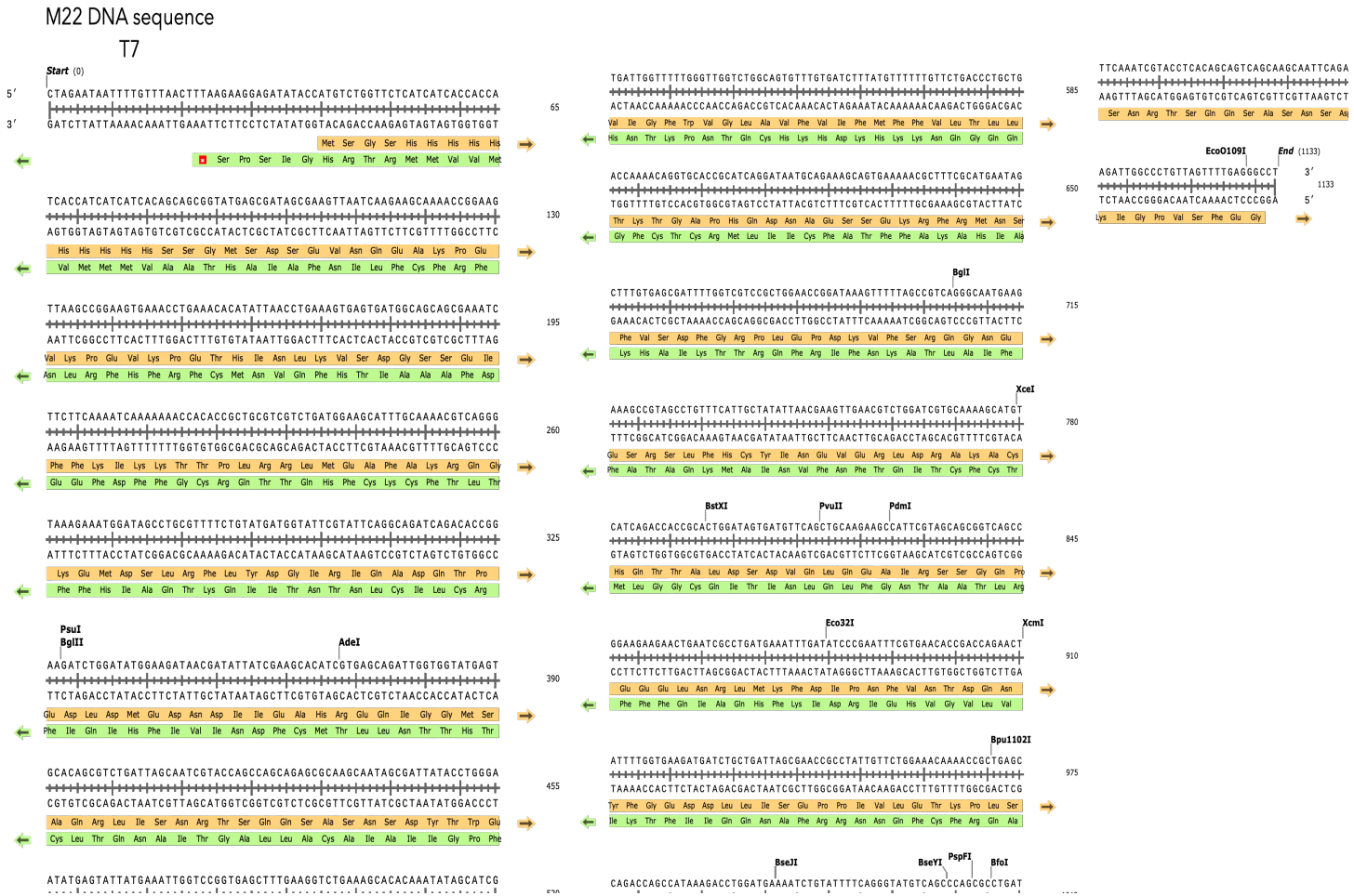
M22 DNA sequence
T7
Start (0)
5′
3′
Met Ser Gly Ser His His His His His His
Ser Pro Ser Ile Gly His Arg Thr Arg Met Met Val Val Met
His His His His His Ser Ser Gly Met Ser Asp Ser Glu Val Asn Gln Glu Ala Lys Pro Glu
Val Met Met Met Val Ala Ala Thr His Ala Ile Ala Phe Asn Ile Leu Phe Cys Phe Arg Phe
Val Lys Pro Glu Val Lys Pro Glu Thr His Ile Asn Leu Lys Val Ser Asp Gly Ser Ser Glu Ile
Asn Leu Arg Phe His Phe Arg Phe Cys Met Asn Val Gln Phe His Thr Ile Ala Ala Ala Phe Asp
Phe Phe Lys Ile Lys Lys Thr Thr Pro Leu Arg Arg Leu Met Glu Ala Phe Ala Lys Arg Gln Gly
Glu Glu Phe Asp Phe Phe Gly Cys Arg Gln Thr Thr Gln His Phe Cys Lys Cys Phe Thr Leu Thr
Lys Glu Met Asp Ser Leu Arg Phe Leu Tyr Asp Gly Ile Arg Ile Gln Ala Asp Gln Thr Pro
Phe Phe His Ile Ala Gln Thr Lys Gln Ile Ile Thr Asn Thr Asn Leu Cys Ile Leu Cys Arg
Glu Asp Leu Asp Met Glu Asp Asn Asp Ile Ile Glu Ala His Arg Glu Gln Ile Gly Gly Met Ser
Phe Ile Gln Ile His Phe Ile Val Ile Asn Asp Phe Cys Met Thr Leu Leu Asn Thr Thr His Thr
Ala Gln Arg Leu Ile Ser Asn Arg Thr Ser Gln Gln Ser Ala Ser Asn Ser Asp Tyr Thr Trp Glu
Cys Leu Thr Gln Asn Ala Ile Thr Gly Ala Leu Leu Ala Cys Ala Ile Ala Ile Ile Gly Pro Phe
65
130
195
260
325
390
455
520
585
650
715
780
845
910
975
1040
PsuI
BglII
AdeI
BstXI
PvuII
PdmI
Eco32I
XcmI
Bpu1102I
BseJI
BseYI
PspFI
BfoI
BglI
XceI
EcoO109I
End (1133)
1133

M22 DNA sequence

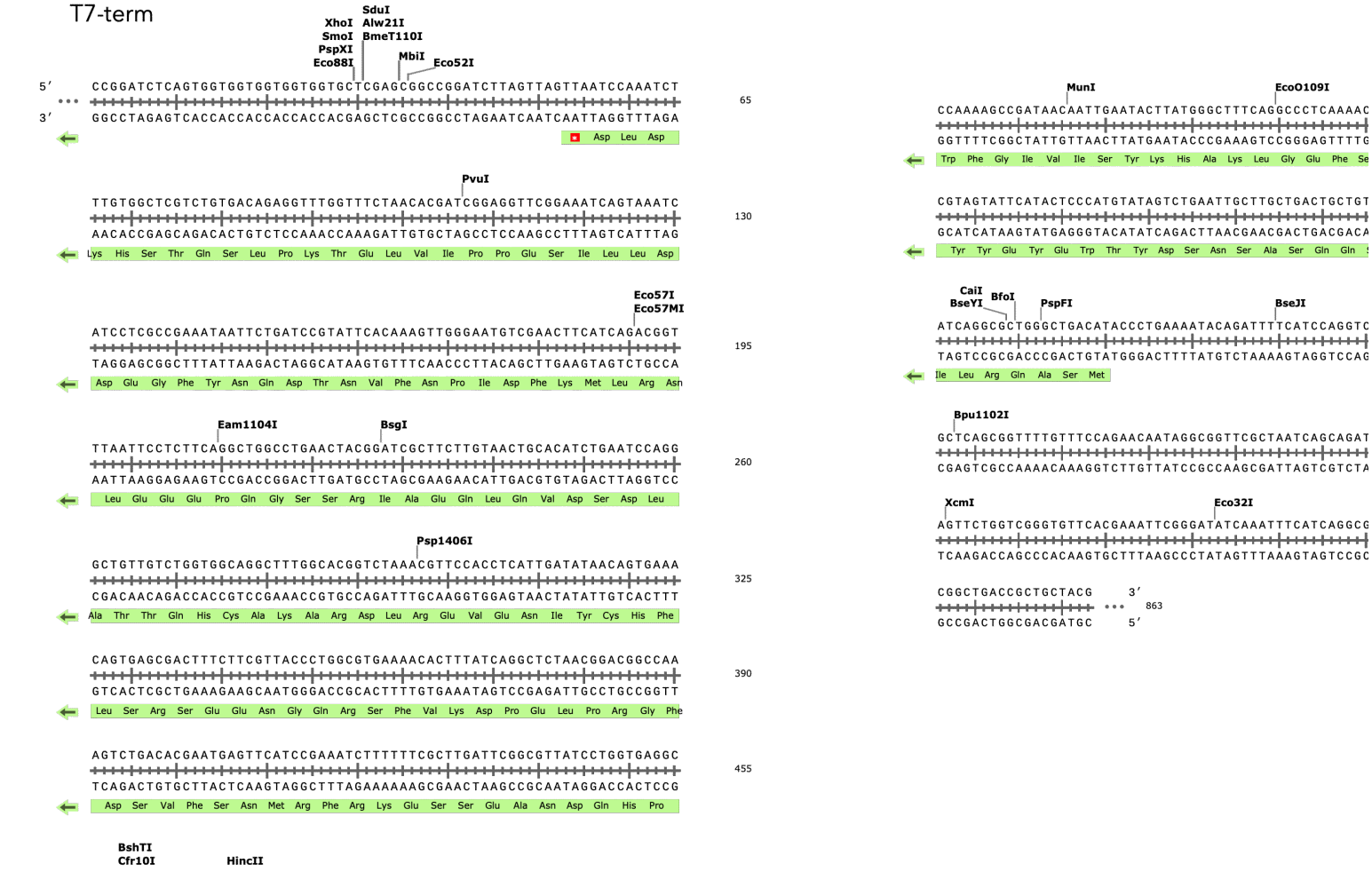

To assess the impact of the fusion tag composed of the histidine tag and the SUMO protease recognition site, spectra were obtained from another protein (NHR2) with the same fusion tag as MRAP2. Comparison of the UV-Vis spectra between the two proteins confirms that the maximum observed in MRAP2 spectra is not a result of the tags present at its N-terminal end.

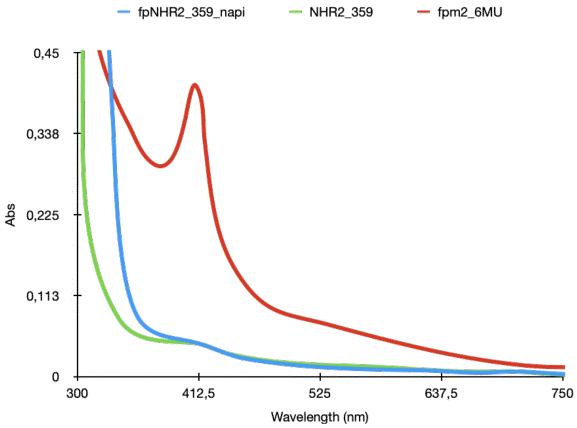

Uv-Vis spectra comparison between fp-NHR2, NHR2, and fp-M2. Here It is confirmed that the presence of His- and SUMO-tag does not influence significantly the UV-Vis profile.

-

Bibliography

[1] G. Tomasello, I. Armenia, and G. Molla, “The Protein Imager: A full-featured online molecular viewer interface with server-side HQ-rendering capabilities,” *Bioinformatics*, vol. 36, no. 9, pp. 2909–2911, 2020, doi: 10.1093/bioinformatics/btaa009.

[2] A. A. Spector and M. A. Yorek, “Membrane lipid composition and cellular function,” *J. Lipid Res.*, vol. 26, no. 9, pp. 1015–1035, 1985, doi: 10.1016/s0022-2275(20)34276-0.

[3] P. W. Bruce Alberts, Alexander Johnson, Julian Lewis, David Morgan, Martin Raff, Keith Roberts, *Molecular Biology of THE CELL*, vol. 53, no. 9. 2013.

[4] S. . Singer and G. L. Nicolson, “The fluid mosaic model of the structure of cell membranes,” *Science*, vol. 175. pp. 720–731, 1972.

[5] H. &E. E. W. Jeffrey R., “The role of alterations in membrane lipid composition in enabling physiological adaptation of organisms to their physical enviroment,” *Prog. Lipid Res.*, vol. 29, no. 4, pp. 167–1222, 1990.

[6] T. Raschle, S. Hiller, M. Etzkorn, and G. Wagner, “Nonmicellar systems for solution NMR spectroscopy of membrane proteins,” *Curr. Opin. Struct. Biol.*, vol. 20, no. 4, pp. 471–479, 2010, doi: 10.1016/j.sbi.2010.05.006.

[7] E. J. Dufourc, “Bicelles and nanodiscs for biophysical chemistry1,” *Biochim. Biophys. Acta - Biomembr.*, vol. 1863, no. 1, p. 183478, 2021, doi: 10.1016/j.bbamem.2020.183478.

[8] G. Van Meer, D. R. Voelker, and G. W. Feigenson, “Membrane lipids: Where they are and how they behave,” *Nat. Rev. Mol. Cell Biol.*, vol. 9, no. 2, pp. 112–124, 2008, doi: 10.1038/nrm2330.

[9] T. Harayama and H. Riezman, “Understanding the diversity of membrane lipid composition,” *Nat. Rev. Mol. Cell Biol.*, vol. 19, no. 5, pp. 281–296, 2018, doi: 10.1038/nrm.2017.138.

[10] G. W. Feigenson, “Phase boundaries and biological membranes,” *Annu. Rev. Biophys. Biomol. Struct.*, vol. 36, pp. 63–77, 2007, doi: 10.1146/annurev.biophys.36.040306.132721.

[11] K. Simons and W. L. C. Vaz, “Model systems, lipid rafts, and cell membranes,” *Annu. Rev. Biophys. Biomol. Struct.*, vol. 33, pp. 269–295, 2004, doi: 10.1146/annurev.biophys.32.110601.141803.

[12] J. Fantini and N. Yahi, “Protein–Lipid Interactions in the Brain,” *Brain Lipids Synaptic Funct. Neurol. Dis.*, vol. 2, pp. 135–162, 2015, doi: 10.1016/b978-0-12-800111-0.00006-0.

[13] H. Yin and A. D. Flynn, “Drugging Membrane Protein Interactions,” *Annu. Rev. Biomed. Eng.*, vol. 18, pp. 51–76, 2016, doi: 10.1146/annurev-bioeng-092115-025322.

[14] A. S. Joseph Martin, “Elucidating the Structure of membrane proteins,” *Biotechniques*, vol. 66, pp. 167–170, 2019.

[15] M. Uhlén *et al.*, “Tissue-based map of the human proteome,” *Science (80-.).*, vol. 347, no. 6220, 2015, doi: 10.1126/science.1260419.

[16] D. M. Boes, A. Godoy-Hernandez, and D. G. G. McMillan, “Peripheral membrane proteins: Promising therapeutic targets across domains of life,” *Membranes (Basel).*, vol. 11, no. 5, 2021, doi: 10.3390/membranes11050346.

[17] V. Monje-Galvan and J. B. Klauda, “Peripheral membrane proteins: Tying the knot between experiment and computation,” *Biochim. Biophys. Acta - Biomembr.*, vol. 1858, no. 7, pp. 1584–1593, 2016, doi: 10.1016/j.bbamem.2016.02.018.

[18] F. Cymer, G. Von Heijne, and S. H. White, “Mechanisms of integral membrane protein insertion and folding,” *J. Mol. Biol.*, vol. 427, no. 5, pp. 999–1022, 2015, doi: 10.1016/j.jmb.2014.09.014.

[19] Z. J. Maben, S. Malik, L. H. Jiang, and P. M. Hinkle, “Dual topology of the melanocortin-2 receptor accessory protein is stable,” *Front. Endocrinol. (Lausanne).*, vol. 7, no. JUL, 2016, doi: 10.3389/fendo.2016.00096.

[20] S. Majeed, A. B. Ahmad, U. Sehar, and E. R. Georgieva, “Lipid membrane mimetics in functional and structural studies of integral membrane proteins,” *Membranes (Basel).*, vol. 11, no. 9, pp. 1–29, 2021, doi: 10.3390/membranes11090685.

[21] C. R. Sanders and J. K. Myers, “Disease-related misassembly of membrane proteins,” *Annu. Rev. Biophys. Biomol. Struct.*,

vol. 33, pp. 25–51, 2004, doi: 10.1146/annurev.biophys.33.110502.140348.

[22] Z. S. Hou, A. Ulloa-Aguirre, and Y. X. Tao, "Pharmacoperone drugs: targeting misfolded proteins causing lysosomal storage-, ion channels-, and G protein-coupled receptors-associated conformational disorders," *Expert Rev. Clin. Pharmacol.*, vol. 11, no. 6, pp. 611–624, 2018, doi: 10.1080/17512433.2018.1480367.

[23] I. Ahmad *et al.*, "Overcoming challenges for amplified expression of recombinant proteins using Escherichia coli," *Protein Expr. Purif.*, vol. 144, no. October 2017, pp. 12–18, 2018, doi: 10.1016/j.pep.2017.11.005.

[24] H. J. Sharpe, T. J. Stevens, and S. Munro, "A Comprehensive Comparison of Transmembrane Domains Reveals Organelle-Specific Properties," *Cell*, vol. 142, no. 1, pp. 158–169, 2010, doi: 10.1016/j.cell.2010.05.037.

[25] D. T. Moore, B. W. Berger, and W. F. DeGrado, "Protein-Protein Interactions in the Membrane: Sequence, Structural, and Biological Motifs," *Structure*, vol. 16, no. 7, pp. 991–1001, 2008, doi: 10.1016/j.str.2008.05.007.

[26] K. D. Tsirigos *et al.*, "Topology of membrane proteins — predictions, limitations and variations," *Curr. Opin. Struct. Biol.*, vol. 50, pp. 9–17, 2018, doi: 10.1016/j.sbi.2017.10.003.

[27] O. Vit and J. Petrak, "Integral membrane proteins in proteomics. How to break open the black box?," *J. Proteomics*, vol. 153, pp. 8–20, 2017, doi: 10.1016/j.jprot.2016.08.006.

[28] E. Wallin and G. Von Heijne, "Genome-wide analysis of integral membrane proteins from eubacterial, archaean, and eukaryotic organisms," *Protein Sci.*, vol. 7, no. 4, pp. 1029–1038, 1998, doi: 10.1002/pro.5560070420.

[29] I. M. Nilsson and G. von Heijne, "Fine-tuning the topology of a polytopic membrane protein: Role of positively and negatively charged amino acids," *Cell*, vol. 62, no. 6, pp. 1135–1141, 1990, doi: 10.1016/0092-8674(90)90390-Z.

[30] G. Von Heijne, "Membrane-protein topology," *Nat. Rev. Mol. Cell Biol.*, vol. 7, no. 12, pp. 909–918, 2006, doi: 10.1038/nrm2063.

[31] V. Goder and M. Spiess, "Topogenesis of membrane proteins: Determinants and dynamics," *FEBS Lett.*, vol. 504, no. 3, pp. 87–93, 2001, doi: 10.1016/S0014-5793(01)02712-0.

[32] C. Masaracchia *et al.*, "Membrane binding, internalization, and sorting of alpha-synuclein in the cell," *Acta Neuropathol. Commun.*, vol. 6, no. 1, p. 79, 2018, doi: 10.1186/s40478-018-0578-1.

[33] E. Jo, J. A. McLaurin, C. M. Yip, P. St. George-Hyslop, and P. E. Fraser, "α-Synuclein membrane interactions and lipid specificity," *J. Biol. Chem.*, vol. 275, no. 44, pp. 34328–34334, 2000, doi: 10.1074/jbc.M004345200.

[34] J. S. O'Brien and E. L. Sampson, "Lipid composition of the normal human brain: gray matter, white matter, and myelin.," *J. Lipid Res.*, vol. 6, no. 4, pp. 537–544, 1965, doi: 10.1016/s0022-2275(20)39619-x.

[35] G. Bénard *et al.*, "Mitochondrial CB 1 receptors regulate neuronal energy metabolism," *Nat. Neurosci.*, vol. 15, no. 4, pp. 558–564, 2012, doi: 10.1038/nn.3053.

[36] S. M. Foord *et al.*, "International Union of Pharmacology. XLVI. G protein-coupled receptor list," *Pharmacol. Rev.*, vol. 57, no. 2, pp. 279–288, 2005, doi: 10.1124/pr.57.2.5.

[37] M. N. Davies *et al.*, "GPCRTree: Online hierarchical classification of GPCR function," *BMC Res. Notes*, vol. 1, pp. 1–5, 2008, doi: 10.1186/1756-0500-1-67.

[38] X. Zhang, S. Dong, and F. Xu, "Structural and Druggability Landscape of Frizzled G Protein-Coupled Receptors," *Trends Biochem. Sci.*, vol. 43, no. 12, pp. 1033–1046, 2018, doi: 10.1016/j.tibs.2018.09.002.

[39] R. Fredriksson, M. C. Lagerström, L. G. Lundin, and H. B. Schiöth, "The G-protein-coupled receptors in the human genome form five main families. Phylogenetic analysis, paralogon groups, and fingerprints," *Mol. Pharmacol.*, vol. 63, no. 6, pp. 1256–1272, 2003, doi: 10.1124/mol.63.6.1256.

[40] B. Mariel, "Mutations and diseases of G protein coupled receptors," *J. Recept. SIGNAL Transduct. Res.*, vol. 15, pp. 131–160, 1995.

[41] J. H. Chaoyang Xue, Yen-Ping Hsueh, "Magnificent seven: roles of G protein-coupled receptors in extracellular sensing in fungi," *FEMS Microbiol Rev*, vol. 32, no. 6, pp. 1010–1032, 2008, doi: 10.1111/j.1574-6976.2008.00131.x.Magnificent.

[42] D. Donnelly and J. B. C. Findlay, "Seven-helix receptors: structure and modelling," *Curr. Opin. Struct. Biol.*, vol. 4, no. 4, pp. 582–589, 1994, doi: 10.1016/S0959-440X(94)90221-6.

[43] R. C. S. Hollenstein, Kaspar, Chris de Graaf, Andrea Bortolato, Ming-Wei Wang, Fiona H. Marshall, "Insights into the structure of class B GPCRs Kaspar," *NIH Public Access*, vol. 35, no. 1, pp. 12–22, 2014, doi: 10.1016/j.tips.2013.11.001.Insights.

[44] B. Gessesse, T. Nagaike, K. Nagata, Y. Shimizu, and T. Ueda, "G-protein coupled receptor protein synthesis on a lipid bilayer using a reconstituted cell-free protein synthesis system," *Life*, vol. 8, no. 4, 2018, doi: 10.3390/life8040054.

[45] T. Haitina, "Function, Pharmacology, Evolution and Anatomical localization of G Protein-coupled receptors and solute carriers," 2009.

[46] D. Donnelly, "The arrangement of the transmembrane helices in the secretin receptor family of G-protein-coupled receptors," *FEBS Lett.*, vol. 409, no. 3, pp. 431–436, 1997, doi: 10.1016/S0014-5793(97)00546-2.

[47] H. Brauner-Osborne, P. Wellendorph, and A. Jensen, "Structure, Pharmacology and Therapeutic Prospects of Family C G-Protein Coupled Receptors," *Curr. Drug Targets*, vol. 8, no. 1, pp. 169–184, 2006, doi: 10.2174/138945007779315614.

[48] N. A. Brown, S. Schrevens, P. Van Dijck, and G. H. Goldman, "Fungal G-protein-coupled receptors: Mediators of pathogenesis and targets for disease control," *Nat. Microbiol.*, vol. 3, no. 4, pp. 402–414, 2018, doi: 10.1038/s41564-018-0127-5.

[49] V. Velazhahan *et al.*, "Structure of the class D GPCR Ste2 dimer coupled to two G proteins," *Nature*, vol. 589, no. 7840, pp. 148–153, 2021, doi: 10.1038/s41586-020-2994-1.

[50] P. S. Klein, T. J. Sun, C. L. Saxe, A. R. Kimmel, R. L. Johnson, and P. N. Devreotes, "A chemoattractant receptor controls development in Dictyostelium discoideum," *Science (80-.).*, vol. 241, no. 4872, pp. 1467–1472, 1988, doi: 10.1126/science.3047871.

[51] R. L. Johnson, C. L. Saxe, R. Gollop, A. R. Kimmel, and P. N. Devreotes, "Identification and targeted gene disruption of cAR3, a cAMP receptor subtype expressed during multicellular stages of Dictyostelium development," *Genes Dev.*, vol. 7, no. 2, pp. 273–282, 1993, doi: 10.1101/gad.7.2.273.

[52] H. J. Sharpe, W. Wang, R. N. Hannoush, and F. J. De Sauvage, "Regulation of the oncoprotein Smoothened by small molecules," *Nat. Chem. Biol.*, vol. 11, no. 4, pp. 246–255, 2015, doi: 10.1038/nchembio.1776.

[53] V. Lam and V. Lam, "Development and Validation of a Novel Quantitative Assay for Cell Surface expression of GPCRs using a Receptor β -lactamase Fusion Protein and the Colourometric Substrate Nitrocefin by Development and Validation of a Novel Quantitative Assay for Cell Prot," 2013.

[54] D. & S. Oesterhelt, FilippOesterhelt, "Rhodopsin-like Protein from the Purple Membrane of Halobacterium halobium," *Nat. New Biol.*, vol. 233, pp. 149–152, 1971.

[55] J. K. Lanyi, "Bacteriorhodopsin," *Annu. Rev. Physiol.*, vol. 66, pp. 665–688, 2004, doi: 10.1146/annurev.physiol.66.032102.150049.

[56] D. Oesterhelt and W. Stoeckenius, "Functions of a new photoreceptor membrane," *Proc. Natl. Acad. Sci. U. S. A.*, vol. 70, no. 10, pp. 2853–2857, 1973, doi: 10.1073/pnas.70.10.2853.

[57] M. Etzkorn *et al.*, "Cell-free expressed bacteriorhodopsin in different soluble membrane mimetics: Biophysical properties and NMR accessibility," *Structure*, vol. 21, no. 3, pp. 394–401, 2013, doi: 10.1016/j.str.2013.01.005.

[58] N. Hasegawa, H. Jonotsuka, K. Miki, and K. Takeda, "X-ray structure analysis of bacteriorhodopsin at 1.3 Å resolution," *Sci. Rep.*, vol. 8, no. 1, pp. 1–8, 2018, doi: 10.1038/s41598-018-31370-0.

[59] S. Schlegel, A. Hjelm, T. Baumgarten, D. Vikström, and J. W. De Gier, "Bacterial-based membrane protein production," *Biochim. Biophys. Acta - Mol. Cell Res.*, vol. 1843, no. 8, pp. 1739–1749, 2014, doi: 10.1016/j.bbamcr.2013.10.023.

[60] K. Mathieu *et al.*, "Functionality of membrane proteins overexpressed and purified from E. coli is highly dependent upon the strain," *Sci. Rep.*, vol. 9, no. 1, pp. 1–15, 2019, doi: 10.1038/s41598-019-39382-0.

[61] Y. He, K. Wang, and N. Yan, "The recombinant expression systems for structure determination of eukaryotic membrane proteins," *Protein Cell*, vol. 5, no. 9, pp. 658–672, 2014, doi: 10.1007/s13238-014-0086-4.

[62] G. L. Rosano and E. A. Ceccarelli, "Recombinant protein expression in Escherichia coli: Advances and challenges," *Front. Microbiol.*, vol. 5, no. APR, pp. 1–17, 2014, doi: 10.3389/fmicb.2014.00172.

[63] S. K. Kwon, S. K. Kim, D. H. Lee, and J. F. Kim, "Comparative genomics and experimental evolution of Escherichia coli

BL21(DE3) strains reveal the landscape of toxicity escape from membrane protein overproduction," *Sci. Rep.*, vol. 5, no. May, p. 16076, 2015, doi: 10.1038/srep16076.

[64] H. Tegel, S. Tourle, J. Ottosson, and A. Persson, "Increased levels of recombinant human proteins with the Escherichia coli strain Rosetta(DE3)," *Protein Expr. Purif.*, vol. 69, no. 2, pp. 159–167, 2010, doi: 10.1016/j.pep.2009.08.017.

[65] D. M. Francis and R. Page, "Strategies to optimize protein expression in E. coli," *Curr. Protoc. Protein Sci.*, no. SUPPL. 61, pp. 1–29, 2010, doi: 10.1002/0471140864.ps0524s61.

[66] C. Klammt *et al.*, "High level cell-free expression and specific labeling of integral membrane proteins," *Eur. J. Biochem.*, vol. 271, no. 3, pp. 568–580, 2004, doi: 10.1111/j.1432-1033.2003.03959.x.

[67] X. Jin and S. H. Hong, "Cell-free protein synthesis for producing 'difficult-to-express' proteins," *Biochem. Eng. J.*, vol. 138, pp. 156–164, 2018, doi: 10.1016/j.bej.2018.07.013.

[68] M. Harbers, "Wheat germ systems for cell-free protein expression," *FEBS Lett.*, vol. 588, no. 17, pp. 2762–2773, 2014, doi: 10.1016/j.febslet.2014.05.061.

[69] F. Katzen, G. Chang, and W. Kudlicki, "The past, present and future of cell-free protein synthesis," *Trends Biotechnol.*, vol. 23, no. 3, pp. 150–156, 2005, doi: 10.1016/j.tibtech.2005.01.003.

[70] D. Schwarz *et al.*, "Preparative scale expression of membrane proteins in Escherichia coli-based continuous exchange cell-free systems.," *Nat. Protoc.*, vol. 2, no. 11, pp. 2945–2957, 2007, doi: 10.1038/nprot.2007.426.

[71] B. Schneider, F. Junge, V. A. Shirokov, D. Schwarz, V. Dötsch, and F. Bernhard, "Chapter 11 Membrane Protein Expression in Cell-Free Systems," vol. 601, pp. 165–186, doi: 10.1007/978-1-60761-344-2.

[72] M. Stech, R. B. Quast, R. Sachse, C. Schulze, and D. A. Wüstenhagen Stefan Kubick, "A continuous-exchange cell-free protein synthesis system based on extracts from cultured insect cells," *PLoS One*, vol. 9, no. 5, 2014, doi: 10.1371/journal.pone.0096635.

[73] M. He, B. M. Edwards, D. Kastelic, and M. J. Taussig, "Ribosome Display and Related Technologies," vol. 805, pp. 75–85, 2012, doi: 10.1007/978-1-61779-379-0.

[74] D. M. Kim and J. R. Swartz, "Prolonging cell-free protein synthesis by selective reagent additions," *Biotechnol. Prog.*, vol. 16, no. 3, pp. 385–390, 2000, doi: 10.1021/bp000031y.

[75] J. Kim, C. E. Copeland, S. R. Padumane, and Y. C. Kwon, "A crude extract preparation and optimization from a genomically engineered escherichia coli for the cell-free protein synthesis system: Practical laboratory guideline," *Methods Protoc.*, vol. 2, no. 3, pp. 1–15, 2019, doi: 10.3390/mps2030068.

[76] J. L. Dopp, Y. R. Jo, and N. F. Reuel, "Methods to reduce variability in E. Coli-based cell-free protein expression experiments," *Synth. Syst. Biotechnol.*, vol. 4, no. 4, pp. 204–211, 2019, doi: 10.1016/j.synbio.2019.10.003.

[77] K. A. Datsenko and B. L. Wanner, "One-step inactivation of chromosomal genes in Escherichia coli K-12 using PCR products," *Proc. Natl. Acad. Sci. U. S. A.*, vol. 97, no. 12, pp. 6640–6645, 2000, doi: 10.1073/pnas.120163297.

[78] L. Frey, N. A. Lakomek, R. Riek, and S. Bibow, "Micelles, Bicelles, and Nanodiscs: Comparing the Impact of Membrane Mimetics on Membrane Protein Backbone Dynamics," *Angew. Chemie - Int. Ed.*, vol. 56, no. 1, pp. 380–383, 2017, doi: 10.1002/anie.201608246.

[79] J. Stetefeld, S. A. McKenna, and T. R. Patel, "Dynamic light scattering: a practical guide and applications in biomedical sciences," *Biophys. Rev.*, vol. 8, no. 4, pp. 409–427, 2016, doi: 10.1007/s12551-016-0218-6.

[80] C. Martin, "Application of Bayesian Inference to Analysis of Dynamic Light Scattering Data to Determine Particle Size Distributions Application of Bayesian Inference to Analysis of Dynamic Light Scattering Data to Determine Particle Size Distributions Submitted in Pa," 2018.

[81] R. Puthenveetil and O. Vinogradova, "Solution NMR: A powerful tool for structural and functional studies of membrane proteins in reconstituted environments," *J. Biol. Chem.*, vol. 294, no. 44, pp. 15914–15931, 2019, doi: 10.1074/jbc.REV119.009178.

[82] G. I. Danmaliki and P. M. Hwang, "Solution NMR spectroscopy of membrane proteins," *Biochim. Biophys. Acta - Biomembr.*, vol. 1862, no. 9, p. 183356, 2020, doi: 10.1016/j.bbamem.2020.183356.

[83] James Keeler, "Understanding NMR Spectroscopy," pp. 9–25, 2010.

[84] M. V. Berjanskii and D. S. Wishart, "Unraveling the meaning of chemical shifts in protein NMR," *Biochim. Biophys. Acta - Proteins Proteomics*, vol. 1865, no. 11, pp. 1564–1576, 2017, doi: 10.1016/j.bbapap.2017.07.005.

[85] D. S. Wishart, "Interpreting protein chemical shift data," *Prog. Nucl. Magn. Reson. Spectrosc.*, vol. 58, no. 1–2, pp. 62–87, 2011, doi: 10.1016/j.pnmrs.2010.07.004.

[86] M. P. Williamson, "Secondary□structure dependent chemical shifts in proteins," *Biopolymers*, vol. 29, no. 10–11, pp. 1423–1431, 1990, doi: 10.1002/bip.360291009.

[87] N. E. Hafsa, D. Arndt, and D. S. Wishart, "CSI 3.0: A web server for identifying secondary and super-secondary structure in proteins using NMR chemical shifts," *Nucleic Acids Res.*, vol. 43, no. W1, pp. W370–W377, 2015, doi: 10.1093/nar/gkv494.

[88] D. S. Wishart, B. D. Sykes, and F. M. Richards, "The Chemical Shift Index□: A Fast and Simple Method for the Assignment of Protein Secondary Structure Through NMR Spectroscopy," *Biochemistry*, vol. 31, no. 6, pp. 1647–1651, 1992, doi: 10.1021/bi00121a010.

[89] Z. Liu, Z. Gong, X. Dong, and C. Tang, "Transient protein-protein interactions visualized by solution NMR," *Biochim. Biophys. Acta - Proteins Proteomics*, vol. 1864, no. 1, pp. 115–122, 2015, doi: 10.1016/j.bbapap.2015.04.009.

[90] P. Aggarwal, P. Kumari, and N. S. Bhavesh, *Advances in liquid-state NMR spectroscopy to study the structure, function, and dynamics of biomacromolecules*. Elsevier Inc., 2022.

[91] N. R. Sibson and K. L. Behar, *Magnetic Resonance Spectroscopy in Neuroenergetics and Neurotransmission*. Elsevier Inc., 2013.

[92] J. Fiaux, E. B. Bertelsen, A. L. Horwich, and K. Wüthrich, "NMR analysis of a 900K GroEL-GroES complex," *Nature*, vol. 418, no. 6894, pp. 207–211, 2002, doi: 10.1038/nature00860.

[93] G. Zhu and X. Yao, "TROSY-based NMR experiments for NMR studies of large biomolecules," *Prog. Nucl. Magn. Reson. Spectrosc.*, vol. 52, no. 1, pp. 49–68, 2008, doi: 10.1016/j.pnmrs.2007.10.001.

[94] K. Jaudzems, T. Polenova, G. Pintacuda, H. Oschkinat, and A. Lesage, "DNP NMR of biomolecular assemblies," *J. Struct. Biol.*, vol. 206, no. 1, pp. 90–98, 2019, doi: 10.1016/j.jsb.2018.09.011.

[95] Y. Kim and C. Hilty, *Applications of Dissolution-DNP for NMR Screening*, 1st ed., vol. 615. Elsevier Inc., 2019.

[96] E. D. Goluch, A. W. Shaw, S. G. Sligar, and C. Liu, "Microfluidic patterning of nanodisc lipid bilayers and multiplexed analysis of protein interaction," *Lab Chip*, vol. 8, no. 10, pp. 1723–1728, 2008, doi: 10.1039/b806733c.

[97] A. E. Saliba, I. Vonkova, and A. C. Gavin, "The systematic analysis of protein-lipid interactions comes of age," *Nature Reviews Molecular Cell Biology*, vol. 16, no. 12. Nature Publishing Group, pp. 753–761, Dec. 01, 2015, doi: 10.1038/nrm4080.

[98] A. L. Plant, "Supported hybrid bilayer membranes as rugged cell membrane mimics," *Langmuir*, vol. 15, no. 15, pp. 5128–5135, Jul. 1999, doi: 10.1021/la981662t.

[99] D. E. Warschawski, A. A. Arnold, M. Beaugrand, A. Gravel, É. Chartrand, and I. Marcotte, "Choosing membrane mimetics for NMR structural studies of transmembrane proteins," *Biochimica et Biophysica Acta - Biomembranes*, vol. 1808, no. 8. pp. 1957–1974, Aug. 2011, doi: 10.1016/j.bbamem.2011.03.016.

[100] S. G. Patching, "Surface plasmon resonance spectroscopy for characterisation of membrane protein-ligand interactions and its potential for drug discovery," *Biochimica et Biophysica Acta - Biomembranes*, vol. 1838, no. 1 PARTA. pp. 43–55, 2014, doi: 10.1016/j.bbamem.2013.04.028.

[101] T. K. Ritchie *et al.*, "Chapter 11 Reconstitution of Membrane Proteins in Phospholipid Bilayer Nanodiscs," *Methods in Enzymology*, vol. 464, no. C. pp. 211–231, 2009, doi: 10.1016/S0076-6879(09)64011-8.

[102] G. G. Privé, "Lipopeptide detergents for membrane protein studies," *Current Opinion in Structural Biology*, vol. 19, no. 4. pp. 379–385, Aug. 2009, doi: 10.1016/j.sbi.2009.07.008.

[103] and S. G. S. Timothy H. Bayburt, Yelena V. Grinkova, "Self-Assembly of Discoidal Phospholipid Bilayer Nanoparticles with Membrane Scaffold Proteins," *Nano Lett.*, vol. 2, 2002.

[104] A. Akbarzadeh *et al.*, "Liposome: Classification, preparation, and applications," *Nanoscale Res. Lett.*, vol. 8, no. 1, 2013, doi: 10.1186/1556-276X-8-102.

[105] A. Jesorka and O. Orwar, "Liposomes: Technologies and Analytical Applications," *Annu. Rev. Anal. Chem.*, vol. 1, no. 1, pp. 801–832, Jul. 2008, doi: 10.1146/annurev.anchem.1.031207.112747.

[106] G. Nasr, H. Greige-Gerges, A. Elaissari, and N. Khreich, "Liposomal membrane permeability assessment by fluorescence techniques: Main permeabilizing agents, applications and challenges," *International Journal of Pharmaceutics*, vol. 580. Elsevier B.V., Apr. 30, 2020, doi: 10.1016/j.ijpharm.2020.119198.

[107] F. Hagn, M. Etzkorn, T. Raschle, and G. Wagner, "Optimized phospholipid bilayer nanodiscs facilitate high-resolution structure determination of membrane proteins," *J. Am. Chem. Soc.*, vol. 135, no. 5, pp. 1919–1925, Feb. 2013, doi: 10.1021/ja310901f.

[108] T. H. Bayburt and S. G. Sligar, "Single-molecule height measurements on microsomal cytochrome P450 in nanometer-scale phospholipid bilayer disks." [Online]. Available: www.pnas.orgcgidoi10.1073pnas.062565599.

[109] T. H. Bayburt and S. G. Sligar, "Membrane protein assembly into Nanodiscs," *FEBS Letters*, vol. 584, no. 9. pp. 1721–1727, May 2010, doi: 10.1016/j.febslet.2009.10.024.

[110] K. Klöpfer and F. Hagn, "Beyond detergent micelles: The advantages and applications of non-micellar and lipid-based membrane mimetics for solution-state NMR," *Progress in Nuclear Magnetic Resonance Spectroscopy*, vol. 114–115. Elsevier B.V., pp. 271–283, Oct. 01, 2019, doi: 10.1016/j.pnmrs.2019.08.001.

[111] M. Falke *et al.*, "α-Synuclein-derived lipoparticles in the study of α-Synuclein amyloid fibril formation," *Chem. Phys. Lipids*, vol. 220, pp. 57–65, 2019, doi: 10.1016/j.chemphyslip.2019.02.009.

[112] T. J. Knowles, R. Finka, C. Smith, Y. P. Lin, T. Dafforn, and M. Overduin, "Membrane proteins solubilized intact in lipid containing nanoparticles bounded by styrene maleic acid copolymer," *J. Am. Chem. Soc.*, vol. 131, no. 22, pp. 7484–7485, Jun. 2009, doi: 10.1021/ja810046q.

[113] A. O. Oluwole *et al.*, "Formation of Lipid-Bilayer Nanodiscs by Diisobutylene/Maleic Acid (DIBMA) Copolymer," *Langmuir*, vol. 33, no. 50, pp. 14378–14388, Dec. 2017, doi: 10.1021/acs.langmuir.7b03742.

[114] M. Pinheiro, J. Magalhães, and S. Reis, "Antibiotic interactions using liposomes as model lipid membranes," *Chemistry and Physics of Lipids*, vol. 222. Elsevier Ireland Ltd, pp. 36–46, Aug. 01, 2019, doi: 10.1016/j.chemphyslip.2019.05.002.

[115] V. Teixeira, M. J. Feio, and M. Bastos, "Role of lipids in the interaction of antimicrobial peptides with membranes," *Progress in Lipid Research*, vol. 51, no. 2. pp. 149–177, Apr. 2012, doi: 10.1016/j.plipres.2011.12.005.

[116] M.-T. Lee, "Biophysical characterization of peptide–membrane interactions," *Adv. Phys. X*, vol. 3, no. 1, p. 1408428, Jan. 2018, doi: 10.1080/23746149.2017.1408428.

[117] A. Ochiai *et al.*, "Crystal structure of rice defensin OsAFP1 and molecular insight into lipid-binding," *J. Biosci. Bioeng.*, 2020, doi: 10.1016/j.jbiosc.2020.02.011.

[118] S. Dowler, G. Kular, and D. R. Alessi, "INTRODUCTION MATERIALS Chemicals and Reagents Antibodies, Cells, and Plasmids EQUIPMENT RECIPES INSTRUCTIONS Purification of Recombinant GST-Fusion Proteins from E. coli Purification of GST-Fusion Proteins from HEK 293 Cells Protein Lipid Overlay Assay TR," no. April, pp. 1–11, 2015, [Online]. Available: www.stke.org/cgi/content/full/OC_sigtrans;2002/129/pl6http://stke.sciencemag.org/Downloadedfromwww.stke.org/cgi/content/full/OC_sigtrans;2002/129/pl6.

[119] C. M. Shirey, J. L. Scott, and R. V. Stahelin, "Notes and tips for improving quality of lipid-protein overlay assays," *Anal. Biochem.*, vol. 516, pp. 9–12, Jan. 2017, doi: 10.1016/j.ab.2016.10.009.

[120] S. Dowler, R. A. Currie, C. P. Downes, and D. R. Alessi, "DAPP1□: a dual adaptor for phosphotyrosine and 3-phosphoinositides," 1999.

[121] L. Ceccato *et al.*, "PLIF: A rapid, accurate method to detect and quantitatively assess protein-lipid interactions." [Online]. Available: www.SCIENCESIGNALING.org.

[122] S. Huang, L. Gao, L. Blanchoin, and C. J. Staiger, "Heterodimeric Capping Protein from Arabidopsis Is Regulated by Phosphatidic Acid," *Mol. Biol. Cell*, vol. 17, 1946, doi: 10.1091/mbc.E05-09.

[123] W. Jin *et al.*, "Lipid binding regulates synaptic targeting of PICK1, AMPA receptor trafficking, and synaptic plasticity," *J. Neurosci.*, vol. 26, no. 9, pp. 2380–2390, Mar. 2006, doi: 10.1523/JNEUROSCI.3503-05.2006.

[124] T. Ganz, "Defensins: Antimicrobial peptides of innate immunity," *Nature Reviews Immunology*, vol. 3, no. 9. pp. 710–720,

Sep. 2003, doi: 10.1038/nri1180.

[125] T. L. R. Ganz, "Defensins," *Pharmac. Ther.*, vol. 66, pp. 191–205, 1995.

[126] V. S. G. Amaral *et al.*, "Psd2 pea defensin shows a preference for mimetic membrane rafts enriched with glucosylceramide and ergosterol," *Biochim. Biophys. Acta - Biomembr.*, vol. 1861, no. 4, pp. 713–728, Apr. 2019, doi: 10.1016/j.bbamem.2018.12.020.

[127] M. Beseničar, P. Maček, J. H. Lakey, and G. Anderluh, "Surface plasmon resonance in protein-membrane interactions," *Chemistry and Physics of Lipids*, vol. 141, no. 1–2. pp. 169–178, Jun. 2006, doi: 10.1016/j.chemphyslip.2006.02.010.

[128] D. G. Myszka, "Kinetic analysis of macro mo le cular inte ractions using surface plasmon resonance biosensors."

[129] K. Narayan and M. A. Lemmon, "Determining selectivity of phosphoinositide-binding domains," *Methods*, vol. 39, no. 2, pp. 122–133, Jun. 2006, doi: 10.1016/j.ymeth.2006.05.006.

[130] J. Charmet, P. Arosio, and T. P. J. Knowles, "Microfluidics for Protein Biophysics," *Journal of Molecular Biology*, vol. 430, no. 5. pp. 565–580, 2018, doi: 10.1016/j.jmb.2017.12.015.

[131] P. Arosio *et al.*, "Microfluidic diffusion analysis of the sizes and interactions of proteins under native solution conditions," *ACS Nano*, vol. 10, no. 1, pp. 333–341, Jan. 2016, doi: 10.1021/acsnano.5b04713.

[132] E. V. Yates *et al.*, "Latent analysis of unmodified biomolecules and their complexes in solution with attomole detection sensitivity," *Nat. Chem.*, vol. 7, no. 10, pp. 802–809, Oct. 2015, doi: 10.1038/nchem.2344.

[133] S. Munusamy, R. Conde, B. Bertrand, and C. Munoz-Garay, "Biophysical approaches for exploring lipopeptide-lipid interactions," *Biochimie*, vol. 170, pp. 173–202, 2020, doi: 10.1016/j.biochi.2020.01.009.

[134] G. Lindblom and G. Gröbner, "NMR on lipid membranes and their proteins," *Current Opinion in Colloid and Interface Science*, vol. 11, no. 1. pp. 24–29, Apr. 2006, doi: 10.1016/j.cocis.2005.09.017.

[135] D. I. Fernandez, J. D. Gehman, and F. Separovic, "Membrane interactions of antimicrobial peptides from Australian frogs," *Biochimica et Biophysica Acta - Biomembranes*, vol. 1788, no. 8. pp. 1630–1638, Aug. 2009, doi: 10.1016/j.bbamem.2008.10.007.

[136] M. S. Baila, J. H. Bowie, and F. Separovic, "Solid-state NMR study of antimicrobial peptides from Australian frogs in phospholipid membranes," *Eur. Biophys. J.*, vol. 33, no. 2, pp. 109–116, Apr. 2004, doi: 10.1007/s00249-003-0342-7.

[137] Y. L. Pan, J. T. J. Cheng, J. Hale, J. Pan, R. E. W. Hancock, and S. K. Straus, "Characterization of the structure and membrane interaction of the antimicrobial peptides aurein 2.2 and 2.3 from Australian southern bell frogs," *Biophys. J.*, vol. 92, no. 8, pp. 2854–2864, 2007, doi: 10.1529/biophysj.106.097238.

[138] L. M. S. Loura, R. F. M. De Almeida, A. Coutinho, and M. Prieto, "Interaction of peptides with binary phospholipid membranes: application of fluorescence methodologies." [Online]. Available: www.elsevier.com/locate/chemphyslip.

[139] B. Christiaens *et al.*, "Tryptophan fluorescence study of the interaction of penetratin peptides with model membranes," *European Journal of Biochemistry*, vol. 269, no. 12. pp. 2918–2926, 2002, doi: 10.1046/j.1432-1033.2002.02963.x.

[140] J. A. González-Vera, "Probing the kinome in real time with fluorescent peptides," *Chemical Society Reviews*, vol. 41, no. 5. pp. 1652–1664, 2012, doi: 10.1039/c1cs15198c.

[141] T. Ehrenschwender and H.-A. Wagenknecht, "4,4-Difluoro-4-bora-3a,4a-diaza-s-indacene as a bright fluorescent label for DNA.," *J. Org. Chem.*, vol. 76, no. 7, pp. 2301–2304, Apr. 2011, doi: 10.1021/jo102519k.

[142] R. Geisler *et al.*, "Aescin - a natural soap for the formation of lipid nanodiscs with tunable size," *Soft Matter*, vol. 17, no. 7, pp. 1888–1900, 2021, doi: 10.1039/d0sm02043e.

[143] M. Marrelli, F. Conforti, F. Araniti, and G. A. Statti, "Effects of saponins on lipid metabolism: A review of potential health benefits in the treatment of obesity," *Molecules*, vol. 21, no. 10, 2016, doi: 10.3390/molecules21101404.

[144] B. Korchowiec, M. Gorczyca, K. Wojszko, M. Janikowska, M. Henry, and E. Rogalska, "Impact of two different saponins on the organization of model lipid membranes," *Biochim. Biophys. Acta - Biomembr.*, vol. 1848, no. 10, pp. 1963–1973, 2015, doi: 10.1016/j.bbamem.2015.06.007.

[145] M. Dudek-Makuch and E. Studzińska-Sroka, "Horse Chestnut - Efficacy and safety in chronic venous insufficiency: An overview," *Rev. Bras. Farmacogn.*, vol. 25, no. 5, pp. 533–541, 2015, doi: 10.1016/j.bjp.2015.05.009.

[146] R. Geisler, C. Dargel, and T. Hellweg, "The biosurfactant β-aescin: A review on the physico-chemical properties and its interaction with lipid model membranes and langmuir monolayers," *Molecules*, vol. 25, no. 1, pp. 1–22, 2020, doi: 10.3390/molecules25010117.

[147] V. R. Netala, S. B. Ghosh, P. Bobbu, D. Anitha, and V. Tartte, "Triterpenoid saponins: A review on biosynthesis, Applications and mechanism of their action," *Int. J. Pharm. Pharm. Sci.*, vol. 7, no. 1, pp. 24–28, 2015.

[148] J. A. Wilkinson and A. M. G. Brown, "Horse chestnut - Aesculus hippocastanum: Potential applications in cosmetic skin-care products," *Int. J. Cosmet. Sci.*, vol. 21, no. 6, pp. 437–447, 1999, doi: 10.1046/j.1467-2494.1999.234192.x.

[149] A. Costantini, "Escin in pharmaceutical oral dosage forms: Quantitative densitometric HPTLC determination," *Farmaco*, vol. 54, no. 11–12, pp. 728–732, 1999, doi: 10.1016/S0014-827X(99)00090-7.

[150] E. E. Pittler MH, "Horse chestnut seed extract for venous insufficiency," *Altern. Ther. Womens Heal.*, vol. 9, no. 4, pp. 25–27, 2007.

[151] R. Geisler, C. Dargel, and T. Hellweg, "The biosurfactant β-aescin: A review on the physico-chemical properties and its interaction with lipid model membranes and langmuir monolayers," *Molecules*, vol. 25, no. 1, 2020, doi: 10.3390/molecules25010117.

[152] J. W. Smalley *et al.*, "HmuY haemophore and gingipain proteases constitute a unique syntrophic system of haem acquisition by Porphyromonas gingivalis," *PLoS One*, vol. 6, no. 2, 2011, doi: 10.1371/journal.pone.0017182.

[153] J. Puerres, M. Díaz, J. Hurtado, P. Ortiz, and M. T. Cortés, "Photoelectrochemical stability under anodic and cathodic conditions of meso-tetra-(4-sulfonatophenyl)-porphyrinato cobalt (ii) immobilized in polypyrrole thin films," *Polymers (Basel).*, vol. 13, no. 4, pp. 1–14, 2021, doi: 10.3390/POLYM13040657.

[154] R. Sreij *et al.*, "Temperature dependent self-organization of DMPC membranes promoted by intermediate amounts of the saponin aescin," *Biochim. Biophys. Acta - Biomembr.*, vol. 1861, no. 5, pp. 897–906, 2019, doi: 10.1016/j.bbamem.2019.01.015.

[155] R. Geisler *et al.*, "Aescin-Induced Conversion of Gel-Phase Lipid Membranes into Bicelle-like Lipid Nanoparticles," *Langmuir*, vol. 35, no. 49, pp. 16244–16255, 2019, doi: 10.1021/acs.langmuir.9b02077.

[156] S. Tsibranska, A. Ivanova, S. Tcholakova, and N. Denkov, *Self-Assembly of Escin Molecules at the Air-Water Interface as Studied by Molecular Dynamics*, vol. 33, no. 33. 2017.

[157] A. M. Dummer, J. C. Bonsall, J. B. Cihla, S. M. Lawry, G. C. Johnson, and R. F. Peck, "Bacterioopsin-Mediated regulation of bacterioruberin biosynthesis in Halobacterium salinarum," *J. Bacteriol.*, vol. 193, no. 20, pp. 5658–5667, 2011, doi: 10.1128/JB.05376-11.

[158] M. Etzkorn *et al.*, "Complex Formation and Light Activation in Membrane-Embedded Sensory Rhodopsin II as Seen by Solid-State NMR Spectroscopy," *Structure*, vol. 18, no. 3, pp. 293–300, 2010, doi: 10.1016/j.str.2010.01.011.

[159] S. Elter *et al.*, "The Use of Amphipols for NMR Structural Characterization of 7-TM Proteins," *J. Membr. Biol.*, vol. 247, no. 9–10, pp. 957–964, 2014, doi: 10.1007/s00232-014-9669-5.

[160] M. Bogdanov, E. Mileykovskaya, and W. Dowhan, "Lipids in the assembly of membrane proteins and organization of protein supercomplexes: Implications for lipid-linked disorders," *Subcell. Biochem.*, vol. 49, pp. 197–239, 2008, doi: 10.1007/978-1-4020-8831-5_8.

[161] J. Tittelmeier, E. Nachman, and C. Nussbaum-Krammer, "Molecular Chaperones: A Double-Edged Sword in Neurodegenerative Diseases," *Front. Aging Neurosci.*, vol. 12, no. October, pp. 1–21, 2020, doi: 10.3389/fnagi.2020.581374.

[162] J. Y. Shin and P. H. Lee, "Mesenchymal stem cells modulate misfolded α-synuclein in parkinsonian disorders: A multitarget disease-modifying strategy," *Stem Cell Res.*, vol. 47, no. February, p. 101908, 2020, doi: 10.1016/j.scr.2020.101908.

[163] K. Juarez-Navarro, V. M. Ayala-Garcia, E. Ruiz-Baca, I. Meneses-Morales, J. L. Rios-Banuelos, and A. Lopez-Rodriguez, "Assistance for folding of disease-causing plasma membrane proteins," *Biomolecules*, vol. 10, no. 5, 2020, doi: 10.3390/biom10050728.

[164] M. Zhu, J. Li, and A. L. Fink, "The association of α-synuclein with membranes affects bilayer structure, stability, and fibril formation," *J. Biol. Chem.*, vol. 278, no. 41, pp. 40186–40197, 2003, doi: 10.1074/jbc.M305326200.

[165] I. Dikiy and D. Eliezer, "Folding and misfolding of alpha-synuclein on membranes," *Biochim. Biophys. Acta - Biomembr.*,

vol. 1818, no. 4, pp. 1013–1018, 2012, doi: 10.1016/j.bbamem.2011.09.008.

[166] B. Uluca *et al.*, "DNP-Enhanced MAS NMR: A Tool to Snapshot Conformational Ensembles of α-Synuclein in Different States," *Biophys. J.*, vol. 114, no. 7, pp. 1614–1623, 2018, doi: 10.1016/j.bpj.2018.02.011.

[167] J. H. Ardenkjaer-Larsen *et al.*, "Facing and Overcoming Sensitivity Challenges in Biomolecular NMR Spectroscopy," *Angew. Chemie - Int. Ed.*, vol. 54, no. 32, pp. 9162–9185, 2015, doi: 10.1002/anie.201410653.

[168] C. Song, K. N. Hu, C. G. Joo, T. M. Swager, and R. G. Griffin, "TOTAPOL: A biradical polarizing agent for dynamic nuclear polarization experiments in aqueous media," *J. Am. Chem. Soc.*, vol. 128, no. 35, pp. 11385–11390, 2006, doi: 10.1021/ja061284b.

[169] T. Viennet *et al.*, "Selective Protein Hyperpolarization in Cell Lysates Using Targeted Dynamic Nuclear Polarization," *Angew. Chemie - Int. Ed.*, vol. 55, no. 36, pp. 10746–10750, 2016, doi: 10.1002/anie.201603205.

[170] M. A. Voinov *et al.*, "Cysteine-Specific Labeling of Proteins with a Nitroxide Biradical for Dynamic Nuclear Polarization NMR," *J. Phys. Chem. B*, vol. 119, no. 32, pp. 10180–10190, 2015, doi: 10.1021/acs.jpcb.5b05230.

[171] T. Maly, D. Cui, R. G. Griffin, and A. F. Miller, "1H dynamic nuclear polarization based on an endogenous radical," *J. Phys. Chem. B*, vol. 116, no. 24, pp. 7055–7065, 2012, doi: 10.1021/jp300539j.

[172] C. Fernández-de-Alba *et al.*, "Matrix-Free DNP-Enhanced NMR Spectroscopy of Liposomes Using a Lipid-Anchored Biradical," *Chem. - A Eur. J.*, vol. 21, no. 12, pp. 4512–4517, 2015, doi: 10.1002/chem.201404588.

[173] A. N. Smith, M. A. Caporini, G. E. Fanucci, and J. R. Long, "A method for dynamic nuclear polarization enhancement of membrane proteins," *Angew. Chemie - Int. Ed.*, vol. 54, no. 5, pp. 1542–1546, 2015, doi: 10.1002/anie.201410249.

[174] P. Wenk, M. Kaushik, D. Richter, M. Vogel, B. Suess, and B. Corzilius, "Dynamic nuclear polarization of nucleic acid with endogenously bound manganese," *J. Biomol. NMR*, vol. 63, no. 1, pp. 97–109, 2015, doi: 10.1007/s10858-015-9972-1.

[175] E. A. W. Van Der Cruijsen *et al.*, "Biomolecular DNP-Supported NMR Spectroscopy using Site-Directed Spin Labeling," *Chem. - A Eur. J.*, vol. 21, no. 37, pp. 12971–12977, 2015, doi: 10.1002/chem.201501376.

[176] B. J. Wylie *et al.*, "Dynamic nuclear polarization of membrane proteins: Covalently bound spin-labels at protein-protein interfaces," *J. Biomol. NMR*, vol. 61, no. 3–4, pp. 361–367, 2015, doi: 10.1007/s10858-015-9919-6.

[177] V. Vitzthum *et al.*, "Magnetically oriented phospholipid bilayered micelles for structural studies of polypeptides. Does the ideal bicelle exist?," *J. Magn. Reson. - Ser. B*, vol. 113, no. 16, pp. 267–271, 1996, doi: 10.1002/cphc.201100630.

[178] T. Viennet *et al.*, "Structural insights from lipid-bilayer nanodiscs link α-Synuclein membrane-binding modes to amyloid fibril formation," *Commun. Biol.*, vol. 1, no. 1, 2018, doi: 10.1038/s42003-018-0049-z.

[179] W. Hoyer, T. Antony, D. Cherny, G. Heim, T. M. Jovin, and V. Subramaniam, "Dependence of α-synuclein aggregate morphology on solution conditions," *J. Mol. Biol.*, vol. 322, no. 2, pp. 383–393, 2002, doi: 10.1016/S0022-2836(02)00775-1.

[180] T. H. Bayburt and S. G. Sligar, "Self-assembly of single integral membrane proteins into soluble nanoscale phospholipid bilayers," *Protein Sci.*, vol. 12, no. 11, pp. 2476–2481, Jan. 2009, doi: 10.1110/ps.03267503.

[181] F. Hagn, M. Etzkorn, T. Raschle, and G. Wagner, "Optimized phospholipid bilayer nanodiscs facilitate high-resolution structure determination of membrane proteins," *J. Am. Chem. Soc.*, vol. 135, no. 5, pp. 1919–1925, 2013, doi: 10.1021/ja310901f.

[182] I. G. Denisov and S. G. Sligar, "Nanodiscs for structural and functional studies of membrane proteins," *Nat. Struct. Mol. Biol.*, vol. 23, no. 6, pp. 481–486, 2016, doi: 10.1038/nsmb.3195.

[183] S. Bibow *et al.*, "Solution structure of discoidal high-density lipoprotein particles with a shortened apolipoprotein A-I," *Nat. Struct. Mol. Biol.*, vol. 24, no. 2, pp. 187–193, 2017, doi: 10.1038/nsmb.3345.

[184] T. Viennet *et al.*, "A structural and kinetic link between membrane association and amyloid fibril formation of α-Synuclein," *bioRxiv*, pp. 1–31, 2017, doi: 10.1101/173724.

[185] M. Rosay, A. C. Zeri, N. S. Astrof, S. J. Opella, J. Herzfeld, and R. G. Griffin, "Sensitivity-enhanced NMR of biological solids: Dynamic nuclear polarization of Y21M fd bacteriophage and purple membrane [18]," *J. Am. Chem. Soc.*, vol. 123, no. 5, pp. 1010–1011, 2001, doi: 10.1021/ja005659j.

[186] M. Hong and K. Jakes, "Selective and extensive," pp. 1–4, 1999, [Online]. Available: papers2://publication/uuid/25DA17A7-C595-4B51-8856-17DBB9B62D99.

[187] E. S. Salnikov *et al*., "Dynamic Nuclear Polarization/Solid-State NMR Spectroscopy of Membrane Polypeptides: Free-Radical Optimization for Matrix-Free Lipid Bilayer Samples," *ChemPhysChem*, vol. 18, no. 15, pp. 2103–2113, 2017, doi: 10.1002/cphc.201700389.

[188] M. Zhu, B. Xu, M. Wang, S. Liu, Y. Zhang, and C. Zhang, "Pharmacological modulation of MRAP2 protein on melanocortin receptors in the sea lamprey," *Endocr. Connect.*, vol. 8, no. 4, pp. 378–388, 2019, doi: 10.1530/EC-19-0019.

[189] P. M. Hinkle and J. A. Sebag, "Structure and function of the melanocortin2 receptor accessory protein (MRAP)," *Mol. Cell. Endocrinol.*, vol. 300, no. 1–2, pp. 25–31, 2009, doi: 10.1016/j.mce.2008.10.041.

[190] S. Chen *et al*., "Palmitoylation-dependent activation of MC1R prevents melanomagenesis," *Nature*, vol. 549, no. 7672, pp. 399–403, 2017, doi: 10.1038/nature23887.

[191] K. D. Quint *et al*., "Melanocortin 1 receptor (MC1R) variants in high melanoma risk patients are associated with specific dermoscopic ABCD features," *Acta Derm. Venereol.*, vol. 92, no. 6, pp. 587–592, 2012, doi: 10.2340/00015555-1457.

[192] J. A. Sebag and P. M. Hinkle, "Regions of melanocortin 2 (MC2) receptor accessory protein necessary for dual topology and MC2 receptor trafficking and signaling," *J. Biol. Chem.*, vol. 284, no. 1, pp. 610–618, 2009, doi: 10.1074/jbc.M804413200.

[193] J. A. Sebag and P. M. Hinkle, "Regulation of G protein-coupled receptor signaling: Specific dominant-negative effects of melanocortin 2 receptor accessory protein2," *Sci. Signal.*, vol. 3, no. 116, pp. 1–8, 2010, doi: 10.1126/scisignal.2000593.

[194] L. Etchevers *et al*., "MC2R/MRAP2 activation could affect bovine ovarian steroidogenesis potential after ACTH treatment," *Theriogenology*, vol. 174, pp. 102–113, 2021, doi: 10.1016/j.theriogenology.2021.08.020.

[195] D. Fridmanis, A. Roga, and J. Klovins, "ACTH receptor (MC2R) specificity: What do we know about underlying molecular mechanisms?," *Front. Endocrinol. (Lausanne).*, vol. 8, no. FEB, pp. 1–23, 2017, doi: 10.3389/fendo.2017.00013.

[196] B. Y. H. Lam *et al*., "MC3R links nutritional state to childhood growth and the timing of puberty," *Nature*, vol. 599, no. 7885, pp. 436–441, 2021, doi: 10.1038/s41586-021-04088-9.

[197] L. F. Chan *et al*., "MRAP and MRAP2 are bidirectional regulators of the melanocortin receptor family," *Proc. Natl. Acad. Sci. U. S. A.*, vol. 106, no. 15, pp. 6146–6151, 2009, doi: 10.1073/pnas.0809918106.

[198] L. E. Pritchard and A. White, "Agouti-related protein: More than a melanocortin-4 receptor antagonist?," *Peptides*, vol. 26, no. 10, pp. 1759–1770, 2005, doi: 10.1016/j.peptides.2004.11.036.

[199] K.-Y. L. yung-Seng Lee, Larry Kok-Seng Poh, "ANovel Melanocortin 3 Receptor Gene (MC3R) Mutation Associated with Severe Obesity," vol. 87, no. 7, pp. 3500–3503, 2002.

[200] A. Shintani *et al*., "MC5R Contributes to Sensitivity to UVB Waves and Barrier Function in Mouse Epidermis," *JID Innov.*, vol. 1, no. 3, p. 100024, 2021, doi: 10.1016/j.xjidi.2021.100024.

[201] M. Cai and V. J. Hruby, "The Melanocortin Receptor System: A Target for Multiple Degenerative Diseases," *Curr. Protein Pept. Sci.*, vol. 17, no. 5, pp. 488–496, 2016, doi: 10.2174/1389203717666160226145330.

[202] J. L. Dopp and N. F. Reuel, "Process optimization for scalable E. coli extract preparation for cell-free protein synthesis," *Biochem. Eng. J.*, vol. 138, pp. 21–28, 2018, doi: 10.1016/j.bej.2018.06.021.

[203] P. J. Jackson *et al*., "Design, pharmacology, and NMR structure of a minimized cystine knot with agouti-related protein activity," *Biochemistry*, vol. 41, no. 24, pp. 7565–7572, 2002, doi: 10.1021/bi012000x.

[204] R. D. Cone, "Studies on the physiological functions of the melanocortin system," *Endocr. Rev.*, vol. 27, no. 7, pp. 736–749, 2006, doi: 10.1210/er.2006-0034.

[205] N. D. Dwyer, E. R. Troemel, P. Sengupta, and C. I. Bargmann, "Odorant receptor localization to olfactory cilia is mediated by ODR-4, a novel membrane-associated protein," *Cell*, vol. 93, no. 3, pp. 455–466, 1998, doi: 10.1016/S0092-8674(00)81173-3.

[206] J. A. Sebag and P. M. Hinkle, "Opposite effects of the melanocortin-2 (MC2) receptor accessory protein MRAP on MC2 and MC5 receptor dimerization and trafficking," *J. Biol. Chem.*, vol. 284, no. 34, pp. 22641–22648, 2009, doi: 10.1074/jbc.M109.022400.

[207] J. A. Sebag and P. M. Hinkle, “Melanocortin-2 receptor accessory protein MRAP forms antiparallel homodimers,” *Proc. Natl. Acad. Sci. U. S. A.*, vol. 104, no. 51, pp. 20244–20249, 2007, doi: 10.1073/pnas.0708916105.

[208] B. E. Hoglin, M. Miner, and R. M. Dores, “Erratum: Pharmacological properties of whale shark (Rhincodon typus) melanocortin-2 receptor and melancortin-5 receptor: Interaction with MRAP1 and MRAP2 (General and Comparative Endocrinology (2020) 293, (S0016648019305453), (10.1016/j.ygcen.2020.113463),” *Gen. Comp. Endocrinol.*, vol. 315, no. October 2021, p. 113915, 2022, doi: 10.1016/j.ygcen.2021.113915.

[209] M. Asai *et al.*, “Loss of function of the melanocortin 2 receptor accessory protein 2 is associated with mammalian obesity,” *Science (80-.).*, vol. 341, no. 6143, pp. 275–278, 2013, doi: 10.1126/science.1233000.

[210] R. L. Ji and Y. X. Tao, “Regulation of Melanocortin-3 and-4 Receptors by Isoforms of Melanocortin-2 Receptor Accessory Protein 1 and 2,” *Biomolecules*, vol. 12, no. 2, pp. 1–14, 2022, doi: 10.3390/biom12020244.

[211] A. A. J. Rouault, D. K. Srinivasan, T. C. Yin, A. A. Lee, and J. A. Sebag, “Melanocortin Receptor Accessory Proteins (MRAPs): Functions in the melanocortin system and beyond,” *Biochim. Biophys. Acta - Mol. Basis Dis.*, vol. 1863, no. 10, pp. 2462–2467, 2017, doi: 10.1016/j.bbadis.2017.05.008.

[212] A. A. J. Rouault, A. A. Lee, and J. A. Sebag, “Regions of MRAP2 required for the inhibition of orexin and prokineticin receptor signaling,” *Biochim. Biophys. Acta - Mol. Cell Res.*, vol. 1864, no. 12, pp. 2322–2329, 2017, doi: 10.1016/j.bbamcr.2017.09.008.

[213] A. Rath and C. M. Deber, “Correction factors for membrane protein molecular weight readouts on sodium dodecyl sulfate-polyacrylamide gel electrophoresis,” *Anal. Biochem.*, vol. 434, no. 1, pp. 67–72, 2013, doi: 10.1016/j.ab.2012.11.007.

[214] A. Rath, M. Glibowicka, V. G. Nadeau, G. Chen, and C. M. Deber, “Detergent binding explains anomalous SDS-PAGE migration of membrane proteins,” *Proc. Natl. Acad. Sci. U. S. A.*, vol. 106, no. 6, pp. 1760–1765, 2009, doi: 10.1073/pnas.0813167106.

[215] Y. Lu, N. Yeung, N. Sieracki, and N. M. Marshall, “Design of functional metalloproteins,” *Nature*, vol. 460, no. 7257, pp. 855–862, 2009, doi: 10.1038/nature08304.

[216] R. Pernil and E. Schleiff, “Metalloproteins in the biology of heterocysts,” *Life*, vol. 9, no. 2, pp. 1–58, 2019, doi: 10.3390/life9020032.

[217] I. B. Robert Jernigan, Gopalan Raghunathan, “Identification and characterization of metal ion binding sites in RNA,” *Methods Enzymol.*, vol. 338, pp. 421–443, 2002, doi: 10.1016/S0076-6879(02)38231-4.

[218] J. Liu *et al.*, “Metalloproteins containing cytochrome, iron-sulfur, or copper redox centers,” *Chem. Rev.*, vol. 114, no. 8, pp. 4366–4369, 2014, doi: 10.1021/cr400479b.

[219] M. M. Harding, M. W. Nowicki, and M. D. Walkinshaw, “Metals in protein structures: A review of their principal features,” *Crystallogr. Rev.*, vol. 16, no. 4, pp. 247–302, 2010, doi: 10.1080/0889311X.2010.485616.

[220] T. Li, H. L. Bonkovsky, and J. T. Guo, “Structural analysis of heme proteins: Implication for design and prediction,” *2010 IEEE Int. Conf. Bioinforma. Biomed. Work. BIBMW 2010*, pp. 834–835, 2010, doi: 10.1109/BIBMW.2010.5703932.

[221] J. H. Brock, “Iron-binding proteins,” *Acta Paediatr. Scand. Suppl.*, vol. 78, no. 361, pp. 31–43, 1989, doi: 10.1111/apa.1989.78.s361.31.

[222] J. Everse, *Heme Proteins*, 2nd ed., vol. 2. Elsevier Inc., 2013.

[223] P. M. Wood, “Why do c-type cytochromes exist? - Reprise,” *BBA - Bioenerg.*, vol. 1058, no. 1, pp. 5–7, 1991, doi: 10.1016/S0005-2728(05)80256-7.

[224] Esther J. Tomlinson and Stuart J. Ferguson, “Loss of either of the two heme-binding cysteines from a class I c-type cytochrome has a surprisingly small effect on physicochemical properties,” *J. Biol. Chem.*, vol. 275, no. 42, pp. 32530–32534, 2000, doi: 10.1074/jbc.M004022200.

[225] T. Y. and K.Okunuki, “Cytochromes,” *Tanpakushitsu Kakusan Koso.*, vol. 10, no. 15, pp. 1589–1595, 1965, doi: 10.1016/b978-0-12-515250-1.50019-9.

[226] H.-G. Koch and D. Schneider, “Folding, Assembly, and Stability of Transmembrane Cytochromes,” *Curr. Chem. Biol.*, vol. 1, no. 1, pp. 59–74, 2008, doi: 10.2174/187231307779814020.

[227] D. I. A. David B.Knaff, “Light-induced oxidation of chloroplast b -type cytochrome at 189°C,” 1969.

[228] C. Ferousi, S. Lindhoud, F. Baymann, E. R. Hester, J. Reimann, and B. Karta, "Discovery of a functional, contracted heme-binding motif within a multiheme cytochrome," *J. Biol. Chem.*, vol. 294, no. 45, pp. 16953–16965, 2019, doi: 10.1074/jbc.RA119.010568.

[229] G. W. Pettigrew, "The amino acid sequence of a cytochrome c from a protozoan Crithidia oncopelti," *FEBS Lett.*, vol. 22, no. 1, pp. 64–66, 1972, doi: 10.1016/0014-5793(72)80220-5.

[230] D. K. Lin, R. L. Niece, and W. M. Fitch, "The properties and amino-acid sequence of cytochrome c from Euglena gracilis [12]," *Nature*, vol. 241, no. 5391, pp. 533–535, 1973, doi: 10.1038/241533a0.

[231] F. A. O. Carvalho, P. S. Santiago, and M. Tabak, "On the stability of the extracellular hemoglobin of Glossoscolex paulistus, in two iron oxidation states, in the presence of urea," *Arch. Biochem. Biophys.*, vol. 519, no. 1, pp. 46–58, 2012, doi: 10.1016/j.abb.2012.01.007.

[232] C.-A. Y. and T. E. Ki. Linda Yu, Young-Ling Chiang, "A TRYPSIN-RESISTANT HEME PEPTIDE FROM CARDIAC CYTO CHROME c1," *Biochim. Biophys. Acta, 379*, vol. 379, pp. 33–42, 1975.

[233] E. M. Kohn, J. Y. Lee, A. Calabro, T. D. Vaden, and G. A. Caputo, "Heme dissociation from myoglobin in the presence of the zwitterionic detergent N,N-dimethyl-N-dodecylglycine betaine: Effects of ionic liquids," *Biomolecules*, vol. 8, no. 4, 2018, doi: 10.3390/biom8040126.

[234] J. W. A. Allen, N. Leach, and S. J. Ferguson, "The histidine of the c-type cytochrome CXXCH haem-binding motif is essential for haem attachment by the Escherichia coli cytochrome c maturation (Ccm) apparatus," *Biochem. J.*, vol. 389, no. 2, pp. 587–592, 2005, doi: 10.1042/BJ20041894.

[235] J. Hallgren *et al.*, "DeepTMHMM predicts alpha and beta transmembrane proteins using deep neural networks," *bioRxiv*, p. 2022.04.08.487609, 2022, [Online]. Available: https://www.biorxiv.org/content/10.1101/2022.04.08.487609v1%0Ahttps://www.biorxiv.org/content/10.1101/2022.04.08.487609v1.abstract.

[236] G. R. M. Graham W.Pettigrew, "Cytochromes c," *Nature*, vol. 215, no. 5101. p. 574, 1967, doi: 10.1038/215574a0.

[237] L. J. Twyman and Y. Ge, "Porphyrin cored hyperbranched polymers as heme protein models," *Chem. Commun.*, no. 15, pp. 1658–1660, 2006, doi: 10.1039/b600831n.